N91-21212

CHEMICAL SPRAY PYROLYSIS of Tl-Ba-Ca-Cu-O HIGH-T_c SUPERCONDUCTORS for HIGH-FIELD BITTER MAGNETS

L. Pierre. de Rochemont, John G. Zhang, Michael R. Squillante
Radiation Monitoring Devices
44 Hunt Street
Watertown
MA 02172

A.M. Hermann, H.M. Duan
University of Colorado at Boulder
Department of Physics
Boulder
CO 80309

Robert J. Andrews, Rome Air Development Center
Solid State Sciences Directorate
Hanson Air Force Base
MA 01731

Warren C. Kelliher
Mail Stop 416A
NASA Langley Research Center
Hampton
VA 23665-5225

I. INTRODUCTION.

This research is part of a NASA program to investigate the feasibility of applying high-T_c superconducting ceramics to the development of a high-field (5-6 Tesla) magnet, with an ultimate objective of utilizing these materials in a liquid nitrogen cooled wind tunnel magnetic suspension balance. The current state of the high-T_c superconducting ceramics inhibits their immediate application to high-field magnets for a number of reasons. Their superconducting properties are strongly anisotropic, with preferential critical performance perpendicular to the perovskite c-axis, i.e., in the a-b plane of the crystal. As a consequence, the bulk ceramics, which have largely random crystal orientations are not suitable for optimal engineering. Epitaxial films can be prepared in which the c-axis is parallel to the plane of the substrate, i.e., perpendicular to the substrate surface. However, since the design and demonstration of a high-T_c superconducting high-field magnet will require preferential c-axis orientation over a large topological surface, many of the vacuum epitaxial deposition techniques are not suited for this application because of the limited surface areas which can be coated.

These issues can be circumvented by advancing chemical spray pyrolysis as a means to deposit large area films on to a tape wire which can then be configured into the geometry necessary to drive the magnetic field. Chemical spray pyrolysis has a number of advantages. It is inexpensive. It can produce good quality films over very large areas. It is an open system deposition technique so continuous strips of film can be prepared, and it has already demonstrated feasibility in a number of electronics applications, particularly in the field of solar cell fabrication.

This paper reports on the deposition of Tl-Ba-Ca-Cu-O thick films by spray pyrolyzing a Ba-Ca-Cu-O precursor film and diffusing thallium into the film to form the superconducting phase. This approach was taken to reduce exposure to thallium and its health and safety hazards. The Tl-Ba-Ca-Cu-O system was selected because it has very attractive features which make it appealing to device and manufacturing engineering. Tl-Ba-Ca-Cu-O will accommodate a number of superconducting phases. This attribute makes it very forgiving to stoichiometric fluctuations in the bulk and film. It has excellent thermal and chemical stability, and appears to be relatively insensitive to chemical impurities. Oxygen is tightly bound into the system, consequently there is no orthorhombic (conductor) to tetragonal (insulator) transition which would affect a component's lifetime. More significantly, the thallium based superconductors appear to have harder magnetic properties than the other high-T_c oxide ceramics. Estimates using magnetoresistance measurements, [1], indicate that at 77 K $Tl_2Ba_2CaCu_2O_{10}$ will have an upper critical field, H_{c2}, of 26 Tesla for applied fields parallel to the c-axis and $\approx$1000 Tesla for fields oriented in the a-b plane. [2]

Results to date have shown that superconducting films can be reproducibly deposited on 100 oriented MgO substrates. One film had a zero resistance temperature of 111.5 K. Furthermore, x-ray diffraction analysis of the films showed preferential c-axis orientation parallel to the plane of the substrate. These results have now made it possible to consider the manufacture of a superconducting tape wire which can be configured into a topology useful for high-field magnet designs. This paper will review the research which lead to the preparation of these films and plans for further development.

II. EXPERIMENTAL RESULTS.

In chemical spray pyrolysis soluble salts of the metallic components of the superconducting ceramic are dissolved in solution in stoichiometric amounts. In this work the nitrate precursors of barium, calcium, and copper, $(Ba(NO_3)_2$, $Ca(NO_3)_2$, $Cu(NO_3)_2)$, were used. Once thoroughly mixed this solution can be sprayed onto a surface which is hot enough to volatilize the transport fluid and then allow the salts to decompose, oxidize and

form a polycrystalline ceramic. Ultrasonic techniques were used to nebulize the solution into droplets. The sprayed surface is thermally treated in the presence of oxygen, air is suitable, to decompose the nitrates into their respective oxides. Once a Ba-Ca-Cu-O oxide precursor film had been formed thallium was diffused into the film which was then thermally processed to produce the superconductive Tl-Ba-Ca-Cu-O phase.

Stoichiometric control is crucial to the electromagnetic performance of high-T_c superconducting ceramics. Thus a primary objective of the Phase I effort is to tune the spray process to produce Ba-Ca-Cu-O precursor thin/thick films with stoichiometric control and uniformity. A second objective of the program is to fuse all the individual metallic ions into a uniform polycrystalline ceramic prior to thallium diffusion processing. Oxides of Ba and Ca fused into crystalline copper oxide structures are less likely to outgas during subsequent thermal annealing and thallium diffusion processing than would amorphous barium or calcium oxides loosely distributed in the film. Furthermore, a fused crystal structure will have better order and chemical uniformity.

It is therefore a fundamental objective of this program to eliminate single species clustering or agglomerations in the films, enhance grain alignment, and to promote superior microstructure. This can be achieved by using a suitable chemical "binder" in the solution which favors thorough dissolution, intermixing and complexation of the different reactants prior to deposition. Ideally, this solvent should enhance mutual reactivity of the salts during the crystal fusion process.

A. Precursor Development and Stoichiometric Control.

To develop stoichiometric control over the process and to avoid single component clustering in the films the effect of solution solvent and substrate temperature on metal ion incorporation, surface morphology and chemical uniformity were evaluated. The thermal behavior of each of the individual nitrate compounds was measured. These measurements were then used to evaluate the effect of a particular solvent by comparison to thermal analysis on a dried residue of that solution in which the nitrates were mixed in stoichiometric amounts.

Since nitrate compounds are generally hygroscopic and their molecular weights can be altered by ambient humidity conditions, stock solutions of each nitrate were prepared. Stock solution concentration was measured using Atomic Absorption spectroscopy, (AA), by Northern Analytical Laboratory, Amherst, NH.

1. Metallic Nitrate Precursor Denitration/Decomposition

The denitration of the individual cation precursors was studied by drying $Ba(NO_3)_2$, $Ca(NO_3)_2$, and $Cu(NO_3)_2$ water solutions on alumina substrates. The thin film material was scratched off the surface and analyzed using differential thermogravimetric analysis, (DTGA). These measurements were performed by Robert J. Andrews with the Solid State Sciences Directorate, of the Rome Air Development Center, Hanscom AFB, MA using a Perkin-Elmer Delta Series TGA7 Thermal Analyzer.

a. Thermal Denitration/Decomposition of $Cu(NO_3)_2$ in Water Solution.

X-ray diffraction spectra on sprayed films shows that $Cu(NO_3)_2$ in an aqueous environment breaks down at elevated temperatures to form $Cu_2(OH)_3{\cdot}NO_3$. DTGA analysis of the dried $Cu(NO_3)_2$-water complex, shown in Figure 1, indicates that the temperature for maximal denitration/dehydration of the $Cu(NO_3)_2$ is 265° C. All thermal analysis measurements were done in oxygen atmospheres. It appears that between 10° and 210° C residual water is driven from the film residue. A very sharp transition is observed between 210° C and 310° C which is attributed to the denitration/dehydration of $Cu_2(OH)_3{\cdot}NO_3$. The 33.7% percentage weight change between 210° C and 1010° C agrees

favorably with the formation of CuO from $Cu_2(OH)_3{\cdot}NO_3$, on the basis of the following fractional weight percents:

	$Cu_2(OH)_3{\cdot}NO_3$	——>	CuO	+	oxides of nitrogen.
fractional wt%	100%		66.2%		33.8%

The chemical stability of CuO in oxygen at higher temperatures is evident.

b. Thermal Denitration/Decomposition of $Ca(NO_3)_2$ in Water Solution.

Analysis on $Ca(NO_3)_2$, (see Figure 2), shows dehydration below 200° C, and a percentage weight change of 66.1% between 400° C and 750° C. Unlike the cupprous reaction, a series of weaker outgassing peaks are observed in the first derivative spectra prior to a very pronounced rate of weight loss at 733° C. This data agrees quite favorably with the formation CaO through the following path:

	$Ca(NO_3)_2$	——>	CaO	+	oxides of nitrogen
fractional wt%	100%		34.16%		65.84%.

CaO appears to be stable in oxygen above 740° C, after denitration.

c. Thermal Denitration/Decomposition of $Ba(NO_3)_2$ in Water Solution.

The barium nitrates, $Ba(NO_3)_2$, are the most stable of the starting compounds. (See Figure 3). First derivative spectra indicates pyrolytic phenomena starts above 600° C. A stable regime is noted between 800° and 900° C. This stability breaks down above 900° C, but first derivative spectra shows the film tends towards stability again above 1010° C. The percentage weight change between room temperature and 1010° is 40.4%, which is close to the fractional weight which would be lost in the formation of BaO:

	$Ba(NO_3)_2$	——>	BaO	+	oxides of nitrogen
fractional wt%	100%		58.65%		41.35%

The stable oxynitrate phase observed in the $Ba(NO_3)_2$ derivative between 800° and 900° C can not be identified at this time. The $Ba(NO_3)_2$ DTGA data suggests that unless the presence of the other nitrates, ($Cu(NO_3)_2$ and its derivatives, or $Ca(NO_3)_2$), can accelerate conversion of $Ba(NO_3)_2$ to BaO at lower temperatures, annealing above 1000 C will be required to completely denitrate the BaCaCuO precursor films.

2. Effects of Solvents and Chemical Binders on Nitrate Denitration/Decomposition in Mixed Precursor Solutions.

To study identify optimal solution chemistry and chemical binder activity the nitrate precursors were mixed in stoichiometric ratios of 212 Ba:Ca:Cu and dissolved in:

A) A water-only solution

B) An ethanol-(20% vol)/water solution

C) A glycerol-(20% vol)/water solution

Each solution was dried on a hot (120° to 230° C depending on solvent volatility) alumina substrate. DTGA scans were run to observe effects of the solvents and the other nitrates on chemical reactivity during denitration. Ethanol solutions were considered to reduce

$Ba(NO_3)_2$ precipitation from solution. Glycerol solutions were considered to reduce single nitrate species agglomerations in solution and to enhance the chemical reactivity between the different nitrate compounds. The glycerol molecule provides a longer chain with hydrogen bonding sites which could conceivably complex different nitrate species in close physical proximity to one another.

The fractional chemical weight distributions for solutions tested were determined using a 212 ratio:

	$Ba(NO_3)_2$	$Ca(NO_3)_2$	$Cu(NO_3)_2$
Ratio	2	1	2
wt%	49.12%	15.49%	35.39%.

a. The Effect of a Water-only Solvent.

Figure 4 shows DTGA spectra for the nitrates when dissolved in water only. Thermogravimetric changes below 200° C are being attributed to water absorbed in the nitrate film by exposure to air. Copper denitration proceeds as before, unaffected by the presence of the other nitrate complexes. Its characteristic spectra in the first derivative is once again observed at 265° C. The percentage weight change observed between 228° C and 369° C was roughly 11%, and is attributed to copper denitration. This is in general agreement with an 11.9% weight differential that would be expected using the fractional weight percentage change observed during $Cu_2(OH)_3{\cdot}NO_3$ denitration/dehydration between 220° C and 300° C.

In mixed-water solutions $Ca(NO_3)_2$ and $Ba(NO_3)_2$ denitration appears to be shifted to lower temperatures. Principal first derivative spectra for the denitration transitions are observed between 375° C and 700° C. This is in rough agreement with the $Ca(NO_3)_2$ spectra, but is contrary to the findings for $Ba(NO_3)_2$. It appears as though $Ca(NO_3)_2$ and $Ba(NO_3)_2$ denitration is accelerated by each other's presence or by the copper oxides in the films. It is also plausible that $Ca(NO_3)_2$ and $Ba(NO_3)_2$ complex together in aqueous solutions. Calculations of the fractional weight percent changes using the individual denitration data predicts a total percentage weight change of 57.56%, in rough agreement with the 54.35% weight change observed in the mixed films. It seems reasonable to assume that in water-only solvents most denitration should be complete above temperatures of 700° C.

b. The Effect of a Water-20% vol Ethanol Solvent.

Figure 5 shows DTGA spectra from the 20%-vol ethanol solution. Spectral signatures in the 0th and 1st derivative spectra are identical, indicating $Cu_2(OH)_3{\cdot}NO_3$ denitration again proceeds unaffected by the presence of either $Ca(NO_3)_2$ or $Ba(NO_3)_2$ in ethanol solvents. An analytical comparison was not possible.

Figure 6 shows the Differential Scanning Calorimetry (DSC) measurements in oxygen on the dried residue of the precursors mixed in water and 20% vol ethanol solution. Strong endothermic peaks are noticeable at temperatures just below outgassing temperatures identified by DTGA. (See Figure 5). This suggests that the individual nitrates are breaking apart seemingly unaffected by each other's presence. The lack of any exothermic peaks in the spectra shows that no latent heats of crystal fusion are being released. Although the use of ethanol may help dissolve $Ba(NO_3)_2$ and prevent its precipitation from solution, it does not promote the formation of fused crystal microstructures.

Furthermore, the addition of ethanol to the solution reduces the liquid surface tension to such a degree that boiling during the drying process caused liquid drops carrying raw materials powders to spew from the substrate. Ethanol experimentation was discontinued at this point because of the adverse effects splattering would have on stoichiometric control.

c. The Effect of a Water-20% Glycerol Solvent.

Experimentation with glycerol solutions was conducted to try to improve film uniformity. Since glycerol is a chain molecule with many hydrogen bonding sites the individual nitrate species have a better chance of being physically complexed closer to each other if they bind at different sites along the chain. It is intended that the close physical proximity of the individual nitrate species provided by the glycerol chain would improve uniformity, inhibit single species clustering, and enhance the formation of BaCaCuO crystallites. Stoichiometric formation of BaCaCuO crystallites is preferred to CuO crystallites segregated from CaO/BaO polymorphous phases. This will help ensure chemical integrity during subsequent processing and single phase formation during thallium diffusion.

Figure 7 shows that the qualitative character of glycerol-complexed BaCaCu-denitration in oxygen changes substantially. DTGA spectra below 182 C, (the boiling point of glycerol) is due primarily to dehydration. Spectra between 182° C and 250° C is attributed to glycerol outgassing. The most notable feature of this spectra is that $Cu_2(OH)_3{\cdot}NO_3$, if it is at all present in the glycerol residue, no longer denitrates by itself. Furthermore, the largest relative change in weight occurs below 500° C. The weight change between 250° and 500° C accounts for roughly 67% of all outgassing above 250° C. This indicates that $Ca(NO_3)_2$ and $Ba(NO_3)_2$ denitration participates in the copper oxide conversions and that BaCaCu complexes are being formed in solution. Roughly one third of the relative weight change occurs above 500° which can be solely attributed to $Ca(NO_3)_2$ and $Ba(NO_3)_2$ (complexed) denitration. This data also shows that the microcrystallites formed with a glycerol binder are relatively stable in oxygen at temperatures up to ≈900° C. Changes in the first derivative spectra above 900° C suggest that the compound could break down at elevated temperature.

Figure 8 shows DSC spectra under oxygen atmospheres for the mixed precursors formed in water/glycerol solvents. Three exothermic peaks are evident at 204° C, ≈300° C, and 341° C. This data, and the marked change in the DTGA spectra for glycerol solutions is direct evidence that the glycerol molecule chemically binds the individual metallic nitrate precursors, promotes reactivity between the precursors and the formation of microstructural crystallites in the sprayed films after thermal processing. An unusual feature of this spectra is that structural relaxation is not observed at temperatures slightly below the principal outgassing band between 250° and 500° C.

3. Effect of Substrate Temperature on Film Deposition

In chemical spray pyrolysis substrate temperature can affect both surface morphology and film stoichiometry. Thermal mass transfer, convection currents, vapor phase dynamics or evaporative effects and secondary chemical reactions can adversely affect chemical incorporation rates into the films. The thermodynamics of this deposition technique has not yet been fully characterized so process control has to be obtained through empirical study uniquely. To identify suitable substrate temperatures chemical incorporation was studied by spraying 223 BaCaCu-nitrate ratios dissolved in all three solvents at substrate temperatures between 180° and 350° C.

Energy Dispersive X-ray Spectroscopy was performed on the films to evaluate atomic ratios. Figure 9 shows the atomic Ca/Cu and Ba/Cu ratios observed in the films sprayed using an ethanol 20%-vol solvent versus substrate temperature. The Ca/Cu and

Ba/Cu ratios used in solution are also shown. By simple inspection it is apparent that during the spray process both Ca and Cu are not fully incorporated since the Ba/Cu film ratio is always greater than the solution ratio and the Ca/Cu film ratio is always less than the solution ratio.

Figure 10 shows copper and calcium incorporation rates against substrate temperature between 180° and 350° C. Incorporation rates were calculated assuming $Ba(NO_3)_2$ is incorporated at 100%. Under this assumption a system of three linearly coupled equations can be constructed for which there are two unknowns. Percentages of Ca and Cu lost can be calculated against Ba incorporation using the ratio of each in the solution. The accuracy of the calculation can be tested by comparing the ratio of Ca/Cu in the films to value obtained through calculation. Figure 11 shows the percentage differences between the calculated and observed values.

A very sharp increase in the copper incorporation and an enhancement in the calcium incorporation was observed at 260° C. This matches the peak denitration temperature for $Cu(NO_3)_2$. This would appear to suggest that film incorporation rates for the metallic cations can be quite sensitive to oxidizing conditions and mass transfer phenomena at the substrate surface.

Since substrate temperature has such a strong influence on the resultant stoichiometry in the hydroxynitrate films a hot plate was constructed to control substrate temperature to within 1° C. This construction employs an Omega(TM) Series 2000 Programmable Temperature Controller capable of ramp and soak temperature cycling.

Films prepared from glycerol 20%-vol solvents were far less susceptible to surface reactivity. Scanning Electron Microscopy (SEM) revealed that a 260° C substrate temperature provided the best surface morphologies. Plates 1-3 show surface characteristics of films prepared using water-only, ethanol (20% vol), and glycerol (20% vol) at that substrate temperature. Both the ethanol and water-only films show signs of single species agglomeration as indicated by the DTGA spectra. Although the films prepared with glycerol had the best submicron microstructures, (See Plate 4), they remained quite porous. (Plate 5), with a high density of weak link interconnections between grain granules.

Continued research using glycerol (20% vol)/water solvents sprayed onto substrates heated to 260° C has shown that solution stoichiometries can be reproduced in the films. Table I shows atomic percents measured in a series of films using semiquantitative Energy Dispersive X-Ray Spectroscopic analysis, by Photometrics, Inc., Woburn, MA.. These results indicate that a strong correlation between solution and film stoichiometries can be achieved using these process parameters. Plate 6 is a backscattered scanning electron micrograph of sample 223-02. Good chemical uniformity and small microstructures can be formed using these process conditions.

B. Effect of Substrates on the Quality of Annealed Films.

Precursor films were prepared on <100> oriented epitaxially polished ytterium-stabilized zirconia (YSZ) and magnesium-oxide substrates. After spraying at a substrate temperature of 260° C in air the films were immediately denitrated by thermal bake out using a temperature cycle determined from thermal analysis measurements.

In both instances microcracking was observed in the oxide precursors. This is a shortcoming to any solution process where the films essentially have to be dried from a slurry and large volumes of reactant by-product is driven from their interior. This results in a generally porous texture. Films sprayed onto YSZ substrate had very poor adhesion to the substrate after the denitration process, and were not suitable for Tl-diffusion. (See Plate 5).

Most of the YSZ-substrate films were damaged during the diffusion step either by film evaporation or flaking.

Films deposited onto MgO substrates had sharply reduced microcrack densities and far superior adhesion. The MgO substrate films did indeed become superconducting after Tl-diffusion when suitable processing parameters were used. No increased microcracking was observed even after electrical characterization in liquid nitrogen. These results suggest very strong suitability of MgO substrates with Tl-Ba-Ca-Cu-O superconducting films prepared using solution processes over a range of temperature from 77 K to 1225 K.

C. Thallium Diffusion Processing.

The superconductive Tl-Ba-Ca-Cu-O phase is formed from the Ba-Ca-Cu-O precursor by diffusing thallium into the film. This can be done with a pellet of thallium oxide in a small porcelain crucible. The pellet is of sufficient size so that it does not totally evaporate during the short annealing step. The substrate containing the precursor films is suspended over the crucible and the assembly is placed in a quartz tube furnace at 850° C for 15 minutes. During the process, argon, air, oxygen, or a mixture of gasses are flowed over the sample. Only oxygen atmospheres were successful in preventing the sprayed precursor films from evaporating off of the substrate. The gas flow rate is adjusted empirically to optimize the oxygen content of the resulting film and to maintain sufficient oxygen overpressures above the films.

D. Electrical Properties of the Superconducting Films.

Figure 12 shows the R-T curve for the first superconducting sample obtained. The transition is sharp and the zero-resistance temperature is 112 K. While this is not the highest temperature reached by the thallium containing superconductors, it exceeds the highest reported value for sprayed films by 15 K. [3] In all five superconducting films were produced with zero resistance temperatures ranging between 97 K and 112 K.

Preliminary measurements of critical currents at 77 K in these spray pyrolyzed films range between 100 and 250 A/cm^2. These values are low for high-field magnet applications and result in major part from the porosity of the films, excessive weak link interconnections, poor grain alignment, and nonuniform crystallographic orientation. Many of these deficiencies can be reduced by finer tuning the process.

E. Crystallographic Orientation of the Ceramic.

An important consideration if the construction of useful magnets is the orientation of the material in the films used. To obtain high critical currents needed for high fields, the crystal grains in polycrystalline films should be oriented with the c-axis perpendicular to the substrate so that the current flows in the a-b plane. Thus, it was important for us to determine whether or not films could be deposited with a preferential orientation. After processing, we analyzed our films using XRD and determined that the films grew with the c-axis perpendicular to the substrate surface.

Table II compares the x-ray diffraction patterns of Tl-Ba-Ca-Cu-O bulk powders to an epitaxial thin film prepared by rf-sputtering and the T_c = 112 K film prepared by chemical spray pyrolysis and thallium diffusion. The epitaxial film has total c-axis orientation in the plane of the substrate, and the powder diffraction has completely random orientations. The c-axis oriented patterns are highlighted and the normalized peak intensities are given to show preferential c-axis orientation in the plane of the substrate for the spray pyrolyzed film.

F. SILVER-DOPING EXPERIMENTATION.

Silver doping into the precursor films can be easily achieved using silver nitrate, $Ag(NO_3)_2$, which dissolves readily into water. Silver incorporation into the Y-Ba-Cu-O has been shown to greatly enhance critical current densities, ductility and other mechanical properties. For these reasons the feasibility of silver-doping by chemical spray pyrolysis was examined in Phase I.

Three silver-doped films (10%-, 20%-, and 30%-wt) were prepared and each showed negligible microcrack densities after denitration baking, regardless of the substrate used, i.e., YSZ or MgO. Unfortunately in an attempt to phase separate the Ba-Ca-Cu-O precursor from the silver, by annealing at 1000 C, the silver-doped films evaporated. An undoped film was annealed at the same time and it did not completely evaporate which suggests that silver incorporation into the Ba-Ca-Cu-O precursor increases the vapor pressure of the compound.

III. PLANS FOR FUTURE DEVELOPMENT.

The successful demonstration of a deposition process for high-T_c superconducting films which can be applied to the preparation of large-area thick films has now made it possible to consider the manufacture of liquid nitrogen-cooled superconducting wire tape. A cross-section of a prototype design for this construction is given in Figure 13. As diagrammed, a stainless steel strength membered copper tape will be used as the base structure. Spray pyrolyzed MgO film will be deposited upon it to provide good adhesion between the superconductor and the support structure. Researchers at the Naval Research Laboratories, Washington, D.C., have successfully demonstrated that spray pyrolysis can be used to deposit 100 oriented MgO films on sapphire, fused silica, and silicon. [4]

Silver-doped TlBaCaCuO films will be sprayed through a mask to form tracks on the MgO-coated base tape. The use of silver is being considered to improve the ceramic's ductility and mechanical workability, [5], as well as to enhance the material's current carrying capability. [6] Applying the superconductor in the wire as tracks should also reduce A.C. losses and improve thermal and electrical shunting of the stored energies and stresses which develop in the films and can quench a superconducting magnetic coil. A silver layer will overlay the superconductor to improve conduction to the copper shunt, and an insulating tape will cap the tape to inhibit high-voltage electrical discharging between windings when the tape is assembled into an operating coil. This design is being considered because it provides sufficient structural support to the mechanical stresses expected from 5-6 Tesla magnetic fields.

A major objective in the successful demonstration of a high-field magnet will be the development of strong flux pinning potentials in the superconducting films. It will be necessary to pin magnetic fluxoids at defect sites with sufficient strength to resist the Lorentz forces induced by the driving currents. The free movement of fluxoids in the superconducting wire tape will dissipate energy and pinch-off critical current densities needed to operate in strong magnetic fields. The value of critical current densities in all type-II superconductors is strongly affected by processing parameters and is not necessarily an intrinsic property of the superconducting system. To achieve this aim significant research will be dedicated to optimizing c-axis orientation of the films by adjusting deposition parameters, and using other salt reactants or chemical binders in fabricating the precursor films. The application of nuclear irradiation [7] and mechanical shock compression [8] can improve flux pinning potentials and will be evaluated in this development as well.

Finally, once large area films have been deposited onto the tape structure which have suitable electrical properties, the spatial characteristics of currents flowing in these films under applied magnetic fields will be measured. These measurements will be crucial to the

determination of the optimal topological surface structure for the high-field magnet. This work will be done with the MIT Francis Bitter National Magnet Laboratory in Cambridge, MA. Once these properties have been assessed, a coil utilizing the wire tape in a pancake, Bitter coil, or hybrid pancake-Bitter coil geometry will be designed to generate a 5-6 Tesla field and tested.

Acknowledgments

The authors are grateful for the contributions made to this paper by Dr. John E.C. Williams and Robert Weggel from the MIT Francis Bitter National Magnet Laboratory, Cambridge, MA.

References

[1] Kang, J.H., Gray, K.E., Kampworth, R.T., and Day, D.W., *Large anistropy in the upper critical field of sputtered thin films of superconducting Tl-Ba-Ca-Cu-O*, Appl. Phys. Lett., **53(25)**, 2562 (1988).

[2] Phase II Proposal, Contract #NAS1-19012, National Aeronautics and Space Administration, NASA Langley Research Center, Hampton, VA 23665-5225.

[3] Barboux, P. Tarascon, J.M., Shokoohi, F., Wilkens, B.J., and Schwartz, C.L., *Thick Films by Solution Processes*, J. Appl. Phys. Lett., **64**, 6382 (1988).

[4] DeSisto, W.J., and Henry, R.L., *Deposition of (100) oriented MgO films on sapphire by a spray pyrolysis method*, Appl. Phys. Lett., **56**, 2522 (1990).

[5] Miller, J., Jr., Holder. S.L., and Hunn, J.D., *Improvement of $YBa_2Cu_3O_{7-x}$ Thick films by Doping with Silver*, Appl. Phys. Lett., **54(22)**, (1989).

[6] Dwir, B., Affronte, M., and Pavuna, D., *Evidence for enhancement of critical current by intergrain Ag in YBaCuO-Ag ceramics*, Appl. Phys. Lett., **55(4)**, 399 (1989).

[7] van Dover, R.B., Gyorgy, E.M., White, A.E., Schneemeyer, L.F., Felder, R.J., and, Waszczak, J.V., *Critical currents in proton-irradiated single-crystal $Ba_2YCu_3O_{7-d}$*, Appl. Phys. Lett., **56(26)**, 2661 (1990).

[8] Weir, S.T., Nellis, W.J., Kramer, M.J., Seaman, C.L., Early, E.A., and Maple, M.B., *Increase in the flux-pinning energy of $YBa_2Cu_3O_{7-d}$ by shock compression*, Appl. Phys. Lett., **56(14)**, 2042 (1990).

TABLE I

SAMPLE I.D.	DESIRED ATOMIC PERCENTAGES Ba	Ca	Cu	MEASURED ATOMIC PERCENTAGES Ba	Ca	Cu	SURFACE UNI-FORMITY
223-02	28.57	28.57	42.86	30%±2	28%±2	42%±2	GOOD
233-02	25.00	37.50	37.50	28%±2	41%±2	30%±2	POOR
243-01	22.22	44.44	33.33	22%±1	46%±2	32%±2	GOOD
253-02	20.00	50.00	30.00	20%±1	48%±2	32%±2	GOOD
224-02	25.00	25.00	50.00	29%±2	29%±2	41%±2	POOR
225-01	22.22	22.22	55.56	26%±2	25%±2	48%±2	POOR

Table I. Stoichiometric control achieved by spraying nitrate precursors dissolved in water and 20%-vol glycerol on substrates heated to 260 C.

Table II-XRD orientation

POWDER (hkl) I/Io	PYROLYSIS (hkl) I/Io	RF SPUTTERING (hkl) I/Io
002/5	**002/2**	**002/9**
	004/2	**004/5**
006/5	**006/4**	**006/8**
		008/4
	103/5	
	105/1	
0010/9	**0010/8**	**0010/9**
107/87	107/3	
	110/2	
200/100		
118/14		
119/5		
205/5		
	0012/100	**0012/100**
210/17		
212/10		
214/8		
220/47		
	1011/1	
	200/2	
	1112/1	
300/18		
	215/1	
	0018/25	**0018/18**
316/14		

X-ray diffraction patterns for $Tl_2CaBa_2Cu_2$. The preferential orientations of a spray pyrolyzed film prepared during Phase I is compared to those of an epitaxial rf-sputtered film, (Yolchikawa, et al., Appl. Phys., July 18, 1988), and to the random orientations of a powder sample, (Hermann, PHYS. REV.) LETT., Vol. 60, No. 16, 1988).

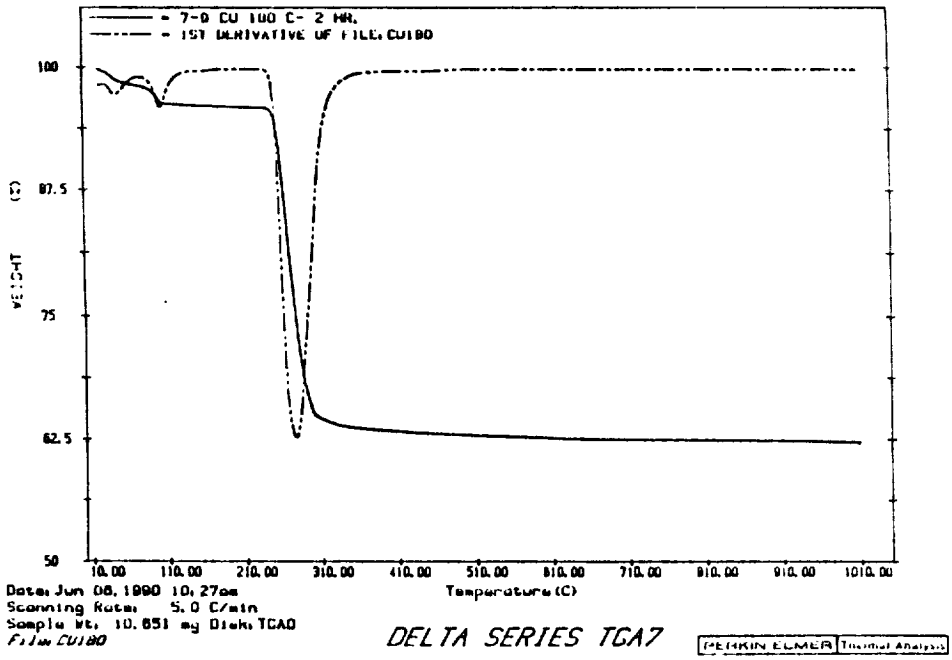

Figure 1. DTGA spectra of $Cu_2(OH)_3{\cdot}NO_3$-the residue of aqueous $Cu(NO_3)_2$ dried at 170 C.

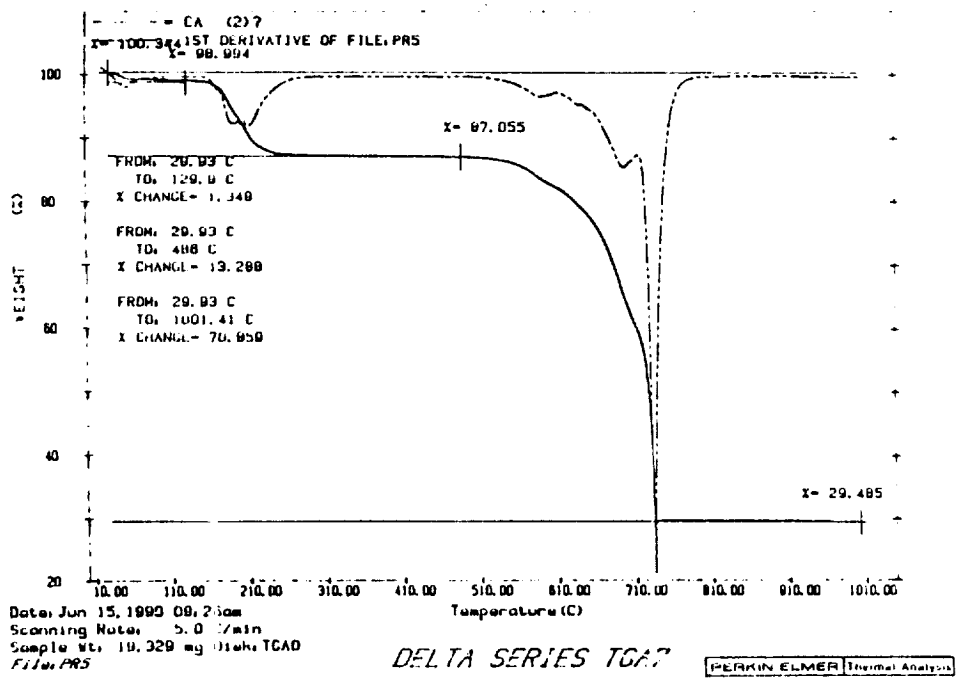

Figure 2. DTGA spectra of aqueous $Ca(NO_3)_2$ dried at 170 C.

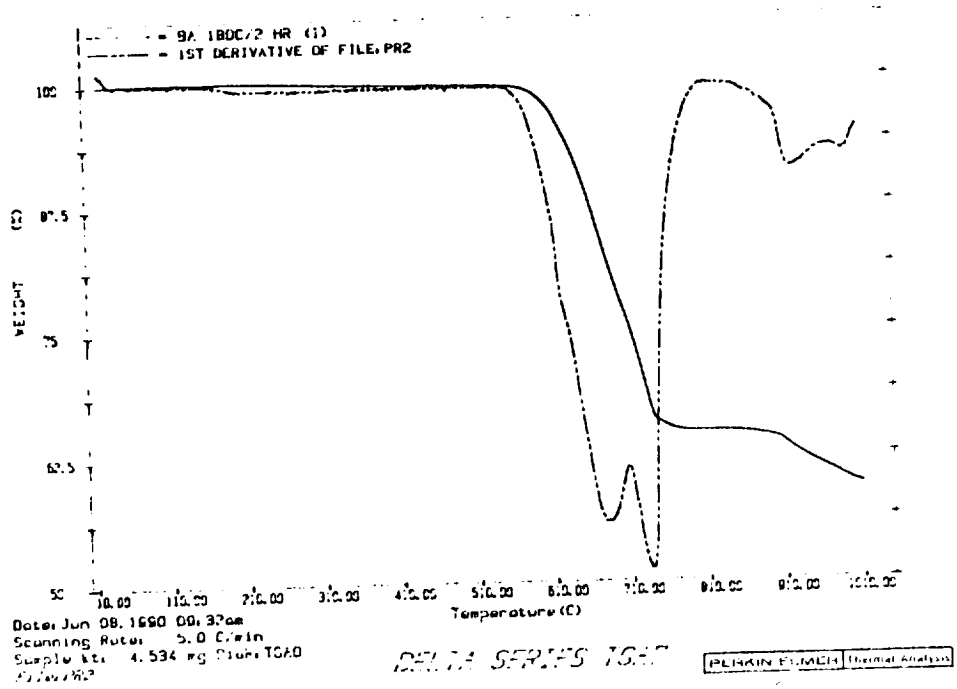

Figure 3. DTGA spectra of aqueous $Ba(NO3)_2$ dried at 170 C.

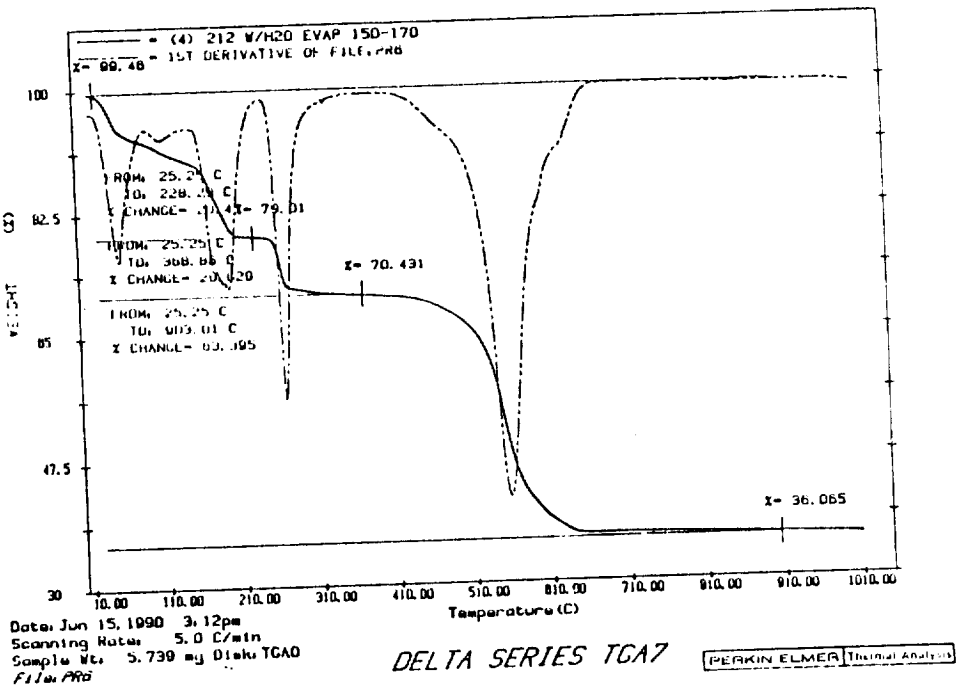

Figure 4. DTGA spectra of mixed 212-Ba-Ca-Cu hydroxynitrates dissolved in water only and dried at 170°C in air.

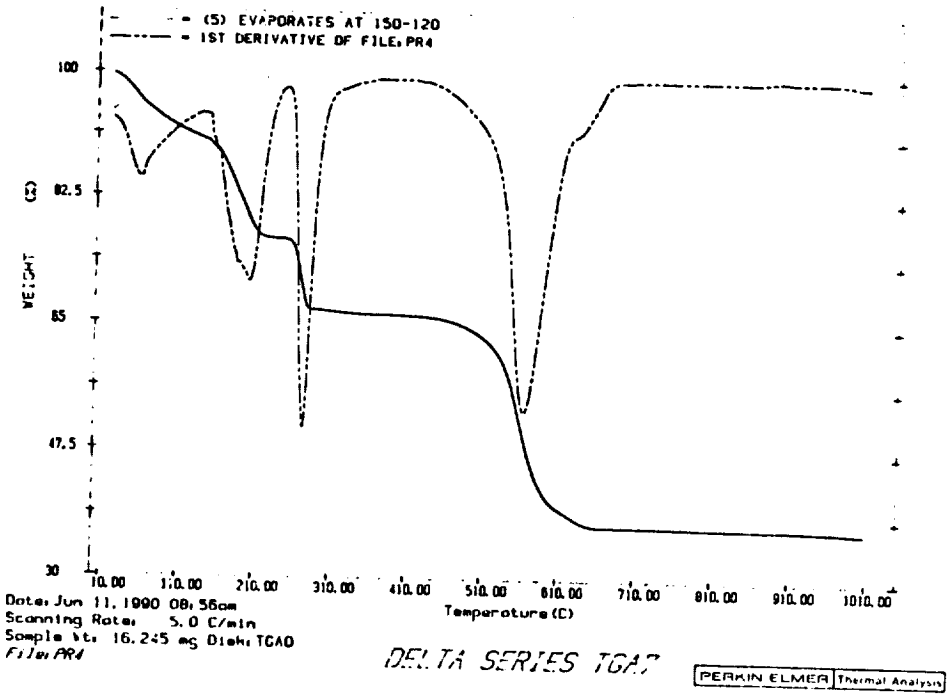

Figure 5. DTGA spectra of mixed 212-Ba-Ca-Cu hydroxynitrates dissolved in water and ethanol (20% vol) and dried at 120 C in air.

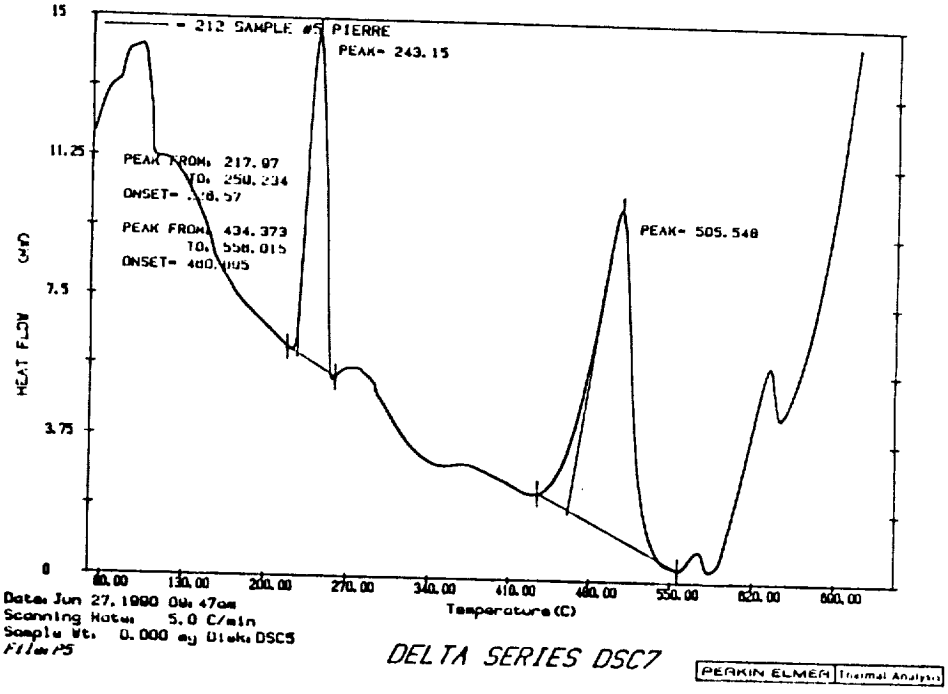

Figure 6. DSC measurement of 2-1-2-Ba-Ca-Cu hydroxynitrate residue mixed in water and 20%-vol ethanol solution in an oxygen atmosphere.

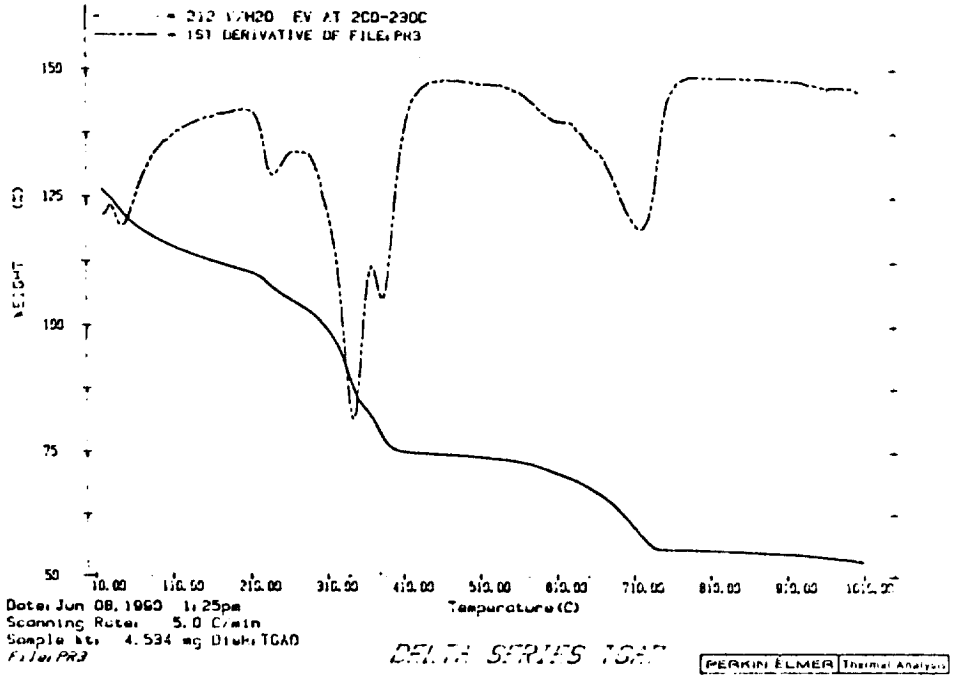

Figure 7. DTGA spectra of mixed 212-BaCaCu hydroxynitrates dissolved in water and glycerol (20% vol) and dried at 210-230 C.

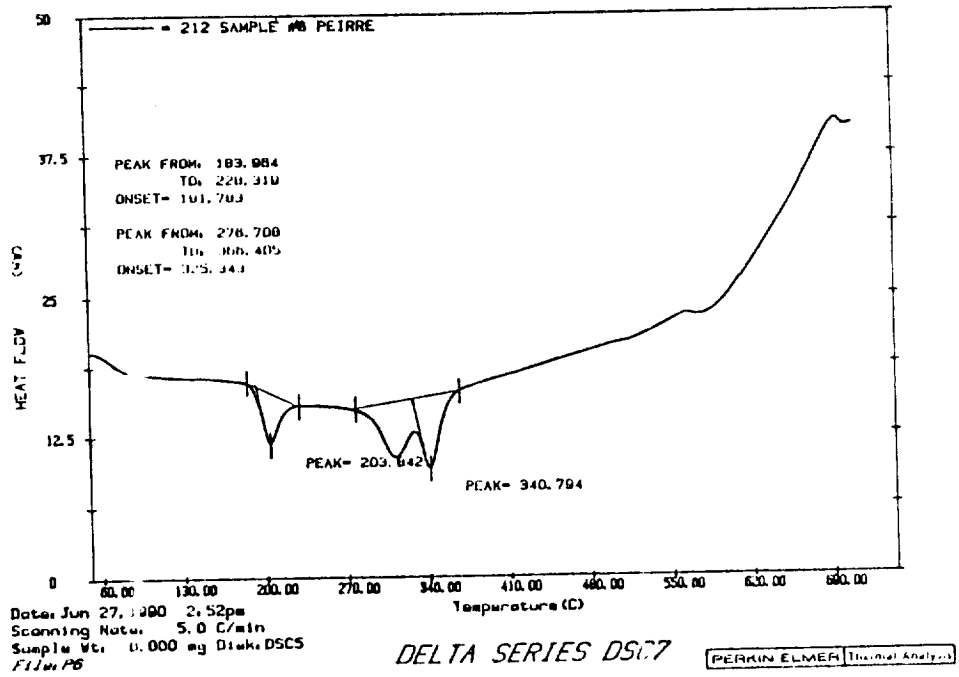

Figure 8. DSC measurement of 2-1-2-Ba-Ca-Cu nitrate residue mixed in water and 20%-vol glycerol solution in an oxygen atmosphere.

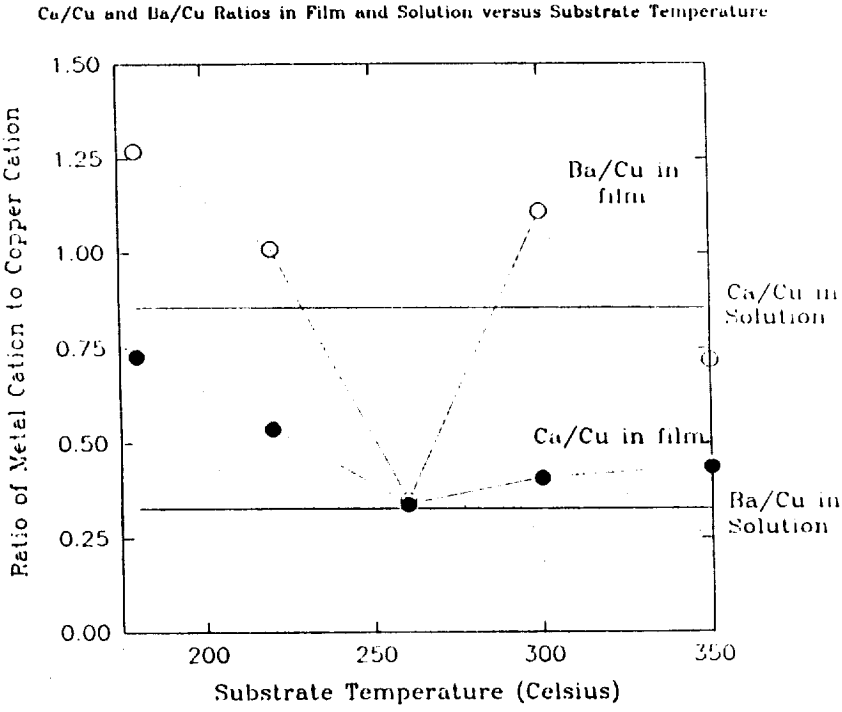

Figure 9. Ba/Cu and Ca/Cu atomic ratios in films sprayed from mixed BaCaCu nitrates dissolved in water and ethanol (20%vol) versus substrate temperature. Ba/Cu and Ca/Cu atomic ratios in solution are marked by the solid lines.

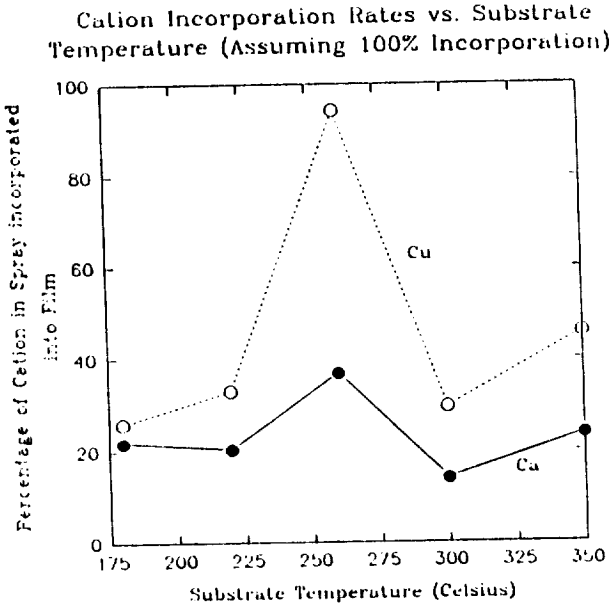

Figure 10. Percent incorporation rates for Ca and Cu sprayed from mixed BaCaCu nitrates dissolved in water and ethanol (20% vol) versus substrate temperature. (Calculated assuming 100% Ba incorporation over substrate temperatures).

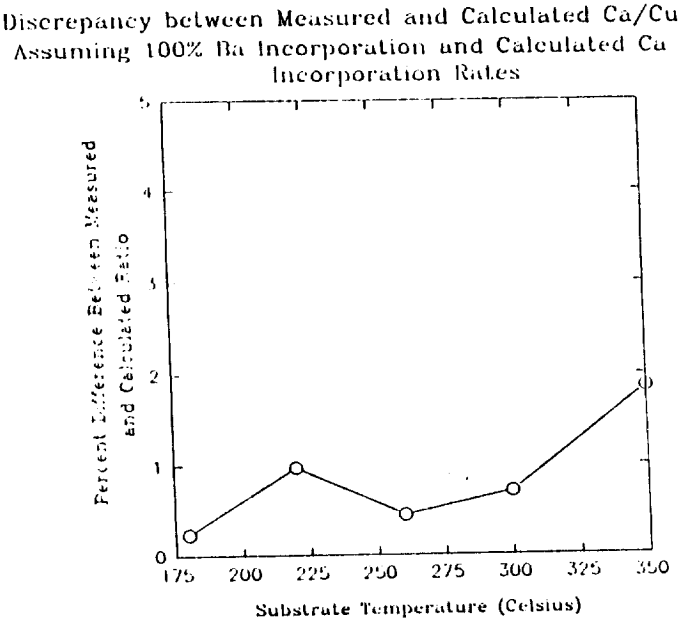

Figure 11. Percentage deviation between Ca/Cu ratios measured in films and Ca/Cu ratios calculated from Ca and Cu loss estimates assuming 100% Ba film incorporation.

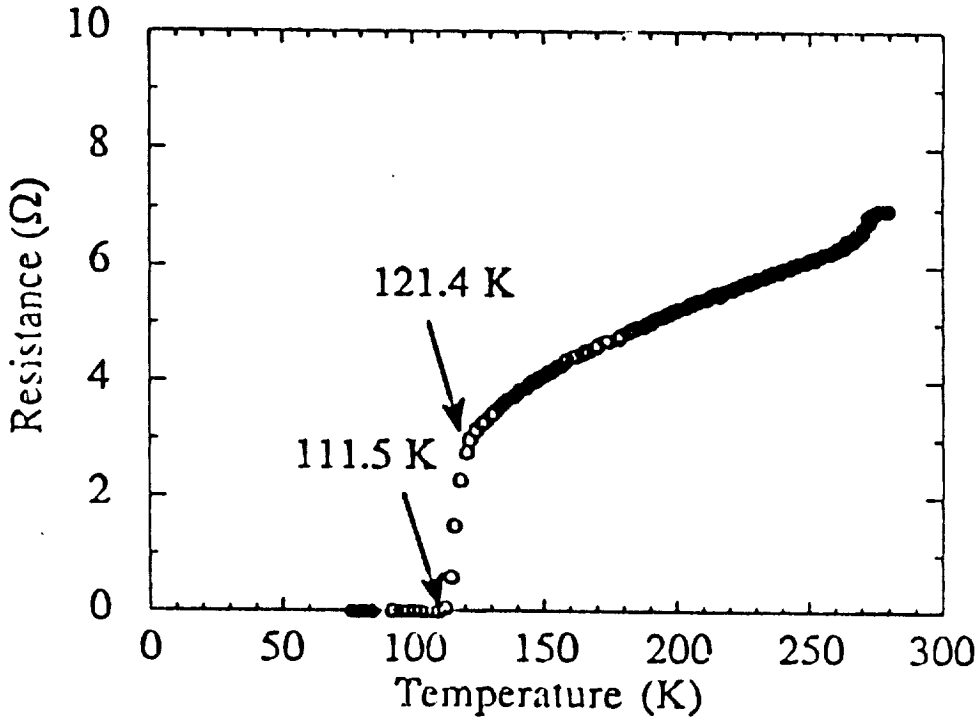

Figure 12. R-T curve for Tl-Ba-Ca-Cu-O superconductor prepared by spray pyrolyzing a Ba-Ca-Cu-O precursor film and thallium diffusion to form the superconductive phase.

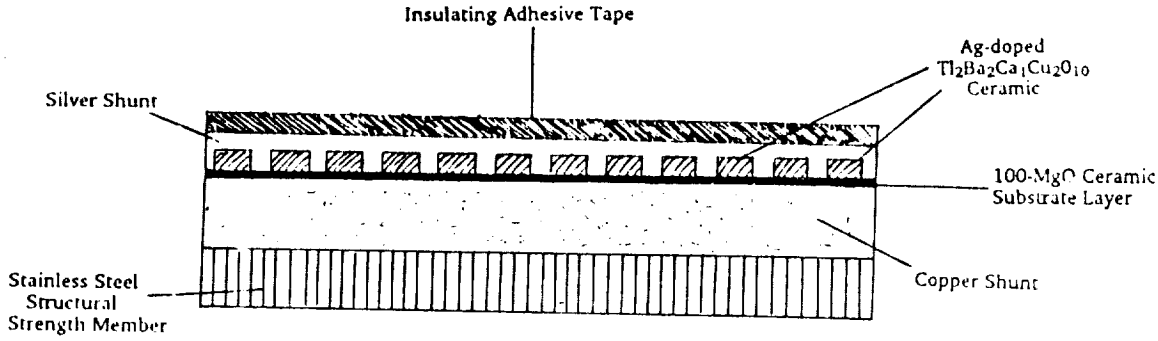

Figure 13. Cross-section of the prototype design of Tl-Ba-Ca-Cu-O wire tape for use in a superconducting magnetic coil. (Not drawn to scale).

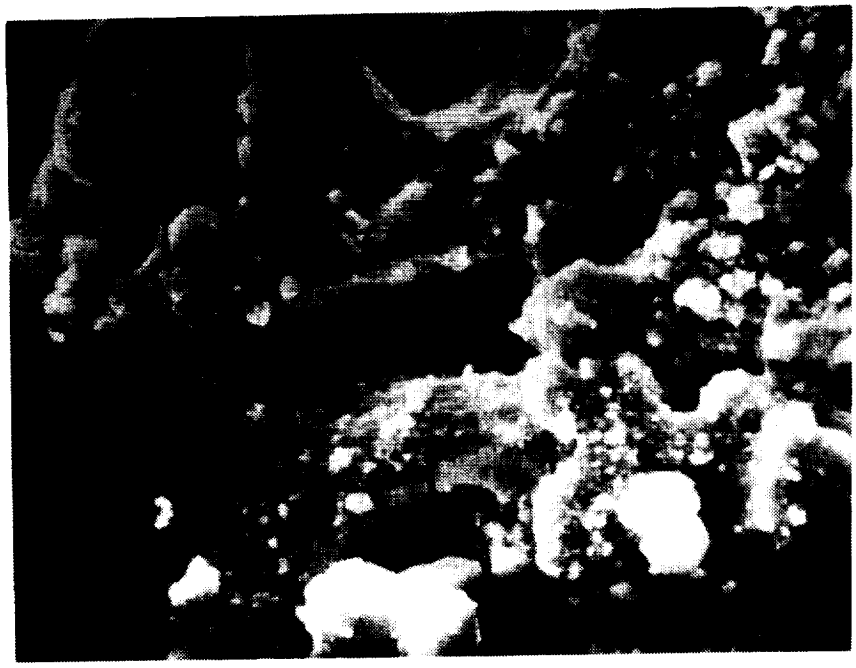

Plate 1. SEM micrograph of a spray pyrolyzed Ba-Ca-Cu-O precursor prepared using a water-only solution. (Magnification 1250 X).

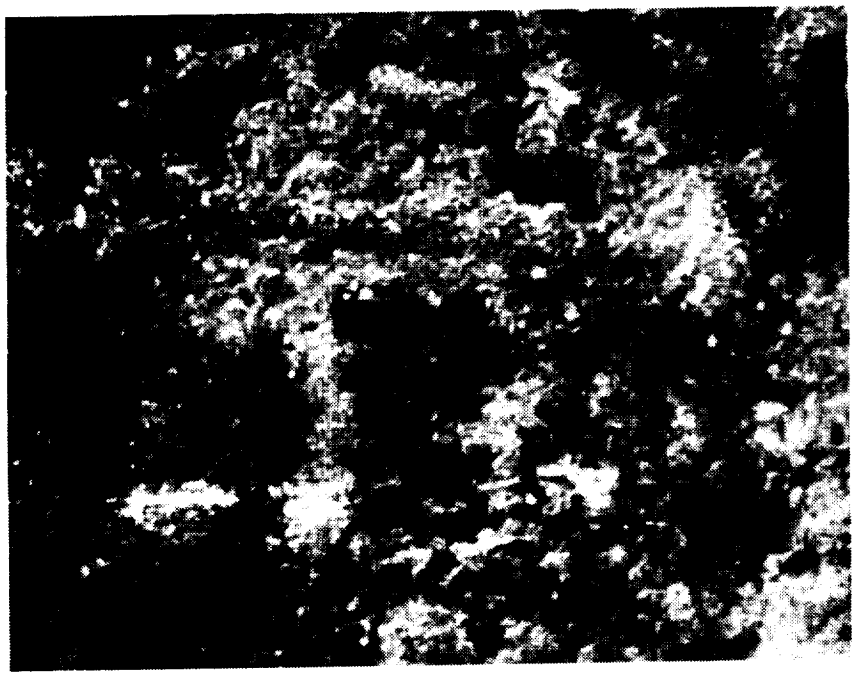

Plate 2. SEM micrograph of a spray pyrolyzed Ba-Ca-Cu-O precursor prepared using a 20%-vol ethanol/water solution. (Magnification 1250 X).

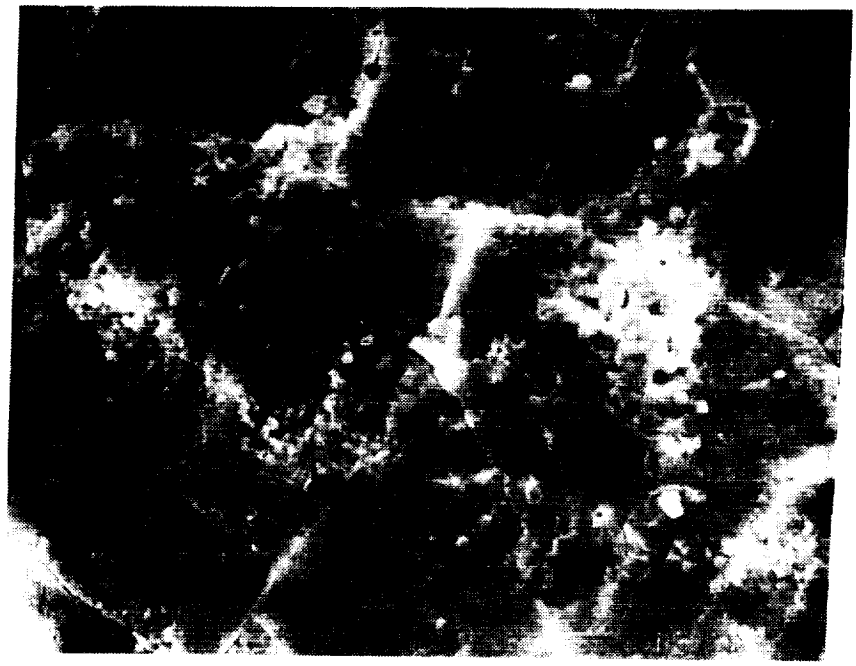

Plate 3. SEM micrograph of a spray pyrolyzed Ba-Ca-Cu-O precursor prepared using a 20%-vol glycerol/water solution. (Magnification 1250 X).

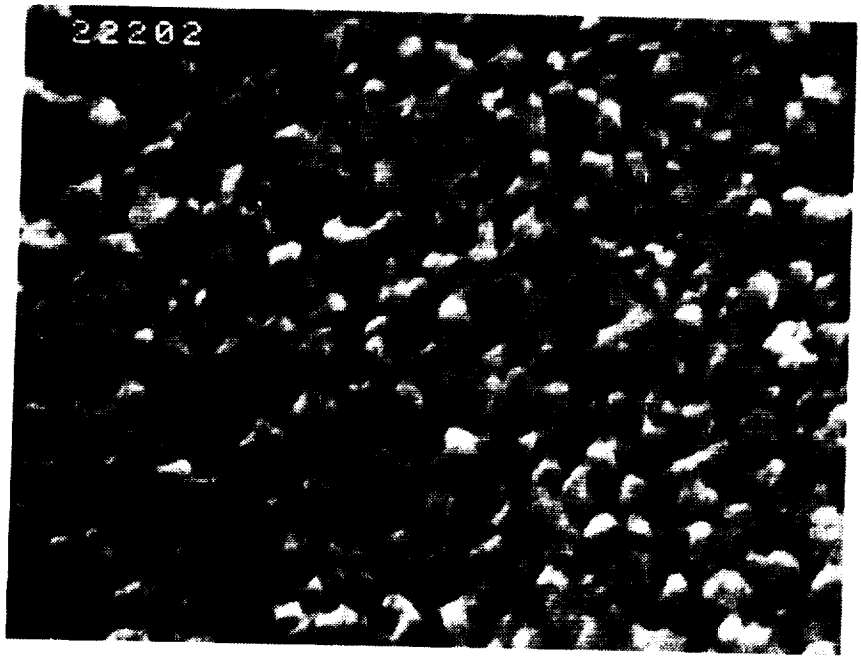

Plate 4. SEM micrograph of the submicron microstructure of the grain granules in a spray pyrolyzed Ba-Ca-Cu-O precursor film prepared using a 20%-vol glycerol/water solution. Weak links connecting granules limit high critical current densities. (Magnification 12.9K X).

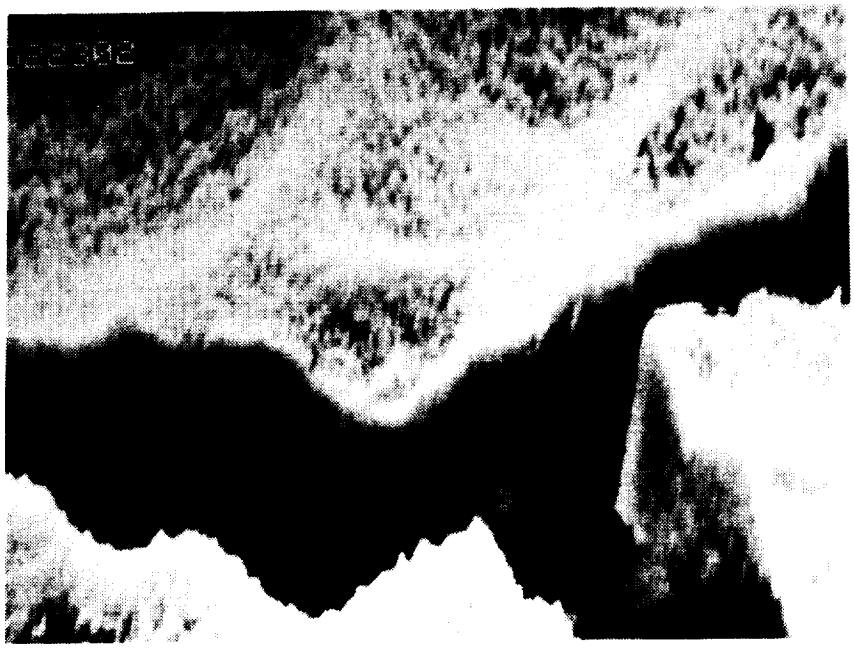

Plate 5. SEM micrograph of a crack in a Ba-Ca-Cu-O precursor film lifting off from a ytterium-stabilized zirconia substrate reveals the porosity of the preliminary films. The high density of weak links in the films will have to be reduced to obtain reasonable critical current densities. (Magnification 3.01K X).

Plate 6. Backscattered electron SEM micrograph showing the baseline chemical uniformity of the Ba-Ca-Cu-O precursor film prepared using a 20%-vol glycerol/water solution. (Magnification 321 X).

PANEL DISCUSSION with audience participation -
APPLICATIONS of SUPERCONDUCTIVITY

Chairman - Dantam K. Rao
Mechanical Technology Incorporated
968 Albany-Shaker Road, Latham, NY 12110

Panel Members - Gerald V. Brown
NASA Lewis Research Center
Mail Stop 23-3, Cleveland, OH 44135

Moustafa K. Abdelsalam
Madison Magnetics Incorporated
216 Walnut Street, Madison, WI 53705

David B. Eisenhaure
SatCon Technology Corporation
12 Emily Street, Cambridge, MA 02139-4507

Warren C. Kelliher
NASA Langley Research Center
Mail Stop 416A, Hampton, VA 23665-5225

Dantam Rao

The purpose of this session is to explore the interest of the magnetic bearing community in applying superconductors to magnetic suspension systems and to discuss the issues related to these applications. As most of you probably know, superconductors have good potential, at least theoretically; the current density of superconductors is an order of magnitude or a couple of orders of magnitude higher than the current density of copper. Typical values are about 10 Amps per square millimeter versus about 100 Amps per square millimeter and flux densities are also fairly high. The flux density of copper as used in magnetic bearings is limited by iron to about 2.3 Tesla compared to the flux density of superconductors which could be demonstrated up to about 20 Tesla for short samples but typically about 5 Tesla normally. So this theoretical potential could be translated into some practical applications to improve performance. I think that this is the particular motivation for this session. We have a panel that consists of people who I suppose most of you know. On the right side we have Gerry Brown from NASA Lewis who was in the superconductivity area about 30 years back dealing with superconducting magnets and Dr. Abdelsalam from Madison Magnetics who has been working for the past 10 years on MSBS and associated systems and on the left side we have Dr. Warren Kelliher from NASA Langley who is working in the area of high T_C superconductor development and applications, and on the left most side we have David Eisenhaure, President of SatCon Corporation who has expertise in Low T_C superconducting suspension applications. The way in which we thought we could organize this panel discussion was to give some time to individual panel members to give us their views about the applications and possible potentials of superconductors and then to have audience participation for interactive discussion to identify other potential applications. We'll start with Gerry Brown to talk about his views.

Gerald Brown

As far as applications go, I will note the ones that we are interested in at NASA Lewis where cryogenic temperatures are inherently available, such as turbo pumps for perhaps the Space Shuttle main engines or orbital transfer vehicles. Liquid hydrogen is the most attractive from a temperature viewpoint because its way below the critical temperatures of the superconductors we are talking about and also its perhaps the safer application. I'm not sure whether people are that ready to accept heavy current windings in a lox pump where every metal present can become fuel. We're also interested in vibration isolation in space at Lewis but because of the associated cryogenic support that you would need with high temperature superconductors I don't really see them as being applicable in that area except perhaps if you have a very large coarse isolation stage. For instance if you were going to isolate the entire experiment payload bay; get a rough isolation at that level where you could afford perhaps the cryogenic support system and then provide finer isolation at the experiment level. One of the key problems of high T_C superconductors (many have already been mentioned), current density, looks as if it will come along. I was talking to John Steckly and he mentioned that there had been reports of current densities that rival that of NbTi, Niobium Titanium. Structural integrity of the ceramics is often focused on but this is not a new problem. It has always been assumed that the inter-metallics like Niobium-Tin and that sort of compound would fail if you ever allowed the superconductor to go into tension so it's always a prestressed compressive situation that you want this type of superconductor to be in. So that is not an entirely new problem. The degree of the problem may be different. AC losses seem to me to be a major consideration and these have been beaten for the lower temperature superconductors to the extent that AC coils can be operated at power line frequencies. There are about three different kinds of AC losses and they all respond to making finer filaments and twisting these filaments with ever tighter pitches and transposing these filaments by twisted twist and so forth. Whether you can actually manufacture the ceramic materials in this form is certainly not clear, we don't even have a big bulk superconductor that's usable yet, but if we expect to carry any substantial component of AC current in the superconductors these items will have to be faced up to. On the other hand, it's been suggested by some of the people at the University of Wisconsin, Roger Boom and company,

that perhaps you don't need to carry the highest frequency components in the superconductor itself. If you do have a normal sheath then that part of the Fourier analyzed current that is of high frequency can perhaps be carried in the sheath and what is of low enough frequency to soak in through the skin depths of that conductor could then be carried by the superconductor, so perhaps you don't have to get the entire AC signal or AC current to soak clear into the core superconductor. Then finally just harking back to the days of the old superconductors, it could take a long time. From the time that people started showing really good current densities in short samples of Niobium Titanium and Niobium Tin it was probably 10 years or more before we had decently stable magnets that you could depend upon. So it won't happen over night in my opinion. As far as the thing that's going to work first, I was very pleased to see what Dantam had presented a couple of talks ago. Everybody's attracted to superconductors because they can produce so much field and since force goes as the square of the field, if you can get five times as much field, say 10 Teslas as versus 2, it's very attractive, but the structural problem is substantial when you take that big of an increase so I think that easiest first application is going to be just the replacement of copper by superconductor as Dantam was talking about. In the first place the conductor is not subjected to very much stress, the relative permeability of the iron or iron cobalt core gives some indication of relative stress. In fact I guess it may even go as a square of that but the winding in an iron core system doesn't see that much stress unless you try to bend it around a square corner or something. Furthermore, the AC loss situation would be easier to handle there. One advantage that Dantam didn't go into in his particular study is that you can push the core materials into the saturated range if you have plenty of ampere turns to burn and I think that is an attractive thing that could yield another factor of 2 on the load capacity. One further thing - people that come to this discussion from superconductivity tend to think of big coils running at 10 Tesla and no core and people that come from magnetic bearings tend to think of just replacing the copper windings. One thing about using the cores is that you do not have much in the way of fringe field. The distance that fringe fields go is going to be more in the order of the gap than of the coil diameters. Many applications that we're interested in such as space applications, may be applications where substantial fringe fields are unacceptable. Without a core it's hard to build a compensating set of windings where the field doesn't project a long distance. If you did go with the pure higher temperature windings without a core you can get pressures that rival the best that you can get in oil films. I forget the numbers exactly, more than 2000 psi I'd say would be easy. At least the field strength indicates you could get that much. If you are willing to put coils on the rotors you can not only get attraction but also repulsion but again the fringe fields are worse. I have already mentioned the AC loss but one final thing before you actually go and design a high temperature superconductor winding for liquid hydrogen temperature: I think an analysis should be done to determine whether high purity aluminum could do better. Somebody this morning or yesterday mentioned that you can get resistance ratios between room temperature and hydrogen temperature of 400 or better with very high purity aluminum so you really ought to check where you'd be better off.

Dantam Rao

Thanks, Gerry, I would now like to hand it over to Moustafa to talk about his experience.

Moustafa Abdelsalam

Mine will be easier than Jerry because I'll talk about the Magnetic Suspension and Balance Systems for example. This is where you have to use superconducting magnets for the support system. If you try to use copper magnets the size would become too large and some of the magnets would get away from the model so that you will not be able to use reasonable size magnets for the wind tunnel. So I think the first application of low temperature superconductors would be in large gap magnetic suspension and levitation and there I think that it would be a mistake for somebody to wait for high temperature superconductors to use for those applications, because as Gerry said, and I think that everybody agrees, that development just to make a superconducting solenoid may be 10 years along the road, not something that will happen in the

next couple of years. The gain that you will get there from high temperature superconductors versus low temperature superconductors is not that great. You still have to use a cryogen to cool the magnet and the structural supports are the same, so unless you can make the high temperature superconductor material itself cheaper than low temperature superconductors, the gain there is not necessarily that much. You gain some on the refrigeration power but that is most of what you get. You know the comment about the aluminum for hydrogen temperature - you can use high-grade aluminum. You could actually get down to 2000 resistance ratio for that current density and that, with liquid Hydrogen, might be in the range of somewhere between 2 kiloamps per centimeter squared and 4 kiloamps per centimeter squared depending on the size and where you can get the surface cooling. The only problem that you find there is that the high-grade aluminum is very soft so something has to be done to structurally support it. Another application where you have to, just by nature, use superconductivity is for energy storage where you can just store energy in superconducting coils and for that you can't use any other methods. You know you are forced to use, just by the nature of the problem itself, superconducting material.

Dantam Rao

Thanks, Moustafa. Now I will turn it over to Warren.

Warren Kelliher

Thank you very much. Can I see a showing of hands of the people who attended the Magnetic Suspension Workshop two years ago? Do we have any of the people here? Just a few of you. One of the things that was outstanding to me is comparing the papers and the presentations that we have today versus what we had there two years ago. Because two years ago the announcements of these superconductors had just come out, you had the hype saying that they will solve the world's problems etcera. Then we went into the dismay of finding that these materials were not that easy to work with and everything else. What we have now is sort of a hard-core group of people who are working with the engineering properties of these materials and putting them into a fabricated shape so they can be put into magnets, both small and large gap type of materials and the work is progressing quite well from what I can see because we've learned an awful lot in those two years about what causes the high J_Cs that are necessary for keeping these materials in the superconducting state. We've got up to, in some of the single crystal materials, 10^6 amperes per square centimeter. It shows the possibilities, even in the bulk, of getting into thousands of amperes per square centimeter and that's all we really need for most wire type applications. One of the things that I disagree with a little bit on the MSBS is that we do have an NTF tunnel here and that handles a cryogen and therefore you automatically have the cryogen to run an MSBS system. However, going to a Helium-cooled system causes the cost to become very prohibitive (a million dollars a day or something like that). So high T_C material will provide a very nice MSBS system, at least for the NTF tunnel here, that will be able to support the model and get rid of the interferences associated with the sting. One of the persons that attended two years ago was Dr. Jack Crowe. I was hoping that he would be able to show up this time but he couldn't. He is in Florida state right now and is now Head of the Magnetics Institute. I hope the problem is solved there between Boston and Florida but this is again its thought of focusing some of the activities in the superconductor materials towards the magnetics field and I see much more of that going to take place in the future. The high T_C materials are going to find much more practical use as a magnetic material in the future.

Dantam Rao

Thanks Warren. I think we appreciate your comments on real world applications and how far we are today towards these real world applications. Now, I would like to turn it over to David.

David Eisenhaure

As advertised, I'm Dave Eisenhaure and I am currently employed by SatCon Technology Corporation up in Cambridge, right down the street from the magnet lab that's in question. In fact we can talk to the people during lunch hour and get their views on the whole problem. SatCon specializes in magnetic bearing and suspension systems; we've worked with both conventional magnetic bearings and superconducting bearings and suspensions. In fact the linear optical disc bearing in the back of the room is one of our products - just to get in a little advertisement while I'm up here and got the mike. What I thought I would do, since I didn't bring any viewgraphs, is tell you a little bit about some of our experiences with superconducting magnetic bearings and what drove us down that path and what really created the need. I think our experience may be very typical of other applications. I think it was four and a half years ago when we received a contract to design an electromagnetic actuation system for laser radar mirrors. For people who aren't familiar with them, these are extremely agile mirrors; they weigh several hundred pounds; they take two to three hundred kilowatts to drive them; and they require control frequencies as high as 400 Hertz. The typical approach to that problem is hydraulic. That's the "competition" in this application. The problem is that if you lose a drop or two of that hydraulic fluid you ruin the optical surface in the mirror so there's a lot of need to go to a magnetic suspension and drive system, or there's a lot of belief that going that way will eliminate some of these problems. The difficulty is when you begin to look into that problem you find out that the inertias associated with conventional soft iron magnetics suspending and driving these systems are so high that you can't meet the system performance specifications. You basically can't drive the actuators themselves even without the laser radar mirror attached. We began looking at superconducting magnetic suspensions and drives and these superconducting suspensions and drives were basically superconducting fields coupled with either normal conducting or hyperconducting armatures. What we found out by going down that path was that with normal conducting armatures we could basically beat the specific performance requirements of hydraulics by a little bit and with hyperconducting armatures we could beat them by a lot. Since then we've had several additional hyperconducting laser radar mirror development programs and we've extended that technology to the advanced concept CMG that Jim Downer reported on yesterday. I think one thing to keep in mind is the comment that Pat Wolke made during his talk describing the different kinds of actuators that are available and which can be built for magnetic suspension and torquing systems. I think you know that when you're developing superconducting systems you have the same options. Every one of those actuators has a superconducting analog and perhaps you have even more because it is not necessary to use iron in all of these applications because of the very high current densities. I have been to a number of these magnetic bearing and suspension conferences and now we're kind of talking about a niche within a niche here because we're talking about superconducting magnetic bearings within the general realm of magnetic bearings and suspensions and if you look at magnetic bearings and suspensions in general it's kind of a niche technology. It's emerging and the place that it can attract research and development funds are the areas where it's either an enabling technology (you can't do it any other way) or just has an overwhelming advantage to conventional technologies. It's got to be a lot better than the way it's currently being done or nobody's going to do it and for magnetic bearings you see a few of those places being found right now. It's happening in canned pumps, it's happening in certain specialized kinds of compressers. Some people believe it's happening in attitude control wheels and in some parts of the world it's happening in machine tool spindles for extremely high speed very precise machining. I think by looking at how that's happening with conventional magnetic bearings and suspensions, you can look at the problem and say: where can we really use superconducting suspensions - where they have a unique place in the world and there are some areas. One area is the application that we found for high performance CMGs, laser radar mirrors, those kinds of very high specific performance requirements. That same kind of requirement is what's driving the people that are trying to build Gigawatt size power systems on space or to put multi-thousand horsepower electrical drives in submarines. They want to make them small, compact, and light. On the other side of things, there are some people that want to build rotating machinery with microwatt kinds of

power levels that they're going to send to Neptune or something and maybe the zero resistivity requirements of superconductivity will enable that. Maybe it's hard to build that machinery with conventional technology. There's a couple of things that haven't been mentioned here (Dave Trumper mentioned it a little bit) that is related to very precise positioning systems. One thing you don't usually think about in servo systems, because usually you're being buffeted by everything, is the internal noise in these systems. If you're building a very quiet, very precise positioning system, what you may find is that the Johnson noise in the actuators is the predominant noise source in the system. Well, superconductors give you a mechanism to eliminate that. I think, along the same lines in very many precise stable systems, like perhaps electron microscope slides, where people are talking about positioning accuracies of an angstrom or better, introducing any heat into those systems is a big problem. You don't have the stability in the materials if you're introducing milliwatts or higher levels of heat and superconductivity provides an enabling mechanism for that kind of a problem. I think one of the things that a group like this can do is to provide some guidance to designers like myself as far as what are the applications that are really needed and what are the requirements for those applications. What should we be designing and why and that's all I have to say, Thank you.

Dantam Rao

Thanks, Dave. Now, I have a few words to say about the experience that we have at MTI. We have, of course, had a couple of contracts dealing with superconducting applications from SDI and NASA and basically the object of the study was to identify potential applications in SDI systems where superconductors could form a good marriage with the system requirements. It is a rather difficult study because of the fact that, as you know, most of the SDI systems are politically oriented - they change from day to day and what you see today in the newspaper may not be found the next day. Within that kind of uncertainty we did in fact study the Phase I architecture of SDI systems and found that there is a certain scope where the cryogenic fluids are naturally available within the system. Basically, in the space based engines, that is the power engines where the cryogenic turbo machinery exists and the cryogenic turbo machinery already has liquid hydrogen available as a fuel. That is one potential application. The other applications which we feel are there, as was pointed out earlier, the space shuttle main engine hydrogen turbo pump and similar turbo pumps that are being planned. The liquid hydrogen is already available and there is a good marriage between the requirements of the superconductor with the applications needs. The application demands that the bearing should be very stiff and high load. The high load and the high stiffness requirements are normally met now by rolling element bearings and it is difficult to meet the same requirements by any other bearing other than a very high stiffness superconducting bearing. In addition to that I may digress a little at this stage to say that when I looked into the applications I saw the basic trends in the world and I saw a divergence in the trends between what Japan does and what the United States does. The Japanese, most of the time, focus mostly on the commercial multi-unit kind of applications where the research dollars are spread over a number of units so that the people will benefit. They probably start to identify an application right at a top level where people will use it, mass produce it, and then develop the technology from that state whereas in the United States I see that most of the applications are targeted at one-of-a-kind applications and the research dollars that the government spends are concentrated on that application and there is actually a problem there. Let me assure you that is basically a socio-economic issue which probably some other audience member could comment on The other applications which we would have in mind - I think most of you are aware of the magnetically levitated trains where superconductors are used by the Japanese to levitate the entire train. You can consider that as basically a 5 degree-of-freedom controlled magnetic bearing except for the fact that the particular device is driven by a linear motor. Instead, the rotary bearings are driven by some prime mover, except for that difference the superconductors are being used there and the advantage of the superconductors there is that they open the gaps quite substantially because of the higher ampere turns that are generated by the superconductors. They use an eddy current levitation mode there and that could be a basic technology which the United States could adopt if the Maglev Trains come around here. The third application I think, which probably some of the members of the

audience are aware of, potentially multi-unit applications, are Cryo-coolers where current Cryo-cooler bearings are right now either rolling element bearings or gas bearings. I believe that there is a potential for the high T_c superconductors playing a role in the sense that they could levitate the rotating shaft permanently. Once it is levitated it could run without contact and that would reduce the wear and the power requirements. Right now the gas bearings they use in the Cryo- coolers are limited by the very short clearances - roughly they are under about a 12 micron clearance. You could see that the wear and tear potential is very high there with the gas bearings and the high T_c passive bearings could be probably be an application there. The other applications which I think some of the members of the audience are already dealing with are the MSBS suspension systems and micro-g isolators. I think there we probably need some participation from the members where we could extend the applications into potential space devices. With this I'll turn over the floor to the members of the audience and invite them to participate in the discussion.

Pat Wolke -Honeywell

Just another chance to editorialize little bit I guess but to reiterate what Dave said these applications have to be enabling technologies, or something where you get a significant performance increase and I would be wary about overselling the capabilities of some of these devices. Maybe in the realm of spacecraft applications we talked about ball bearings having a limited life and wear out mechanisms. One of the key wearout mechanisms is eventual loss of lubrication and I see in superconductivity that you also have effectively a consumable in the cryogen and if we talk about applications where they've got a lot of liquid hydrogen onboard anyway, all for this other stuff, we've got it available for us. Well typically, in control applications where you might be using magnetic bearings, those are operational for the entire life of the spacecraft and the other consumables are sitting ready for a particular application. They don't want to pop the canister for those. Once you pop the can you can't reseal it, it leaks. So that consumable that you have is part of your control system and must be included in calculations of the lifetime of your device, so we have to be careful about overselling these things, getting people too excited and then being basically disappointed at the end. We have to be realistic up front and include all of the things that are necessary in the system.

Dantam Rao

Thanks, Dave, it is your turn to answer the question.

Dave Eisenhaure

I get to answer that? Yes, I agree and I think we see two kinds of things; one thing is people are going to send up satellites that they really need and they are going to get data back from those; the other is the kind of thing we see at SDI and that is where some grandiose Battle Station is going to be built in the sky and that may never happen. I guess there are two levels. My thought was that superconductivity is a niche within a niche. I personally think that for a lot of spacecraft applications, conventional room temperature bearings without superconductors are just fine. It is not at all that clear you need superconductors to do those things. If you go down the path a little bit and you say, "we have some applications where we really need superconductors, we have to build a torquer that weighs 5 pounds and produces 4-5000 foot/pounds of torque in a direct drive application," maybe what we need is a space-rated refrigerator to really use these things. That's what the people that are trying to put superconducting electric drives into ships believe. They believe that one of the critical pieces of equipment they need in order to use these guys is a refrigerator and whether that refrigerator makes 70 degree Kelvin or whether it makes 4, it's a critical part and we don't have it. You can buy it for your lab, but you can't buy one to put in a ship and you certainly don't have one that can fly. Now, maybe magnetic bearings, either superconducting or maybe not superconducting are a part of that system, and you know, I'm a little bit prejudiced and I think that perhaps they are, but you know that's one of the things that has

to be thought about. If this is going to happen, that's one of the pieces that has to be done and someone has to do it and someone has to pay for it.

Dantam Rao

Thanks, Dave. I think that I'm going to offer a small comment on that. I would tend to agree with Pat's comment that there might be a likelihood of overselling, because of the fact that for over the past 50 years of activity in the superconductivity area we have a very few mature applications where the dynamic environment is involved. One particular application where the experience was gathered over 15-20 years that comes to my mind was the superconducting alternator program and the government spent a lot of money on that program and the only comments I heard from the funding agencies were that the multimegawatt alternators haven't produced a single watt.

Gerald Brown

Just one quickie, in some missions the cryogen may not be a consumable. If it's supposed to last long enough so that they've found a refrigerator is better than just a certain amount of storage, then you're just using power instead of the fluid.

John Stekly - Intermagnetics General Corporation

I'd just like to make a comment. When you mention the superconducting alternator, I think that this is certainly one area that has been explored. However, magnetic resonance imaging is an area where superconductors are being applied on a commercial basis. It's the largest single commercial application of superconductivity. For those of you who are older you probably know what it's all about, for those younger fellows that don't need to have MRI scans this is a Computer Tomography (CT) type device and you use 1 meter bore superconducting magnets. Now these didn't show up all of a sudden fully developed. You needed to have extremely high uniformity, measured in parts per million. You had to have magnets that didn't decay to better than one part in ten to the seventh per hour and you also needed to have a refrigeration system that was compatible with use in a hospital. Now, I think that this goes back to the system comment, you need all of this in order to make it work, plus you have to have it economical. You can't just have somebody that wants to use superconducting wire for MRI because it just won't work. You have to use the wire that's available with the cryogenics system that exists now with a cryostat and with the costs that it takes to assemble all of this. I think again that this is the reason magnetic resonance imaging is a viable application today. I think that any other application needs all of these elements. The other area that's very successful, again it's not quite as difficult, is high energy physics. They make large accelerators; there's 1000 superconducting magnets that are operating at Fermilab that have been operating for the better part of a decade and there's the supercollider which is just in the process of being started in Texas that will have 12000 superconducting magnets. All very successful applications of superconductivity, but again, it involves cryogenics, it involves magnetic design that is particular to that application and the correct economics, and I think that when you have that the application will work.

Dantam Rao

Would anybody like to add to what John said?

Moustafa Abdelsalam

I think I agree with John, that if you have the application, you don't wait and I think that this was part of that recommendation that I will offer. For example, for MRI, if we waited until we had high temperature superconducting wires to make the magnets, we would still be waiting. And at the same time, we would have lost all the experience that we got along the way. Somebody

else might have built them. For space applications, let me add that since we have hydrogen on the space station, it would make sense to use high temperature superconductor energy storage. Since you are not going to pay for the refrigerant, you know for hydrogen you can actually store it in the system and you can use the magnetic energy storage system instead of batteries in space. There are some studies that use toroids, in that case, you don't have any stray fields on the station and you can actually store energy there and it's weight effective compared to other systems. Another area for the high temperature superconductor that I think can probably be done soon, is the leads for low temperature superconductors. A major part of the losses for low temperature superconductors, especially for magnets, is the leads for those magnets, I'm talking about for example MSBS where you have to have the leads connected all the time for control and then if you can make those leads high temperature superconductor then you can decrease a lot of the refrigeration power that you need for that.

Dantam Rao

Thanks, Moustafa. Regarding John's comment, I think that I would fully agree with what John said, that the current experience of superconducting magnets is quite extensive, that is we have very mature and technologically proven applications; as he pointed out, there are quite a lot of MRI systems which are being used all of the time. The superconducting supercollider is one of the systems that is being projected and an MSBS system could probably be one of the potential applications but what I was trying to point out when I selected the cryo-alternator or superconducting alternator for my comments was that in my mind when we are dealing with magnetic suspensions we are dealing with mechanical devices and when the mechanical devices are rotating or vibrating or whatever, they are distinctly different from steady-state devices like MRI and superconducting supercolliders. Its dynamic machines that we are dealing with and their dynamic environment. The distinct and unique opportunity that the superconducting community had to demonstrate the utility of the superconductors in a dynamic environment was the superconducting alternator and that was the only system I thought could be compatible with the magnetic suspension requirements which the superconductors may face in the future if we think of inserting the superconductors into mechanical systems.

Robert Humphris - University of Virginia

I have a question for the panel concerning superconductivity in magnetic bearings for rotating machinery. In most of the magnetic bearings with rotating machinery today they are using switching amplifiers as the power amplifier, to save power again, and of course these switching amplifiers work at frequencies from 20 kilohertz up to 100 kilohertz, and I can just imagine the AC losses involved at these frequencies. Is this going to be a real problem?

Dantam Rao

Let me comment on that. I think that there are 3-4 ways in which we could see the superconductors inserted into magnetic bearings. One approach was, which Gerry Brown probably feels comfortable with, and I also feel comfortable, was immediate insertion by replacing the copper by superconductors. That is an approach which could be viable. If you do that then you are going to face the problem which you mentioned but there are alternative approaches. That is, instead of trying to expose the superconductors to high frequencies you can design the flux circuit such that the superconductors will act as permanent magnets in persistent current mode and the flux circuit is away from the alternating fields in a decoupled mode. If you do that then you can avoid the problem.

Bob Humphris

In that case, what would be the advantage of superconductivity over a permanent magnet bias?

Dantam Rao

Okay, there I think the answer is that permanent magnets have a maximum flux-density of 1.3 Tesla whereas the magnetic materials saturate at around about 2.3 Tesla. There's a difference of 1 Tesla, so probably the superconductors could play a role by increasing the bias flux-density.

Un-identified Speaker

I'm intrigued by the idea of energy storage that was alluded to a little bit ago. Maybe this is slightly out of the field which you're discussing here, can somebody give me a thumbnail sketch of what you're alluding to?

Moustafa Abdelsalam

Okay, there was a study at the University of Wisconsin, on superconducting magnetic energy storage for space applications, where you can ship toroids, D-shaped toroids, to the space station and use them to store energy. What you do there is like a persistent mode electromagnet, where you have the current flowing all of the time in the electromagnet. You are storing the energy as a magnetic field and you can draw in and take part of that energy, you can charge and discharge the electromagnet. It works much like a battery except that you are storing the energy as a magnetic field not as a chemical reaction and actually there is a Defense Nuclear Agency (DNA) Phase I contract study on building 20 megawatt hour superconducting magnetic energy storage. That's for utility applications where you level the utility power. You charge it over night where you don't have much load for the utility and discharge it during the day when you have a peak load and this way you can level the load on the utility. The first phase of this study was just submitted, I think, in August, beginning of August of this year and DNA is studying two designs and I think that sometime next year DNA will decide which design is going to be built for the next four years so that's Phase II of the study.

Kirk Logsdon

I had a question for the panel. Given the practical limitations of keeping flux contained in the circuit and not spewing all over the place in certain applications, does anyone on the panel feel that research on better soft magnetic materials should be pursued in light of the superconducting coils that we have potentially coming on the scene some day?

Dantam Rao

I don't know, maybe I'll try to answer that question. It depends upon the system which you have in mind. If you have in mind aerospace systems, at least the systems that I have come across - the SDI space systems, most of them are extremely sensitive to flux lines. Let me back up. I think that there are two types of systems in SDI. There are Sensor Systems which sense the oncoming missile where they use infrared detectors. Those systems are very sensitive to magnetic flux lines. There are Weapons Systems which throw the missiles on the oncoming missile and those Weapons Systems may not be that sensitive, like lasers for example. But the Sensor Systems are going to be quite sensitive to flux lines. One way of containing the flux lines is soft magnetic materials as you were suggesting. The other way could be using the superconductor in a diamagnetic mode, which could probably be attractive, I don't know. Probably there is a need to see the system tradeoff between the weight of a diamagnetic shield versus the weight of the

magnetic material shield. I think that is a systems study, every specific system has to be looked at to see which approach looks better. The approach which we thought could be better is to channel the flux, to solve that particular problem using iron, at least right in the beg nning.

Don Rote - Argonne National Laboratory

We did a study a couple of years ago on applications of superconductors and high temperature superconductors to transportation, and one of the things that we looked at was the question of SMES, Superconducting Magnetic Energy Storage, and what we found was that in terms of the amount of energy that you could store per unit weight you simply cannot beat a battery for storing energy. There's no way around it, the mechanical stresses are sufficiently great that by the time you include the components necessary to retain the magnet form, and it gets even worse in the case of a toroid, that you simply cannot beat the battery. But there are certain cases under which you can beat a battery and it therefore becomes the same question that was raised before and that is what are the special applications where superconductivity does provide some benefit. It does not provide benefit in terms of energy per unit mass stored, but it does provide benefits in terms of how fast you can charge the system, how fast you can discharge it, how many cycles you can go through. Chemical batteries are very bad, notoriously bad, when you try to charge them very fast, discharge them very fast, or expose them to many deep cycles. If the superconducting coil is properly designed you can charge it fast, discharge it fast, and recycle it many, many times provided the mechanical stresses can be properly accounted for. So there may be applications in the space environment, as there are on the ground, where you can take advantage in that regard, but don't be mislead by the notion that you can beat a battery for energy storage per unit mass, because to our knowledge, at least at the present time, it can't be done.

Dantam Rao

Yes, that is an interesting observation, and I think that Moustafa would be the right person to answer the questions raised. I'm aware that the sponsor to the SMES project had the object of demonstrating the trade-off between the energy storage device versus batteries by experiments. Probably Moustafa would be able to add something more to that.

Moustafa Abdelsalam

I tend to agree with you. I'm talking about power per unit mass. If you try to get a certain level of power from batteries, you will not be able to do it. You will have an energy storage magnet to do that. Its not energy per unit mass. I should have mentioned that.

David Eisenhaure

One of the things that hasn't been mentioned too much today and which we hear about in the newspapers is the need to ground-test large space structures and I hear stories about NASA and other agencies flying larger and larger space structures and the question of how these things can be ground-tested and how you simulate a space environment. There hasn't been much discussion of that here and it seems like we're probably at the right NASA Center to discuss that. I was wondering if any of the NASA people could comment on what the needs are and whether some of these large gap suspensions would be applicable to that task?

Dantam Rao

I think the comment is open to NASA personnel here.

Nelson Groom - NASA Langley Research Center

Well, in answer to that question, I think that there are applications for magnetic suspension to ground tests. As you pointed out, ground testing is very important. There are problems testing anything on the ground, as you know, but with large space structures, it is even more so. The less influence that you have on a structure, the better off you are, so the answer is yes.

John Murphy, Rockwell

I'd like to comment on current space vehicle design and currently it s influenced very heavily by the propulsion system and currently we think that the HO propulsion system (Hydrogen-Oxygen) is the best for specific impulse. There are other servicing fluids that we could pick, but for other reasons, the current design is for that. That leads you to hydrogen and oxygen in a cryogenic form or a slush form with high density fuel cells that we currently know about through Air Force technology. It looks like superconducting technology as a complement to that is very applicable to future space vehicle design and I have alluded to this with several of the speakers but it is certainly a fertile area that we should explore for future space vehicle design, specifically for SEI or interplanetary application where maintenance becomes a big problem and in-flight maintenance becomes a reality which you must address.

Dantam Rao

I tend to agree with what we tentatively conclude in our SDI sponsored study - that is basically liquid hydrogen was one of the most abundant fluids in the SDI systems and maybe the applications could target liquid hydrogen temperatures. But instead of targeting an application like that before you start experimenting with liquid hydrogen fluid straight away, maybe you could start gaining experience by conducting demonstrations using liquid nitrogen at a higher temperature, gaining experience then go down to liquid hydrogen. The two-tier approach could be a viable approach to develop and demonstrate the technologies.

Colin Britcher - Old Dominion University

I have a comment. I guess I'm sort of a believer in technology demonstration exercises for their own sake. I think that is a throwback to the early operations of NASA where they built X-Aircraft because they were kind of nifty things to build. (They learned an awful lot on the way of course.) I guess the LGMSS experiment that was described this morning counts as a technology demonstration exercise and I got the impression from Pierre DeRochemont that there was some effort to build a high temperature superconducting magnet with the National Magnet Lab, which may also qualify. Are there other efforts underway or should there be other efforts underway? Is it the right time for people to try to build large magnets that can carry high AC currents, that kind of thing?

Dantam Rao

If I understand your question, I think the question was--are there applications other than the MSBS for the large magnets--am I right?

Colin Britcher

No. The question is: should people be trying to do technology demonstration exercises; build hardware almost for its own sake, just to show the practicality of using superconductors on large scales or for unsteady load applications or for large force applications, that kind of thing.

Dantam Rao

I don't know. My comment may sound personal but the research dollars available are rather stringent unless a specific application is targeted. It will be very difficult to get funding to start demonstrating that High-T_C magnets or Low-T_C magnets could be used for a specific dynamic environment. I think that maybe my comment is to target the application first, to understand the dynamic environment, then try to simulate the dynamic environment, simultaneously keeping in mind that there could be a potential payoff. Payoff is very critical to demonstrate that the dollars are spent wisely. I think that a rather difficult issue is to see that payoff. In superconductors most of the current payoffs come from paper studies but unless it is demonstrated it is difficult to have the continued funding from the government.

David Eisenhaure

I have another perspective on that. If you look at some of this technology, conventional magnetic bearings have been around for about 50 years and you could build quite nice ones for the last 20 and the question is--why aren't they flying? Why can't you get a program manager to put them on his spacecraft or into his submarine or whatever? I think that the other view is you know no one believes paper studies. If you are going to put things in space, put them into real systems. You have to do some demonstrations. I agree with you. I think you've got to build some things and you've got to fail a few times and if you do that, you are really going to demonstrate the technology that people will believe. The question of how you get the research dollars vectored into those programs, I don't know, I think that's an institutional problem and I think you have to figure out a way that all the money just doesn't go into funding, that some of the money is kept out and some of these things we're going to do. So I believe what you said, that's a good thing and it should happen.

John Murphy

David, to comment that the next flight vehicle that is a good candidate for demonstration is the X-30, the NASP experimental vehicle, that is due to come on line in about 1997 to the year 2005, to demonstrate some of the space application for this new complementary technology.

John Stekley

I just wanted to make a comment on the fact that low temperature superconductors have been developed recently with very low filament sizes using matrices that are resistive rather than copper and these have been developed in order to be used at power frequencies, for things like transformers, power control equipment, and again these are available today. You can't buy them in the same sense you can buy Niobium-Titanium but they are available for a few individual magnets and I think certainly for some of the applications here. I think it makes a lot of sense to see how these operate before you get up into very large sizes. I think you need some experience. Generally the losses are frequency dependent, only so much per cycle, and these conductors typically operate reasonably well up to fields of about one Tesla (AC operation).

Dexter Johnson, NASA Lewis

I've only been on board with NASA Lewis for about 4 weeks now and I'm just getti ig into learning about magnetic applications and so forth but I was a NASA Fellow and I did my Masters thesis research here at NASA Langley. Just to address your inquiry into the suspension of large space structures, earth-bound testing and so forth. My Masters thesis had to do with trying to minimize the dynamics which you have coupling to the suspension system, in which you're doing testing on an earth-bound structure. I see from my experience that most of the work that has been done has been passive applications. My particular work was active, and I could see very well

where magnetic bearings or magnetic actuation could play a part. Some of the other things that have been used have been air tables and that type of thing, although those have caused problems. I'm sure that magnetic suspension could very well be used and it's a big area that magnetic suspension could be applied to.

David Eisenhaure

Where did you do your thesis?

Dexter Johnson

In the Structural Dynamics Branch, but now it's Spacecraft Dynamics Branch here at Langley and I did it with the University of Buffalo.

Dantam Rao

Are there questions? I think we have stretched it a little bit beyond our scheduled time, because it's tea time. Anyway I hope you are very, very thirsty. In conclusion, I would like to thank all of the audience who participated in the discussion and hope we have increased the awareness of superconductors in the magnetic bearing community and that the next time that we meet, we will have the opportunity of listening to more presentations where superconductors have been used in bearings or suspensions or similar devices. Thanks very much.

DEVELOPMENT and DESIGN of a MAGNETIC INERTIALLY REFERENCED ISOLATION SYSTEM for MICROGRAVITY EXPERIMENTATION

Kirk Logsdon, Carlos M. Grodsinsky
NASA Lewis Research Center
Mail Stop 23-3
Cleveland
OH 44135

NASA
Lewis Research Center

SPACE EXPERIMENTS DIVISION

SFSD
Space Flight Systems Directorate

1. Introduction
   - Vibration Sources
   - Spacecraft Environment

2. Active Magnetic Isolation
   - Advantages
   - Disadvantages

3. Development of Active Inertial Magnetic Isolation System
   - Inertially Referenced Magnetic Control

4. Design of Active Inertial Magnetic Isolation System
   - Conceptual Configuration of Isolation Platform
   - Prototype System
   - Preliminary Results

5. Summary

Vibration sources present on the Space Transportation System (STS) and in the future the Freedom Station. These sources are catagorized by frequency range, from DC up to > 10^1 Hz.

Quasi-Static (DC to 10^{-3} Hz)

- Aerodynamic Drag: function of atmospheric conditions and surface area
- Gravity Gradient: function of distance to orbiter center of gravity
- Photon Pressure: function of projected surface area viewing Sun

Low Frequency (10^{-3} to 10^1 Hz)

- Large Flexible Elements
  - Solar Arrays
  - Antennae
- Crew Motion
- Attitude Control
- Robotic Motion

Medium-High Frequency (> 10^1 Hz)

- On Board Equipment: pumps, motors, and other dynamic facility equipment

NASA Lewis Research Center

SPACE EXPERIMENTS DIVISION

SFSD
Space Flight Systems Directorate

G-Level Tolerence for Monochromatic Oscillatory Disturbances (Stuhlinger)

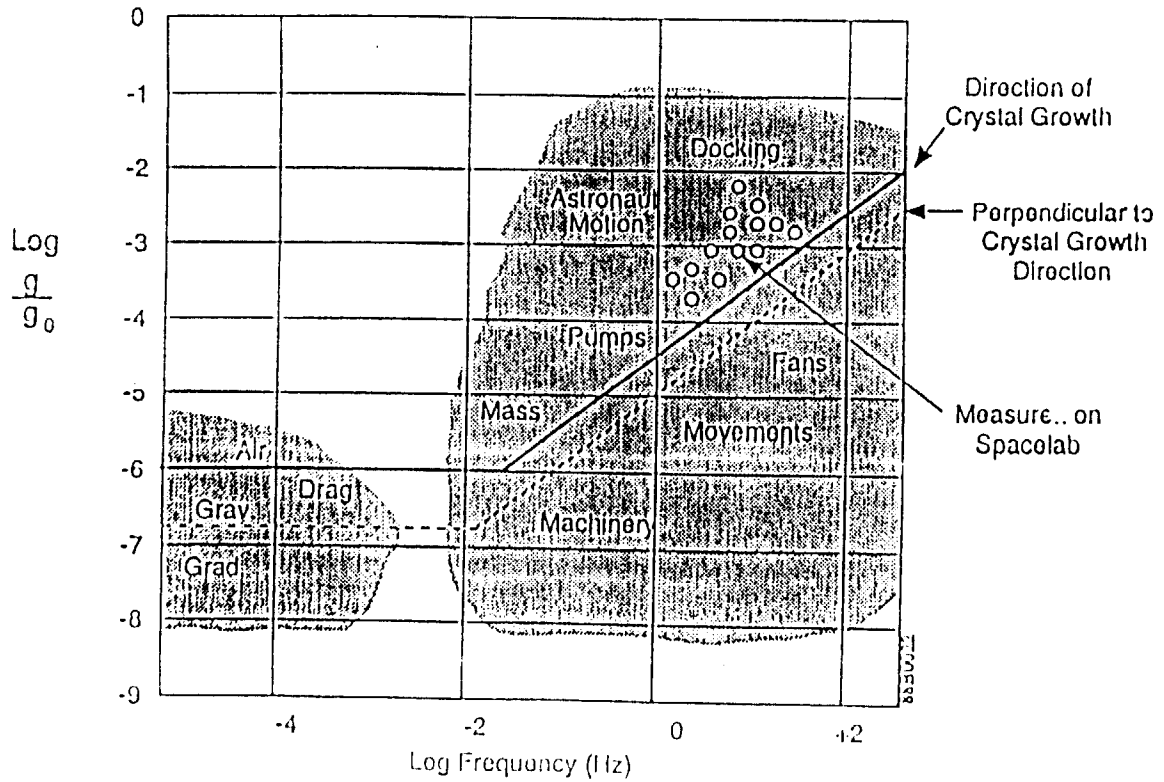

Plot gives magnitudes of various disturbances verses their characteristic frequencies.

Active magnetic isolation systems advantages in disturbance rejection for sensitive payloads.

Advantages

- Variable Stiffness and Damping
- "Adaptive" Control Capability
- Isolation of Direct and Base Disturbances
- Adaptable to Various Payload Masses
- Payload Centering Under Load

Disadvantages

- Greater Complexity

One degree-of-freedom differential equation of motion demonstrating the conceptual approach to an inertially referenced isolated payload.

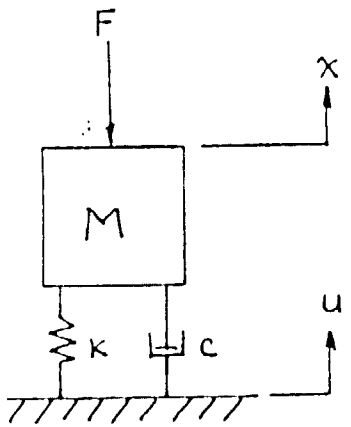

Without Inertial Isolation:

$$m\frac{d^2x}{dt^2} + c\left\{\frac{dx}{dt} - \frac{du}{dt}\right\} + k(x - u) = 0$$

With Inertial Isolation:

$$m\frac{d^2x}{dt^2} + c\left\{\frac{dx}{dt} - \frac{du}{dt}\right\} + c\frac{du}{dt} + k(x - u) = 0$$

One degree-of-freedom block diagram of inertially referenced payload control system.

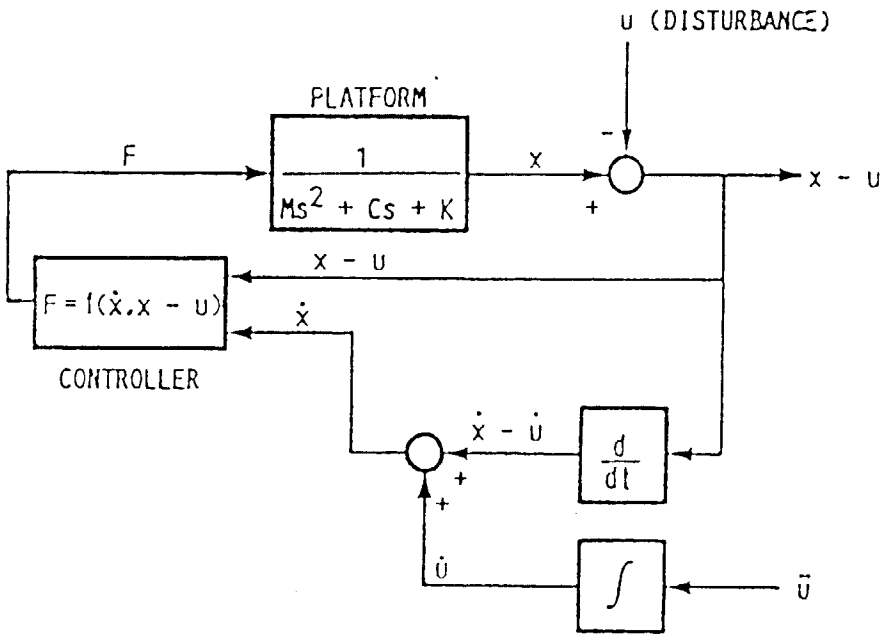

NASA
Lewis Research Center

SPACE EXPERIMENTS DIVISION

SFSD
Space Flight Systems Directorate

Transmissibility curves of an inertially damped one degree-of-freedom control system as compared to a relatively referenced active system.

INERTIAL DAMPING TRANSMISSIBILITY CURVES

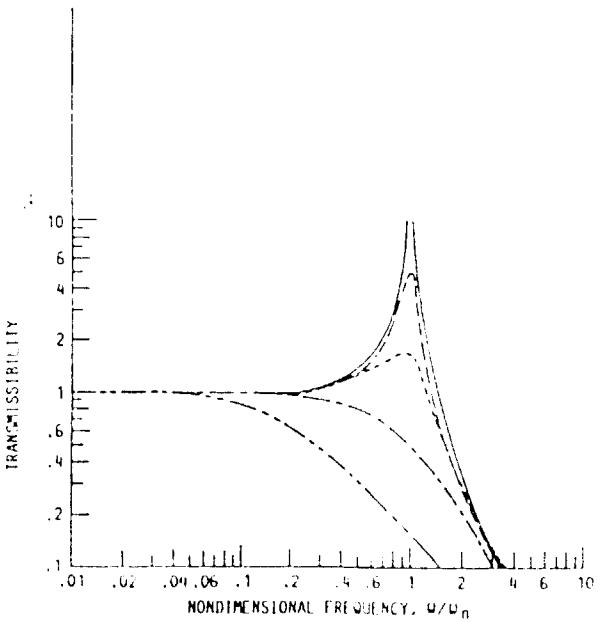

RELATIVE FEEDBACK TRANSMISSIBILITY CURVES

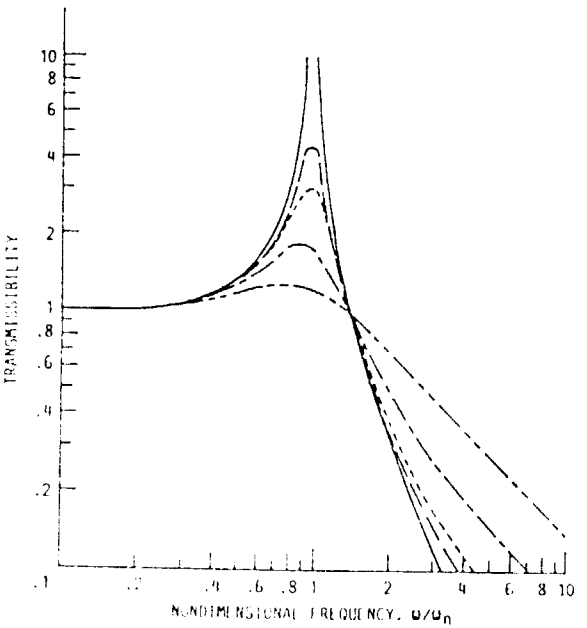

Conceptual configuration of a six degree-of-freedom isolation platform.

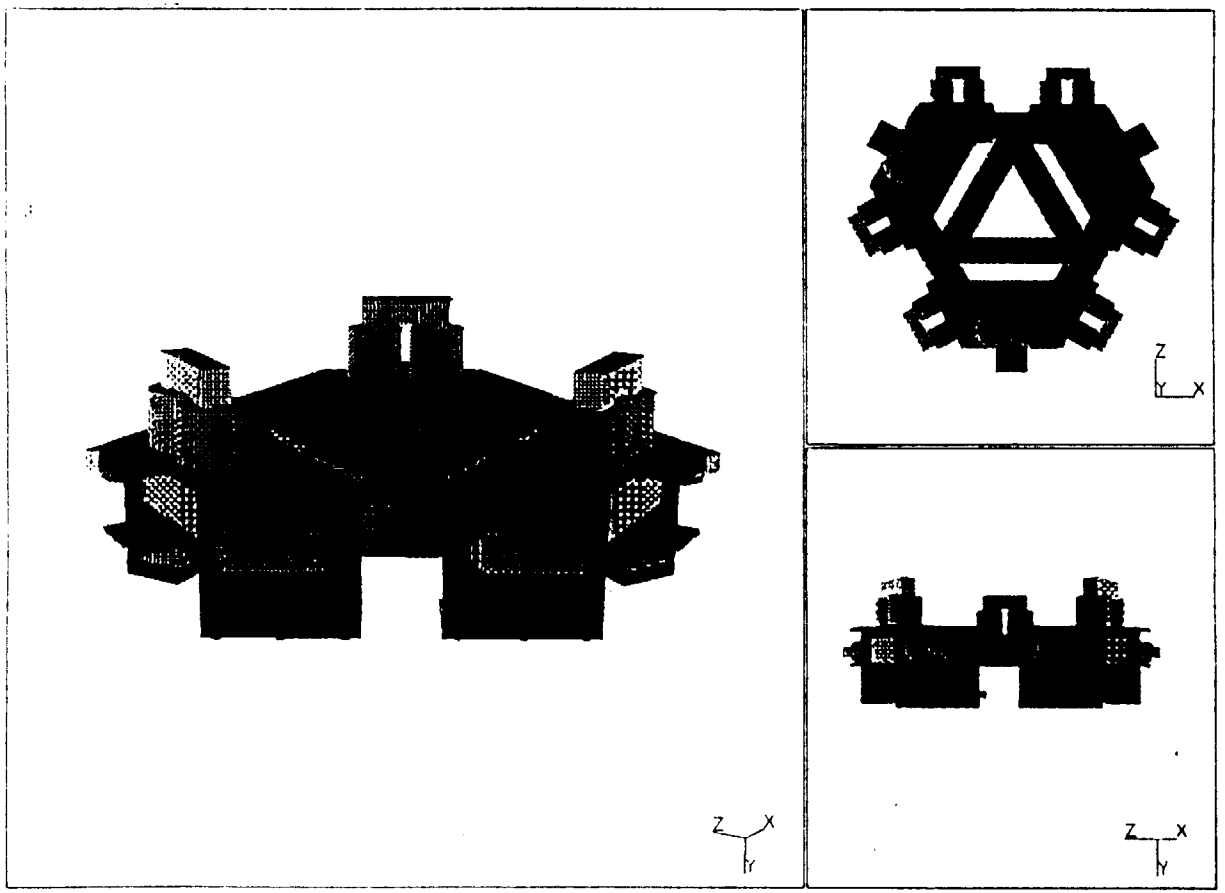

NASA
Lewis Research Center

SPACE EXPERIMENTS DIVISION

SFSD
Space Flight Systems Directorate

Preliminary isolation results of a three degree-of-freedom configuration.

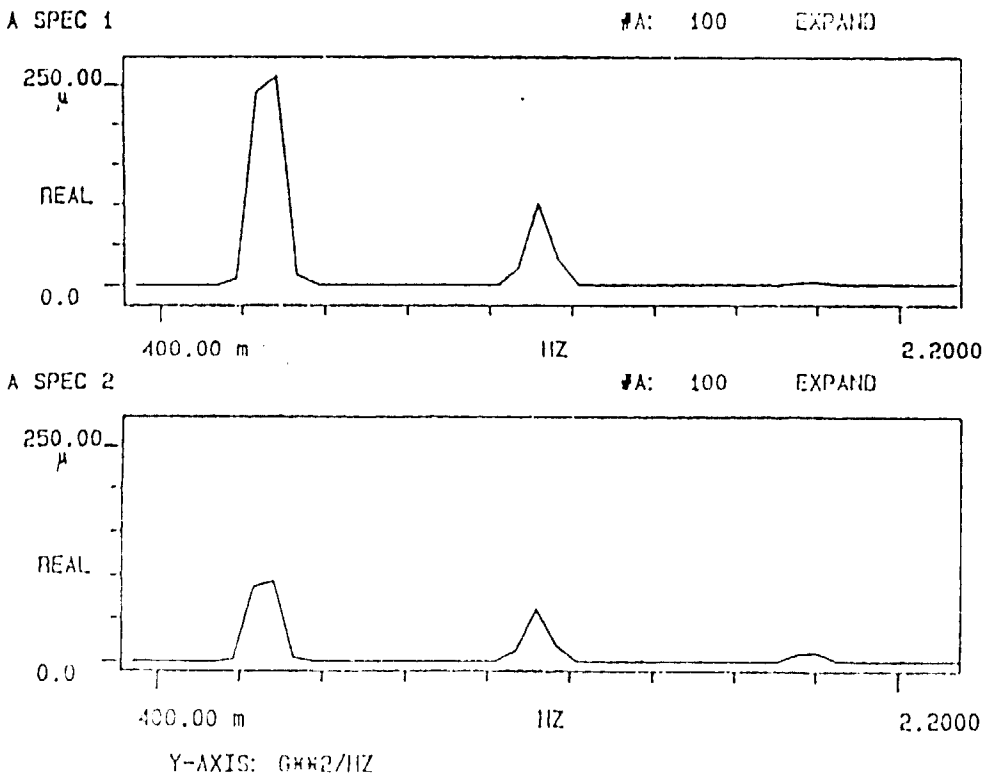

SUMMARY

1. Active magnetic systems can substantially improve isolation at low frequencies.

2. Active magnetic systems can be adaptively controlled to optimally isolate a payload in a random environment.

3. Ability of systems to use inertially sensed information in order to decouple the mass from a dynamic environment.

4. Active isolation systems can be designed for several payload configurations and thus, can be used as a microgravity experimentation support facility.

5. Response of the system can be adapted by using various sensing feedback methods in the feedback control loop.

ACTIVE VIBRATION ISOLATION MOUNTS

H. Ming Chen, Richard Dorman, Donald Wilson
Mechanical Technology Incorporated
968 Albany-Shaker Road
Latham
NY 12110

Active Vibration Isolation Mounts

By

H. Ming Chen

Richard Dorman

Donald Wilson

Abstract

Several approaches toward reduction of vibration from operating machinery to ground through active electromagnet mounts are discussed. The basic approach to active mount design is to take advantage of the force attenuation characteristics of soft mechanical spring mounts and supplement their limitations with an active electromagnetic system. Techniques discussed include vibration cancellation approaches, as well as a method of altering mount stiffness and damping properties at the disturbing frequencies. Analytical and experimental results are presented encompassing the magnitude of force reduction and the stability characteristics of each technique.

Description of Figures

Figure 1

The advantages and capabilities of an active mount are summarized in the tabulation of Figure 1.

Figure 2

The objective of the active mount as summarized in Figure 2 is to isolate machinery or platforms from ground. This is accomplished by sensing the force transmitted to ground to drive an electromagnet.

Figure 3

This figure illustrates a typical mount using an elastomer to support the weight and an electromagnet to provide dynamic forces.

Figure 4

Vibration control techniques to be reviewed include the use of filters to control the stiffness and damping properties of the support (fixed or tracking filters), or the use of an inverse transfer function.

Figure 5

The force transmissibility curve illustrates the reduction in transmitted forces that can be achieved by altering the support stiffness and damping properties. This figure also illustrates that the primary advantages of force attenuation occur at the lower frequency range.

Figure 6

Figure 6 further illustrates the influence of stiffness and damping modifications to the transmissbility of forces through the mount.

Figure 7

Controls of the active mount depend upon adjusting the stiffness and damping of the electromagnet as a function of the transmitted force as detected by a force gage or load cell.

Figures 14, 15

These figures refer to the technique used in developing an inverse transfer function. The test rig is excited with a sinusoidal signal to the electromagnet. The amplitude and phase are recorded at the force gage relative to the excitation. This information comprises the transfer function across the mount. The control technique is to develop a similar amplitude and phase function through a series of filter networks. A 180° phase inversion of this signal will drive in opposition to the force gage signal and cancel the transmitted force.

Figure 16

Figure 15 is a block diagram of the proposed filter network to create the inverse transfer function.

Figures 17, 18

These figures illustrate the constructed circuit to duplicate the characteristics of Figures 14 and 15. Tests are presently in progress to check out the performance of this approach.

Figures 8, 9, 10

These figures illustrate a test rig used to demonstrate force attenuation techniques. In Figure 8, the mount supporting a vibration shaker is shown in the foreground. The control function is performed digitally in a desk-top IBM-PC. The control signal is amplified with a linear amplifier shown as the box alongside the rig. A close-up of the rig in Figure 9 shows the force gage used as the control pickup. In Figure 10, the electromagnet is visible with the mount disassembled.

Figure 11

This figure shows the computer CRT screen and the software control commands.

Figure 12

In this figure, the real time vibration wave is shown above an FFT plot of the vibration as picked up on the force gage. In this figure, the force gage is inactive.

Figure 13

This is a repeat plot of Figure 13 with the active mount activated. The output from the force sensor has been reduced from an amplitude of 0.3151 v. to 0.0252 v., as noted from the value of Y at the bottom of the plots.

Active Isolation Mounts

- Isolate Machinery Base Using Elastomer and Electromagnetic Mount Combination
- Electromagnets React to Dynamic Disturbance
- Attenuation of >20 dB Over Standard Elastomer Mount in Laboratory
- Easily Retrofitted with Most Dynamic Machinery
- Failsafe Design Provides Passive Mount Backup

891704

FIGURE 1

Mechanical Technology Incorporated

ACTIVE MAGNETIC ISOLATION MOUNTS

Objective:

Isolate Platform from Both Platform Induced and Ground Induced Vibrations

Method:

Sensor Driven, Actively Controlled Electromagnet to Cancel Dynamic Forces

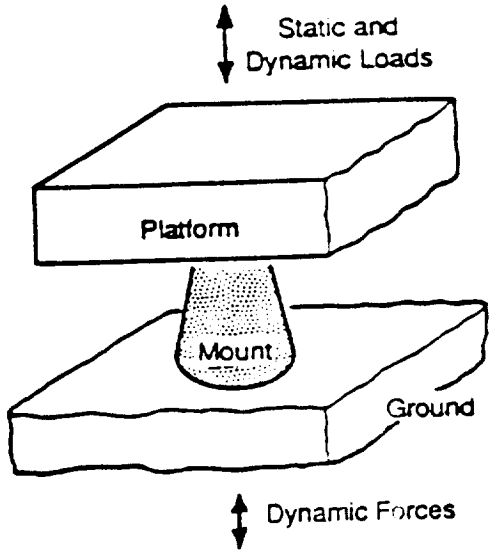

Potential Benefit

- *15 to 1 Amplitude Reduction*
- *Eliminate Multiple Rafting*
- *Compatible with Current Mount Designs*
- *New or Retrofit Capability*
- *Applicable to a Variety of Platforms*

FIGURE 2

Mechanical Technology Incorporated

ACTIVE MAGNETIC ISOLATION MOUNTS

Approach:

- Electromagnetic Support in Parallel with Existing Mount
- Elastomer/Spring Mount Carries Gravity Load
- Electromagnet Reacts Dynamic Load Only

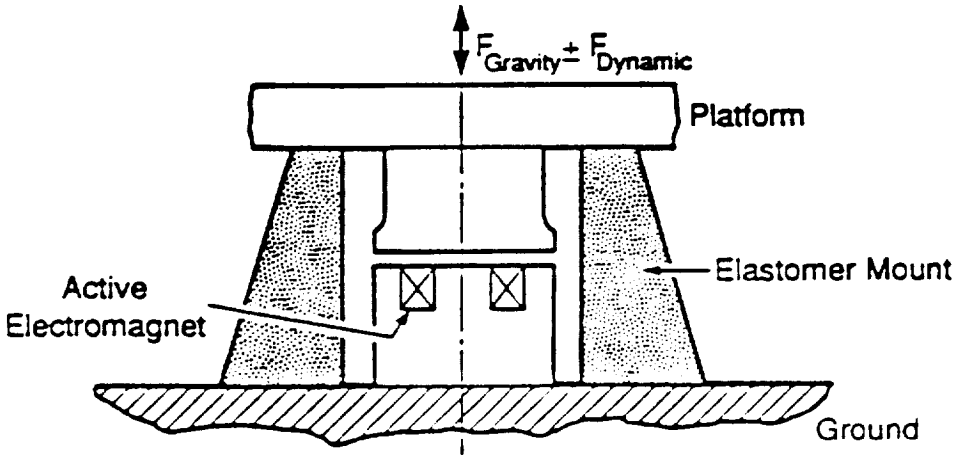

Result

Minimize Size, Weight, and Complexity of Active Mount

FIGURE 3

VIBRATION CONTROL TECHNIQUES

- BAND PASS FILTERS
- TRACKING FILTERS (LMS)
- INVERSE TRANSFER FUNCTION

FIGURE 4

Mechanical Technology Incorporated

ACTIVE MAGNETIC ISOLATION MOUNTS

Approach:

Minimize Dynamic Force Transmission
by Actively Altering Support Stiffness and Damping

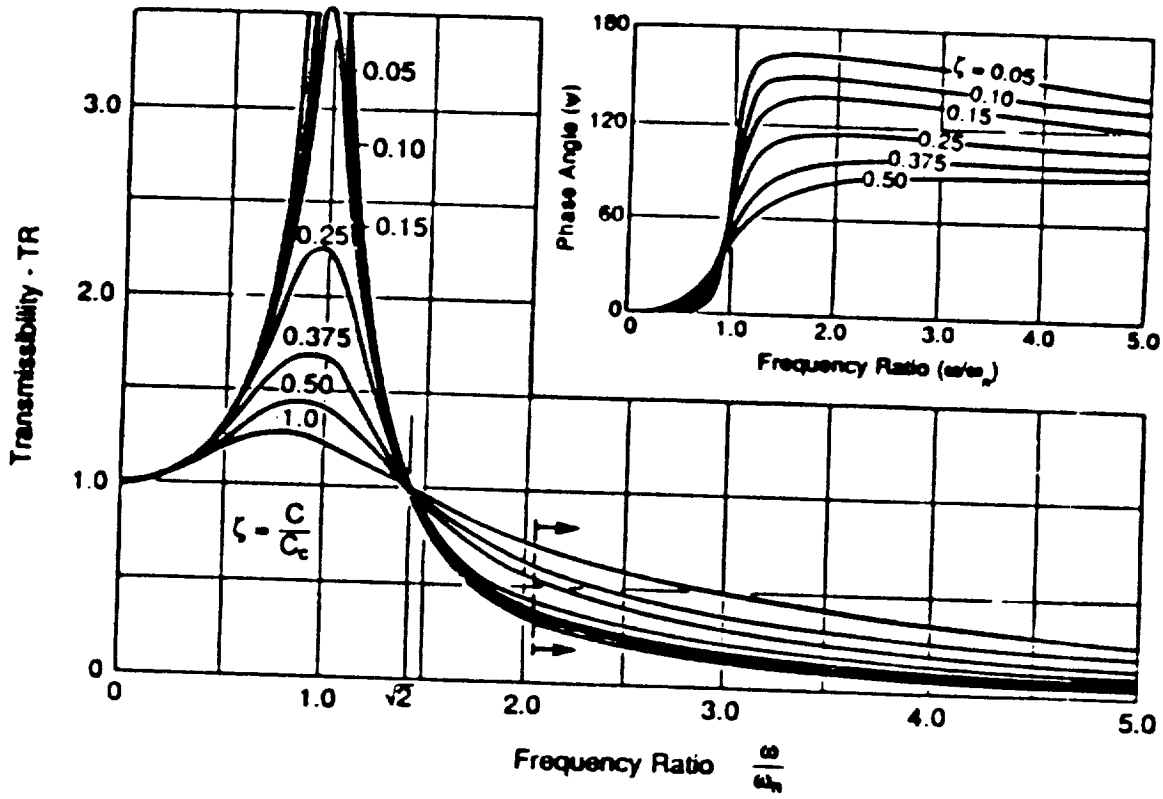

Result

20 to 30 dB Attenuation
at Discrete Frequencies

FIGURE 5

INFLUENCE OF REDUCED STIFFNESS AND INCREASED DAMPING ON FORCE TRANSMISSION

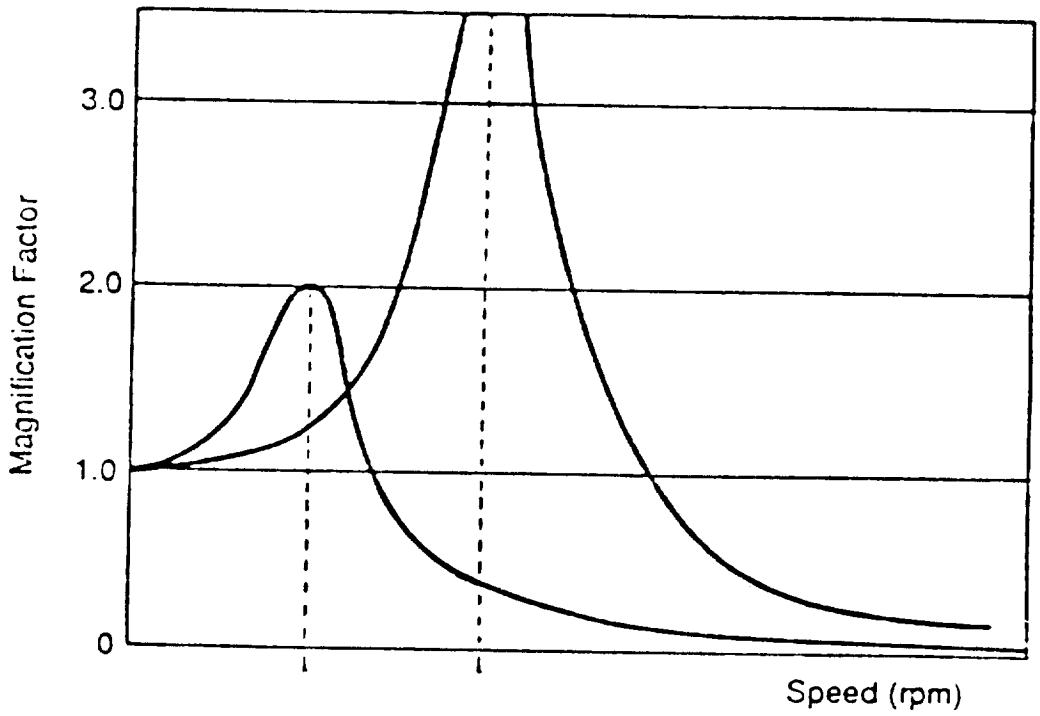

FIGURE 6

Mechanical Technology Incorporated

ACTIVE MAGNETIC ISOLATION MOUNTS

Approach:

Control Circuit Alters Stiffness and Damping

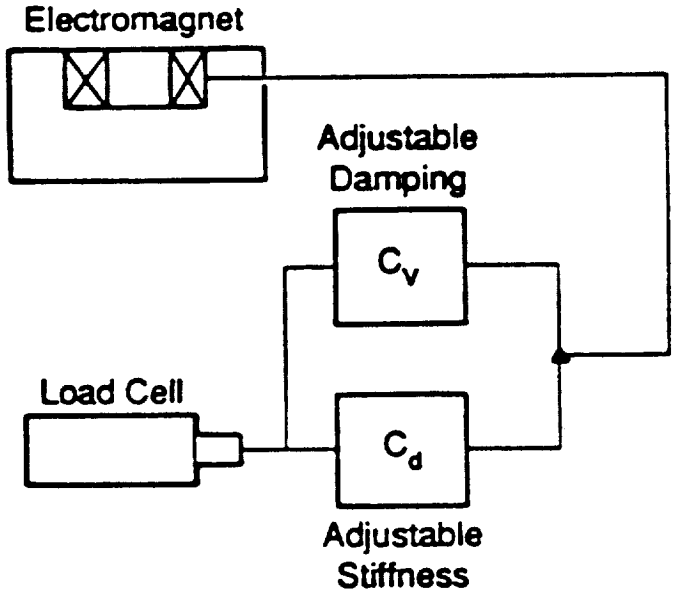

Result

Control Parameters to Achieve
Reduced Elastomer Stiffness

FIGURE 7

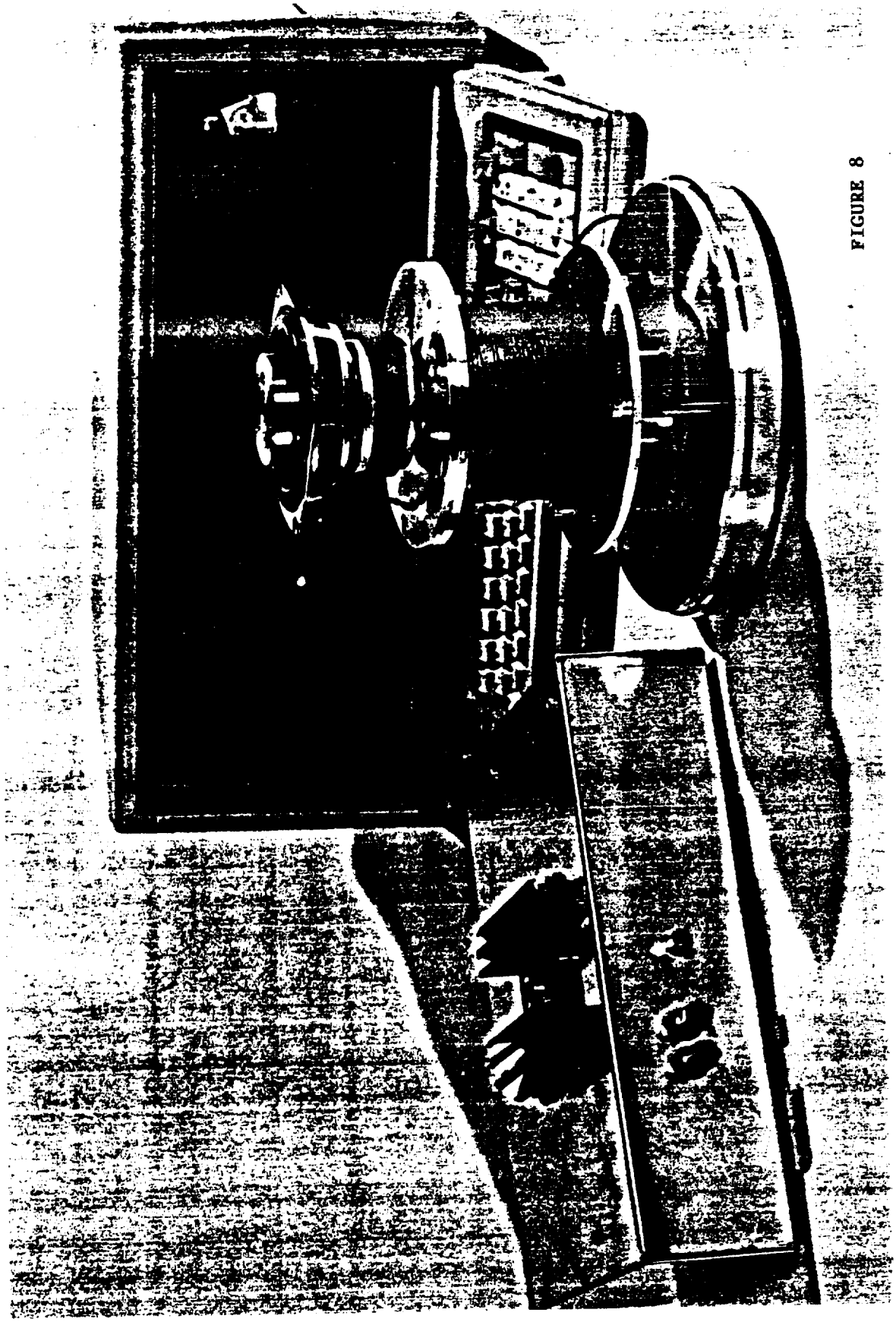

FIGURE 8

FIGURE 9

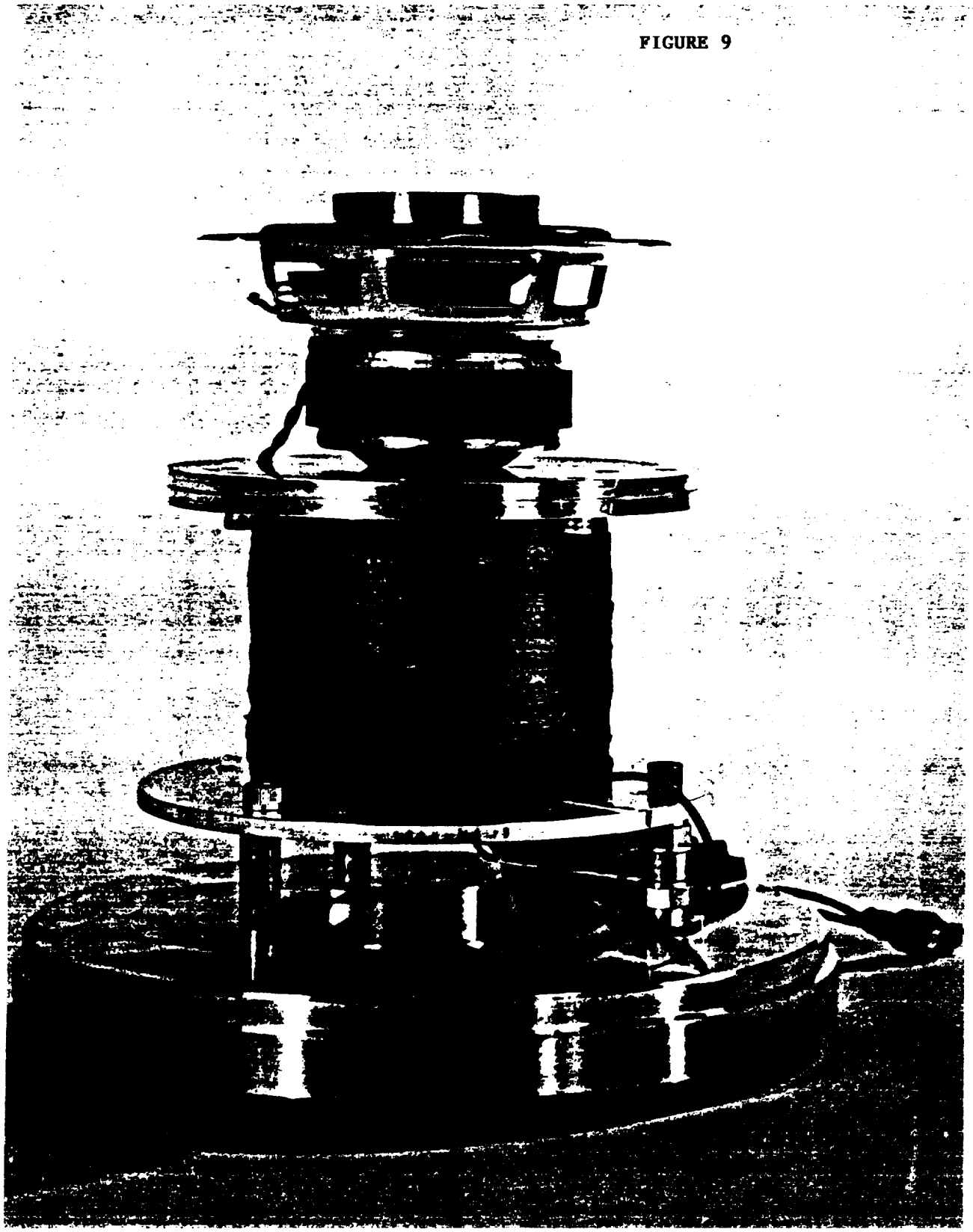

FIGURE 10

FIGURE 11

Mechanical Technology Incorporated

ACTIVE ISOLATION MOUNT TEST RESULT

-- WITHOUT AIM CONTROL --

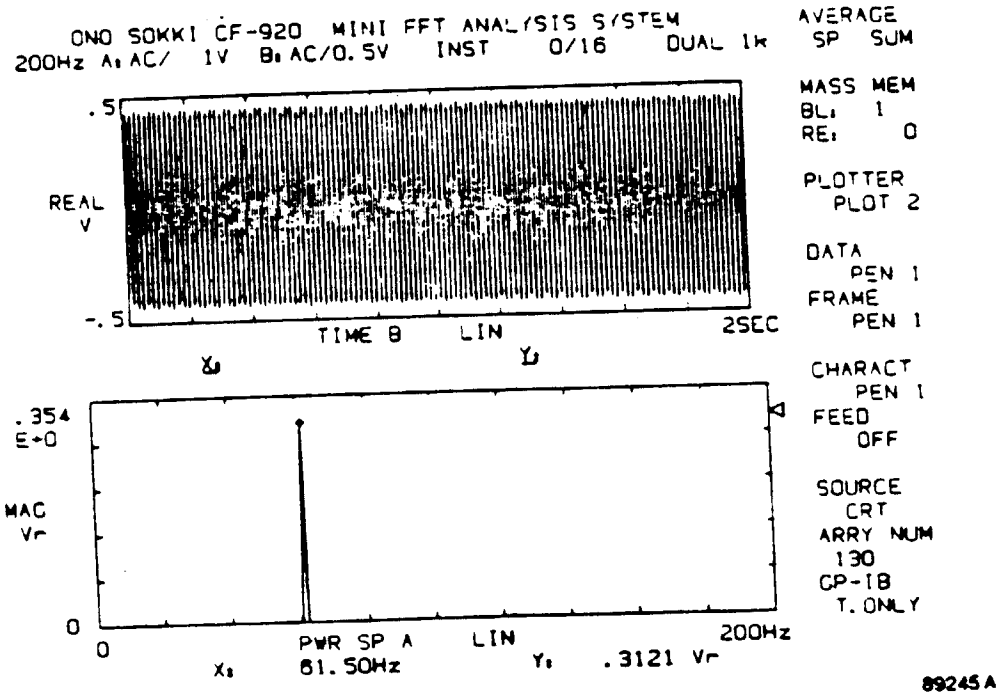

FIGURE 12

Mechanical Technology Incorporated

ACTIVE ISOLATION MOUNT TEST RESULT

-- WITH AIM CONTROL --

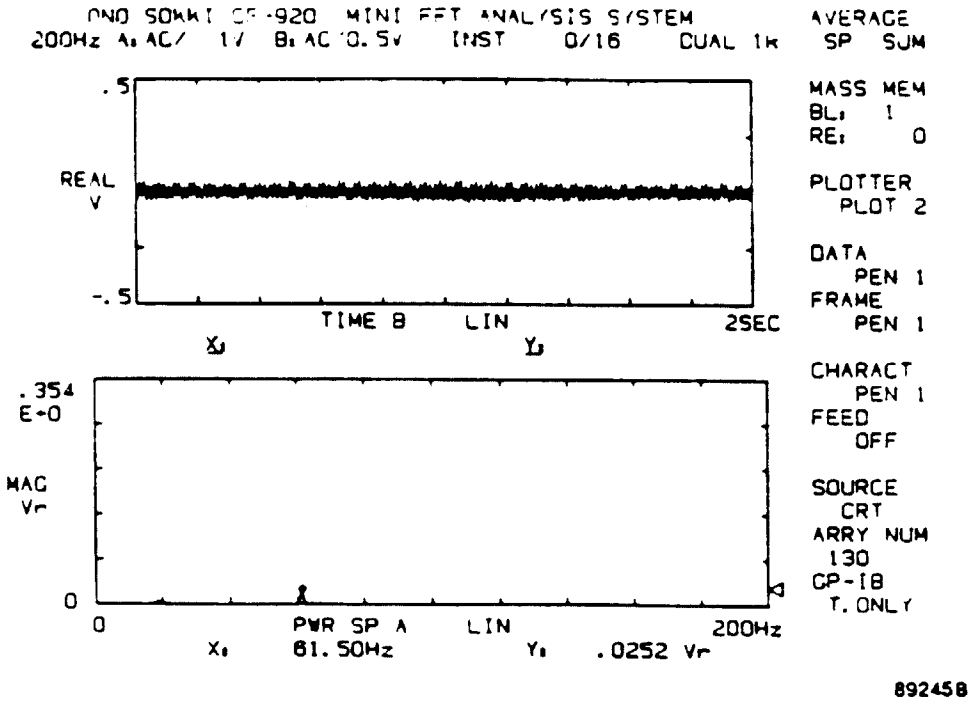

FIGURE 13

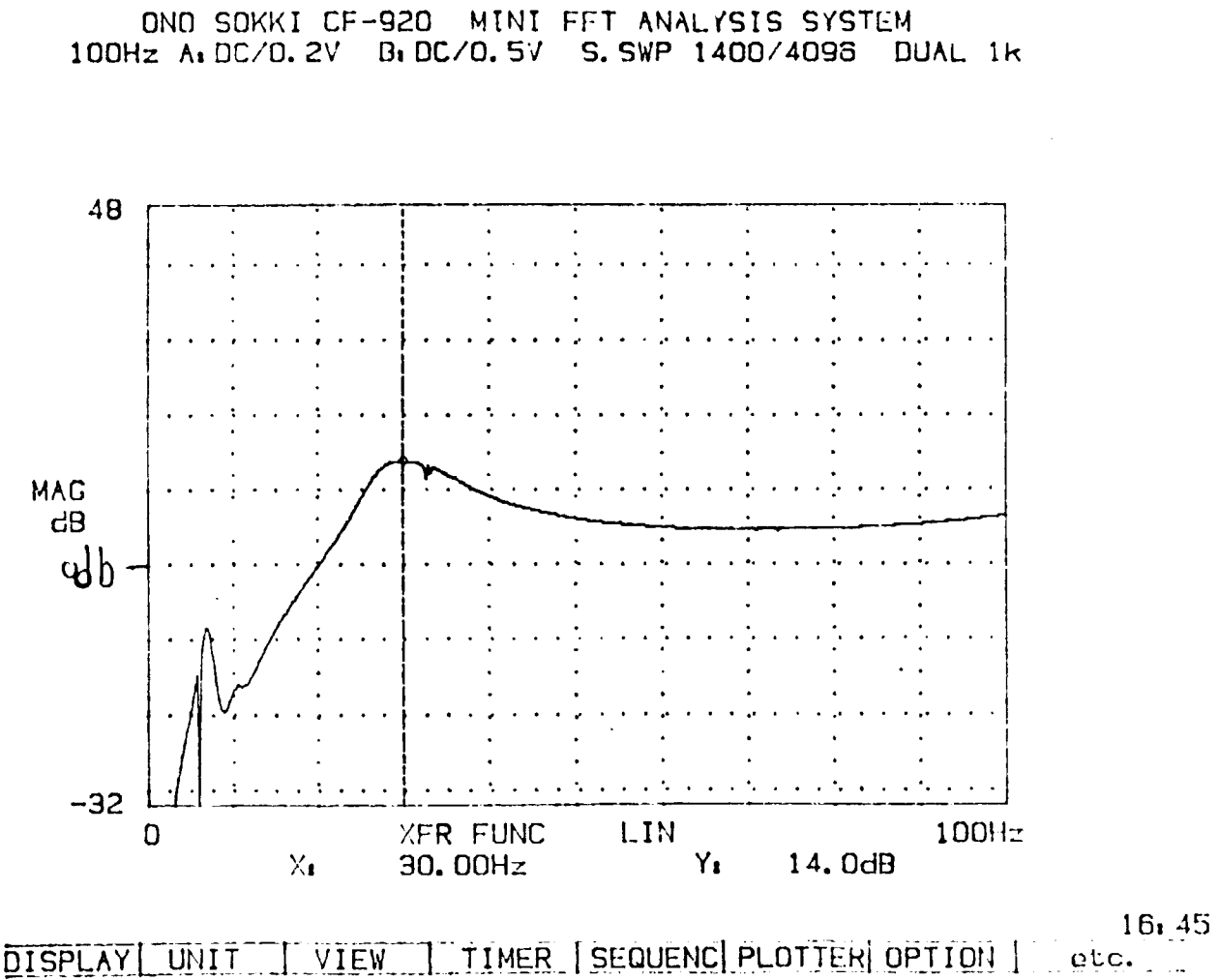

FIGURE 14

STRUCTURAL AMPLITUDE RESPONSE

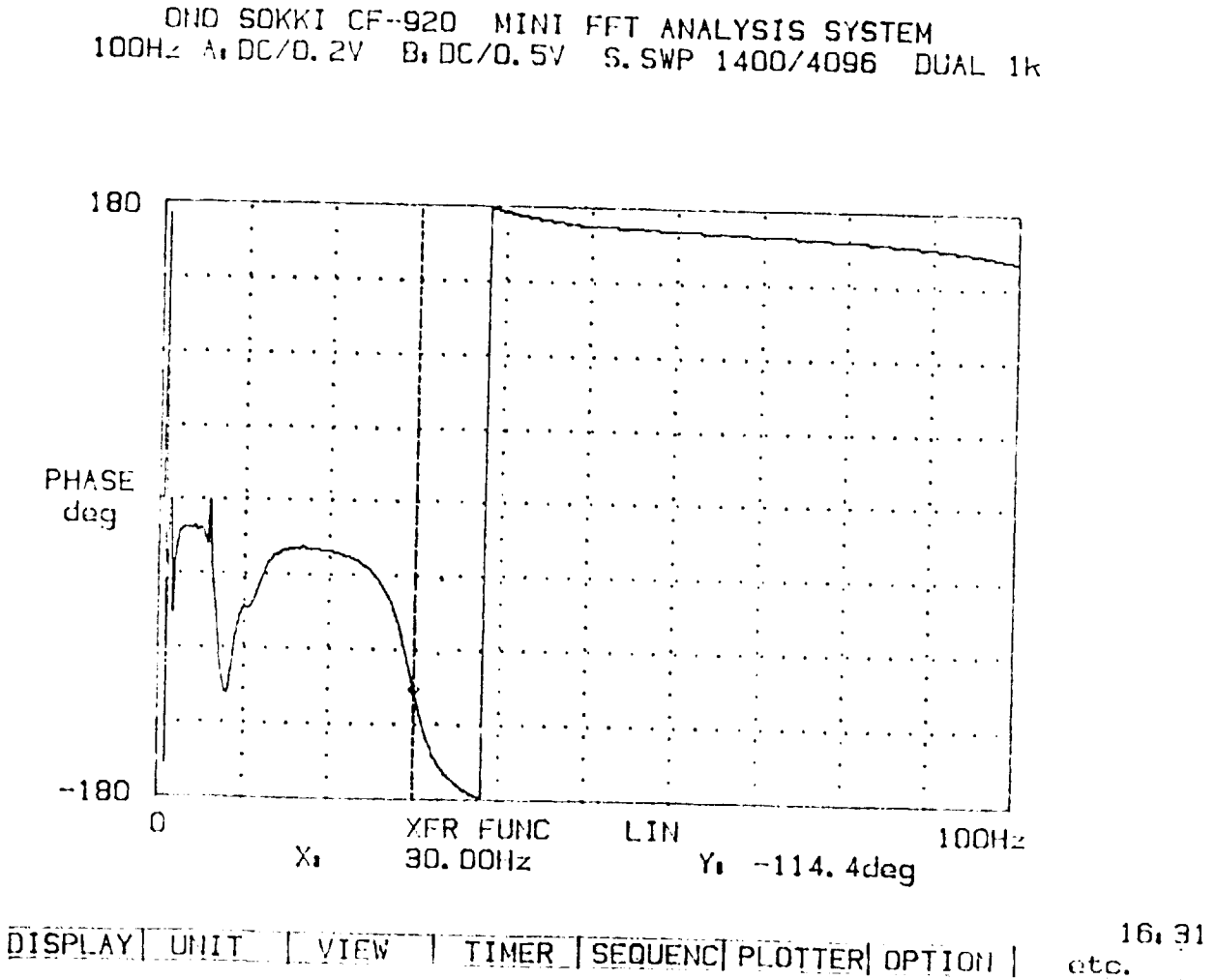

FIGURE 15 - STRUCTURAL PHASE RESPONSE

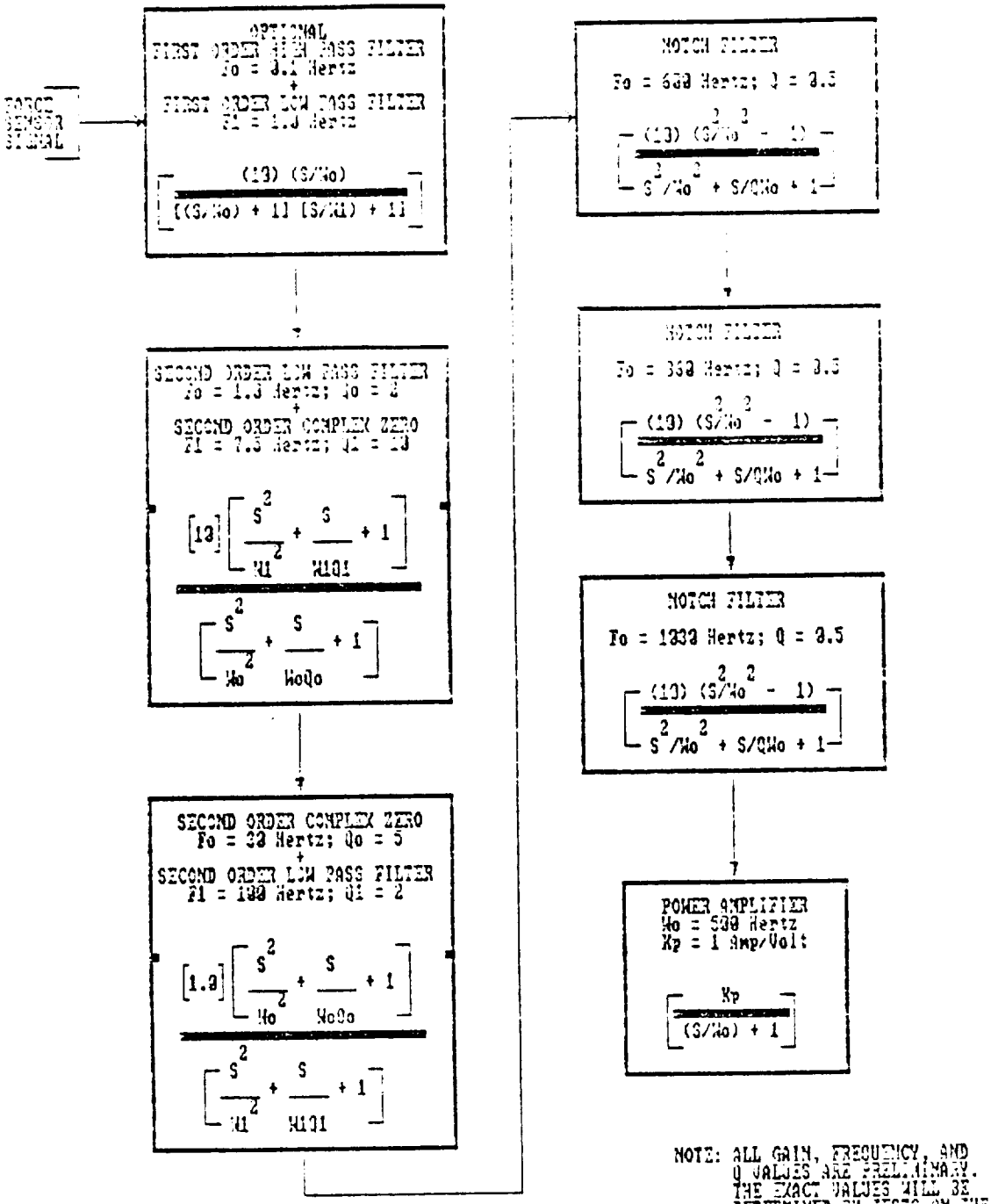

FIGURE 16

R. DORMAN
5/24/90

PROPOSED COMPENSATION CIRCUIT

CLOSED LOOP/FORCE SENSOR

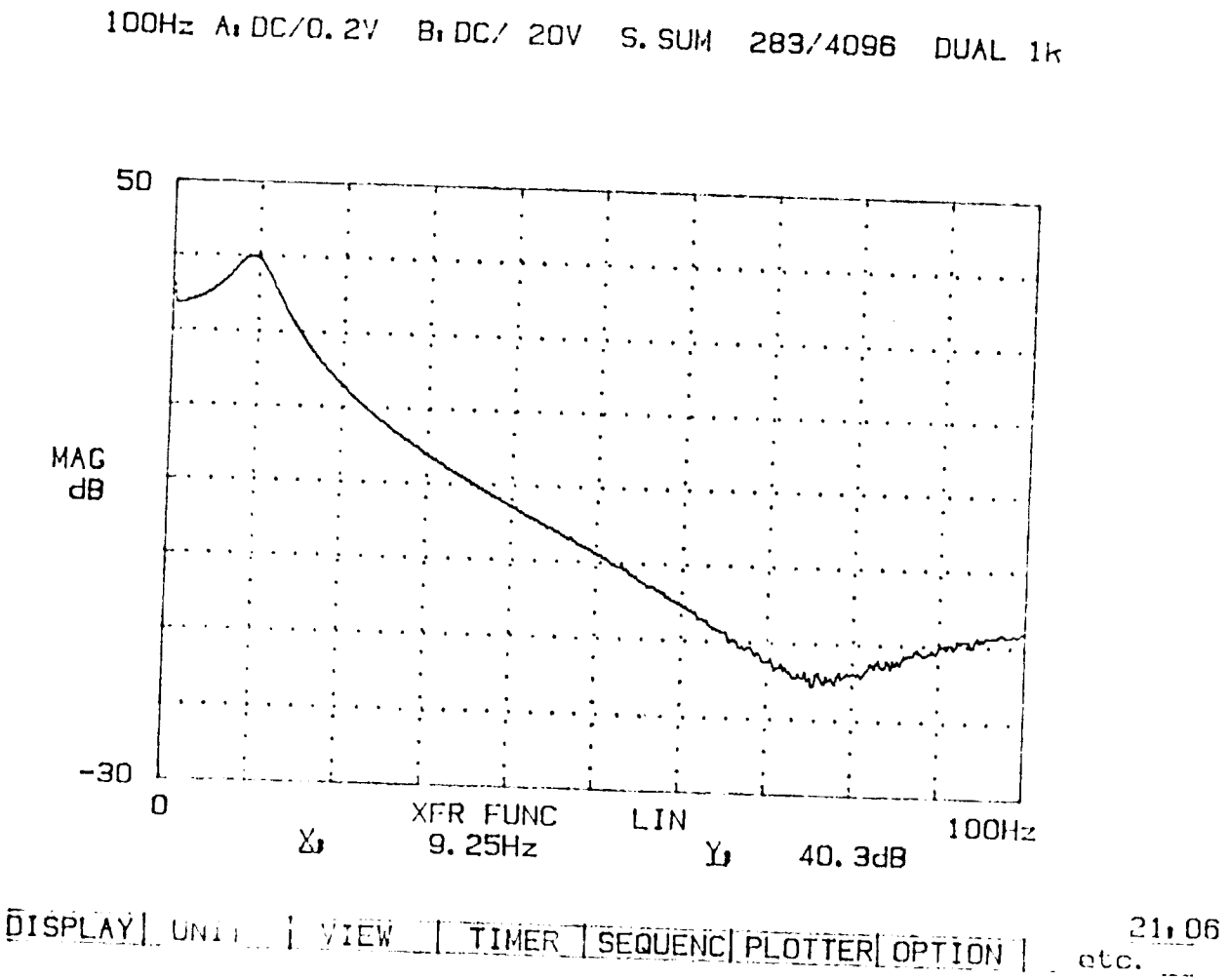

FIGURE 17 - AMPLITUDE RESPONSE OF CONTROL CIRCUIT

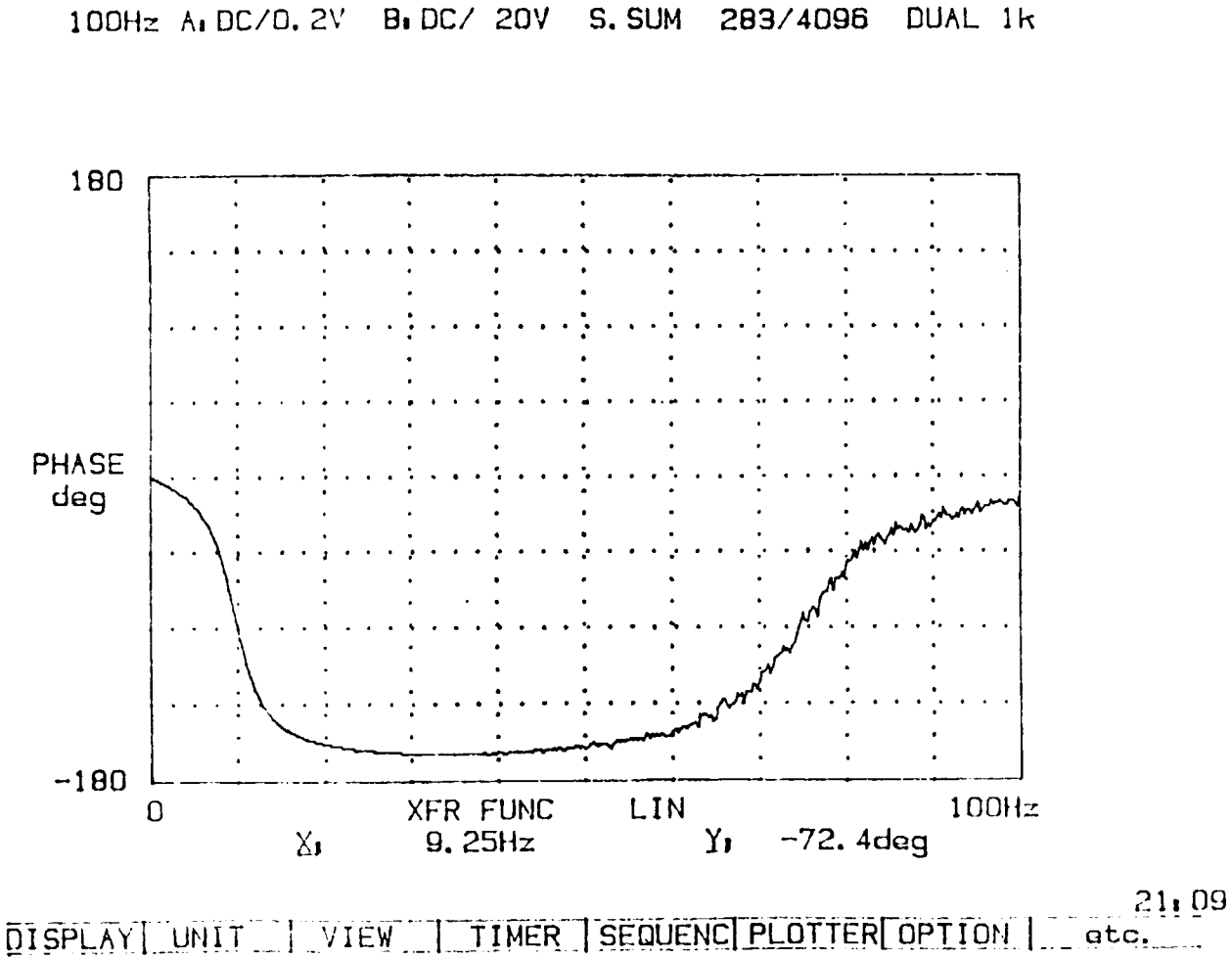

FIGURE 18 - PHASE RESPONSE OF CONTROL CIRCUIT

VIBRATION ISOLATION of SCIENCE EXPERIMENTS in SPACE - DESIGN of a LABORATORY TEST SETUP

Bibuti B. Banerjee, Paul E. Allaire, Carl R. Knospe
Department of Mechanical and Aerospace Engineering
University of Virginia
Thornton Hall, McCormick Road
Charlottesville
VA 22901

University of Virginia / NASA Lewis

DISTURBANCE LEVELS

Quasi-Steady or "DC" Accelerations

Relative Gravity	Frequency (Hz)	Source
1E-7	*0 to 1E-3*	*Aerodynamic Drag*
1E-8	*0 to 1E-3*	*Light Pressure*
1E-7	*0 to 1E-3*	*Gravity Gradient*

Periodic Accelerations

Relative Gravity	Frequency (Hz)	Source
2E-2	*9*	*Thruster Fire (orbital)*
2E-3	*5 to 20*	*Crew Motion*
2E-4	*17*	*Ku Band Antenna*

Non-Periodic Accelerations

Relative Gravity	Frequency (Hz)	Source
1E-4	*1*	*Thruster Fire (Attitudinal)*
1E-4	*1*	*Crew Push-Off*

University of Virginia / NASA Lewis

VIBRATION ISOLATION OBJECTIVES

1. The Problem

   - Vibration Causes
     - Thruster fire
     - Machinery operation
     - Crew motion

   - Desired Isolation Range
     - 10E-5 to 10E-6 g
     - 0 to 10 Hz frequency

   - Passive Isolation Capabilities
     - 10E-2 to 10E-3 g
     - Not good at low frequencies

2. The Solution

   - Active Control Isolation
     - Electromagnetic Actuators
     - Low Frequency Accelerometers
     - Digital Control
     - Effects of Umbilicals

University of Virginia / NASA Lewis

INITIAL EXPERIMENT : 1-D ISOLATION

1. Long-stroke Shaker
2. Umbilicals
3. Electromagnetic Actuator
   - Lorentz Type
   - Long Action Magnetic Actuator (LAMA)
4. Sensors
5. "Experiment" Mass
6. Magnetic Supports
7. Base

University of Virginia / NASA Lewis

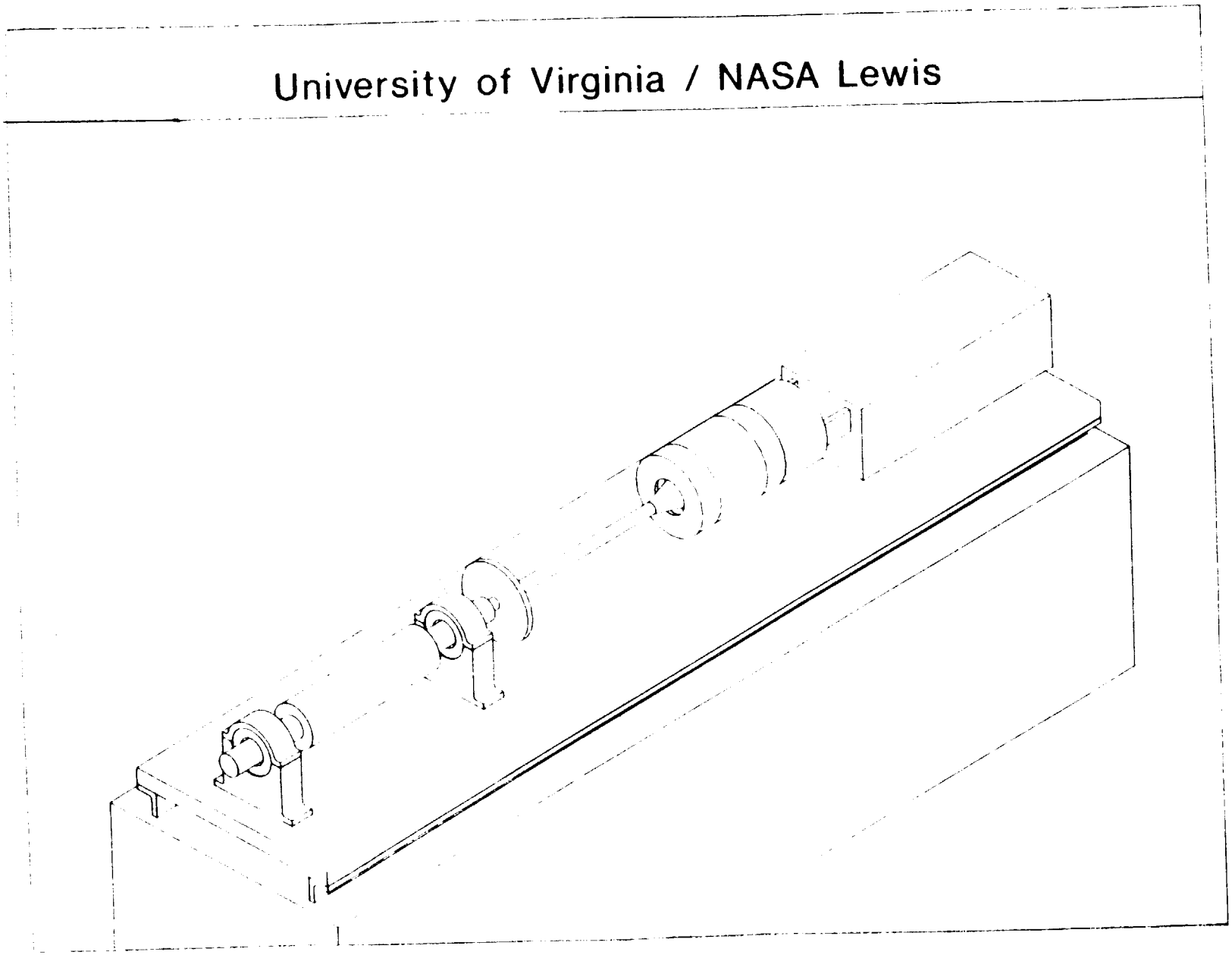

University of Virginia / NASA Lewis

University of Virginia / NASA Lewis

LONG STROKE SHAKER

6.25-in, 158-mm p-p stroke

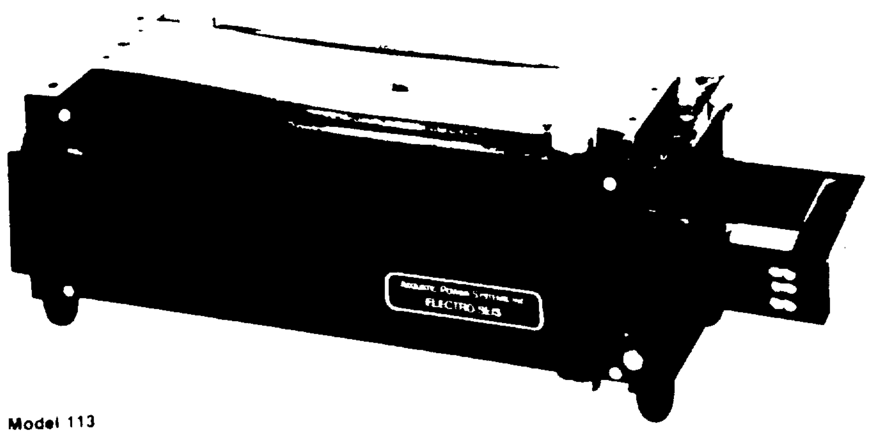

Model 113

ELECTRO-SEIS

SPECIFICATIONS

Model 113

[illegible]

APPLICATIONS

[illegible]

FEATURES

[illegible]

University of Virginia / NASA Lewis

Model 114 Power Amplifier

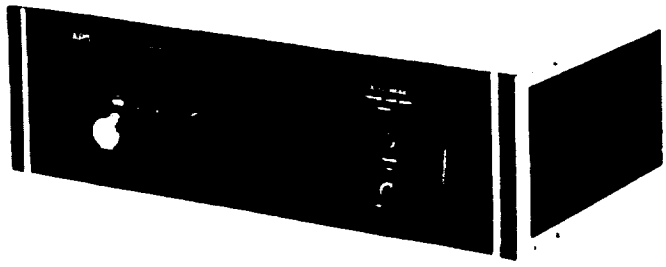

DESCRIPTION

The APS 114 and APS 124 **DUAL-MODE** Power Amplifiers are designed specifically to provide drive power for electrodynamic shakers. The output stage uses proven high reliability power operational amplifiers arranged to produce a balanced output.

The amplifiers have features which make them uniquely suited for studying the dynamic characteristics of structures. They may be operated in either a voltage or current amplifier mode, selectable from the front panel. This operating mode selector switch facilitates shaker drive power interruption in either a current or voltage mode for observation of resonance decay in structures.

The completely self-contained units are packaged in rugged aluminum enclosures suitable for bench or rack mounting. Forced air cooling and massive heat sinks for the output devices ensure continuous operation with a shaker delivering rated force into blocked, resistive or reactive loads.

A current monitor signal available on the rear panel permits monitoring of the instantaneous output current amplitude and phase. Electronic protection circuitry will detect an output short to ground or overload conditions and remove the drive signal.

The Model 124-EP features an extended power option which provides higher peak power with the same average power of the basic Model 124.

SPECIFICATIONS	Model 114
Average Output, into shaker reactive load	125 V-A rms
Peak Output, into shaker reactive load	250 V-A rms
Current Output, peak (random noise)	5.0 A peak
Current Output, continuous	4.0 A rms
Frequency Range	0-10000 Hz
Input Signal Voltage	2 V peak
Input Impedance	100 K ohm
Noise, referred to max. output	-90 dB
Current Monitor Output	250 mV/A
Input Power	120 V 50-60 Hz 300 W 220-240 V (optional)
Rear Panel Connectors	
Power Output	MK3-3*S Cannon
Input, Current Monitor	BNC Type Jack
AC Power	Std 3-Pin Receptacle
Weight	35 lb (15.9 kg)
Size HxWxD	5.22 x 17 x 9.25 inches 133 x 432 x 235 mm

University of Virginia / NASA Lewis

DASHPOT SERIES 160

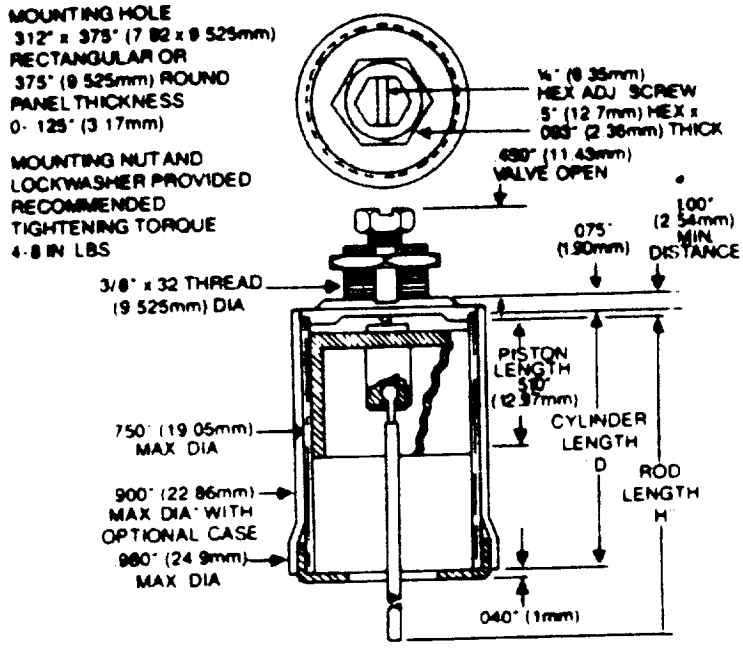

Bore:
.627" (16.0mm)

Damping Coefficient:
Regular damping: 2.5#/in./sec.
Super damping: 10#/in./sec.

Maximum Pull Force:
4# (1.8kg.)

Maximum Friction Force:
Less than 1gm.

Operating Temperature Range:
-75°C to +150°C

Approximate Piston Weight:
3gm.

Cylinder Weight: 1st inch: 8gm.
Each additional inch: 3.6gm.

University of Virginia / NASA Lewis

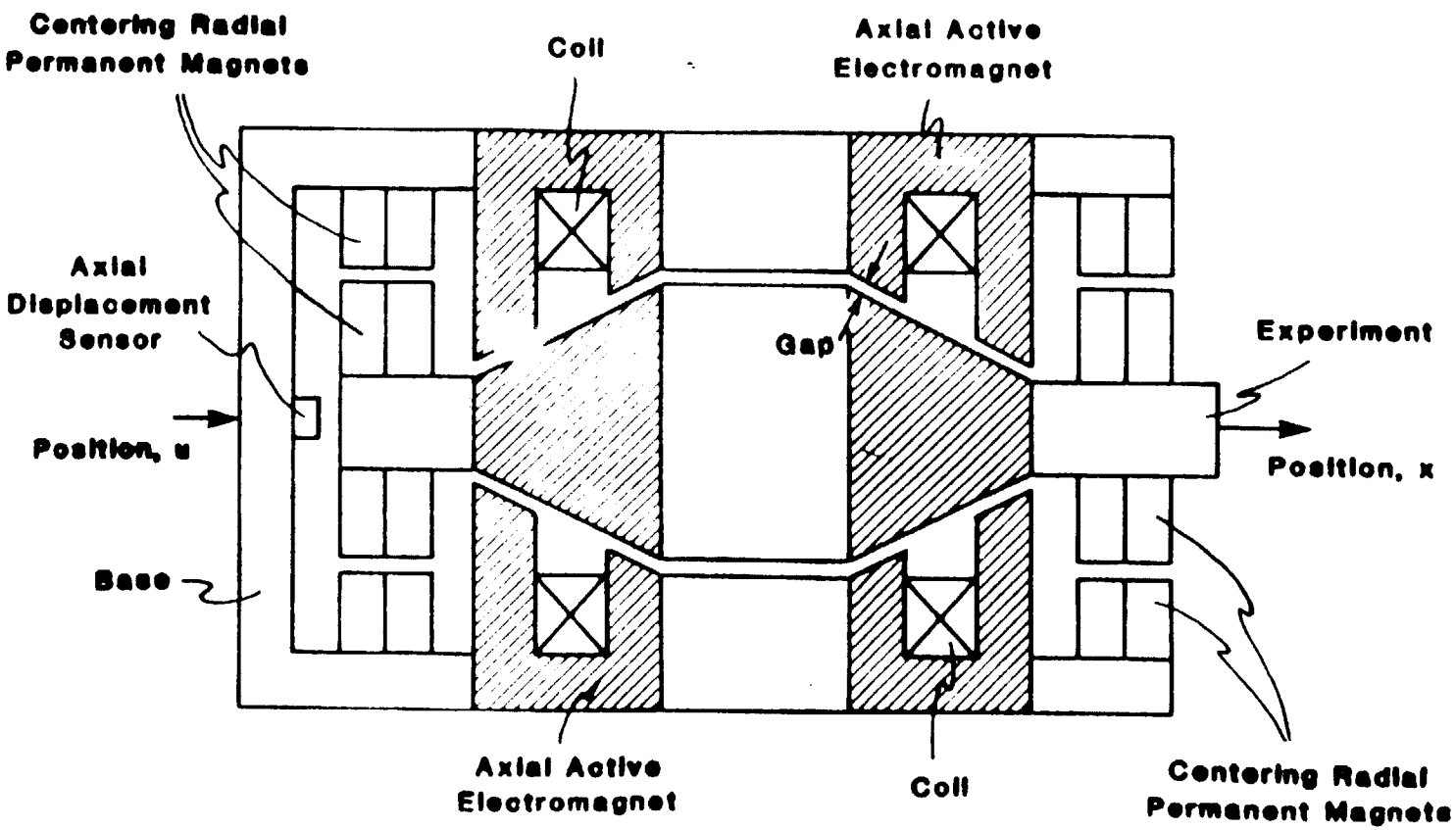

Long Action Magnetic Actuator (LAMA) Diagram

University of Virginia / NASA Lewis

QA-700

SUNDSTRAND DATA CONTROL'S Q-FLEX® SERVO ACCELEROMETER

Features

- Cost-Effective High Accuracy
- Field-Adjustable Voltage Sensitivity and Range
- Consistently Repeatable Accuracy and Stability
- Self-Contained Sensor and Electronics in One Small Hermetic Package
- Better than 1 micro g Threshold and Resolution
- Dual Built-In Test Capability
- Wide Dynamic Range
- Internal Temperature Sensor Thermal Modeling

QA-700 Technical Data

PERFORMANCE

Output Range	±30g
Bias	8mg max
Bias Thermal Coefficient	70µg/°C max
Current Scale Factor	1.3mA/g nom
Scale Factor Thermal Coefficient	200 ppm/°C nom
Linearity Error	48µg/g² max
Input Axis Misalignment	1 mrad
Resolution Threshold	1µg max
Frequency Response	
0-100 Hz	±0.1% max
100-200 Hz	±5% max
200-800 Hz	±10% max
Natural Frequency	1300 Hz
Damping Ratio	0.3 to 0.8

ELECTRICAL

Input Voltage	±13 VDC to ±18 VDC
Quiescent Current max	20mA per supply
Isolation case to all pins	10 megohms at 50 VDC
Temperature Sensor Output*	1µA/°K

University of Virginia / NASA Lewis

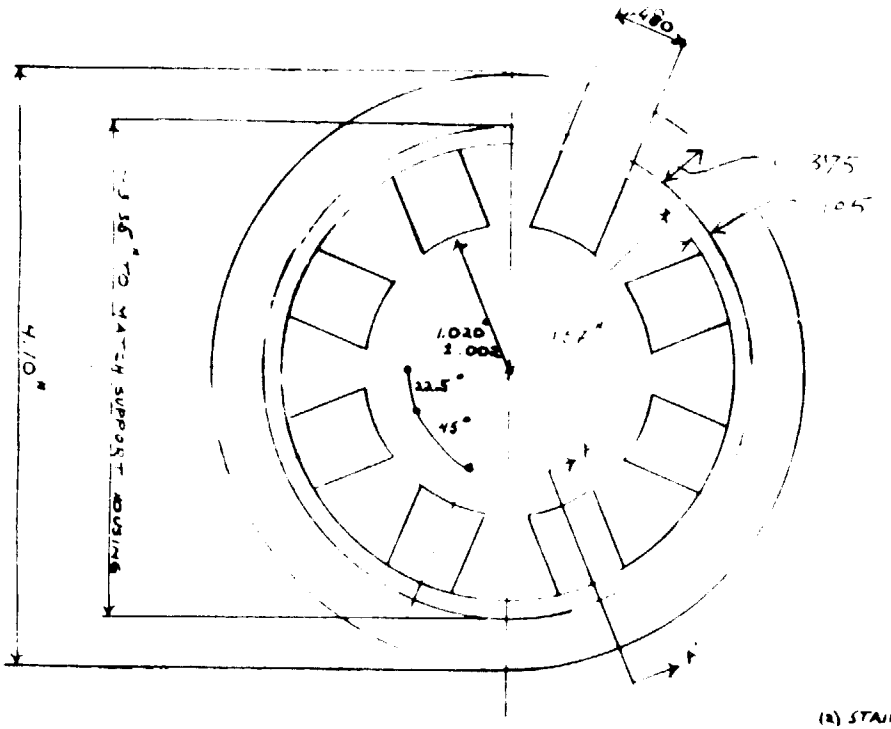

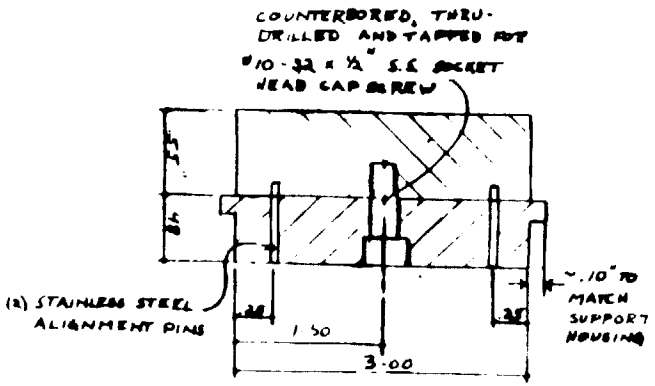

SECTION A-A'

MAGNETIC SUPPORT
MATERIAL: MAGNET IRON
DIMENSIONS: X XX ± .01"
X.XXXX ± .005"
UNLESS NOTED

MODEL: lrntz1 DATE: SEP-14-90

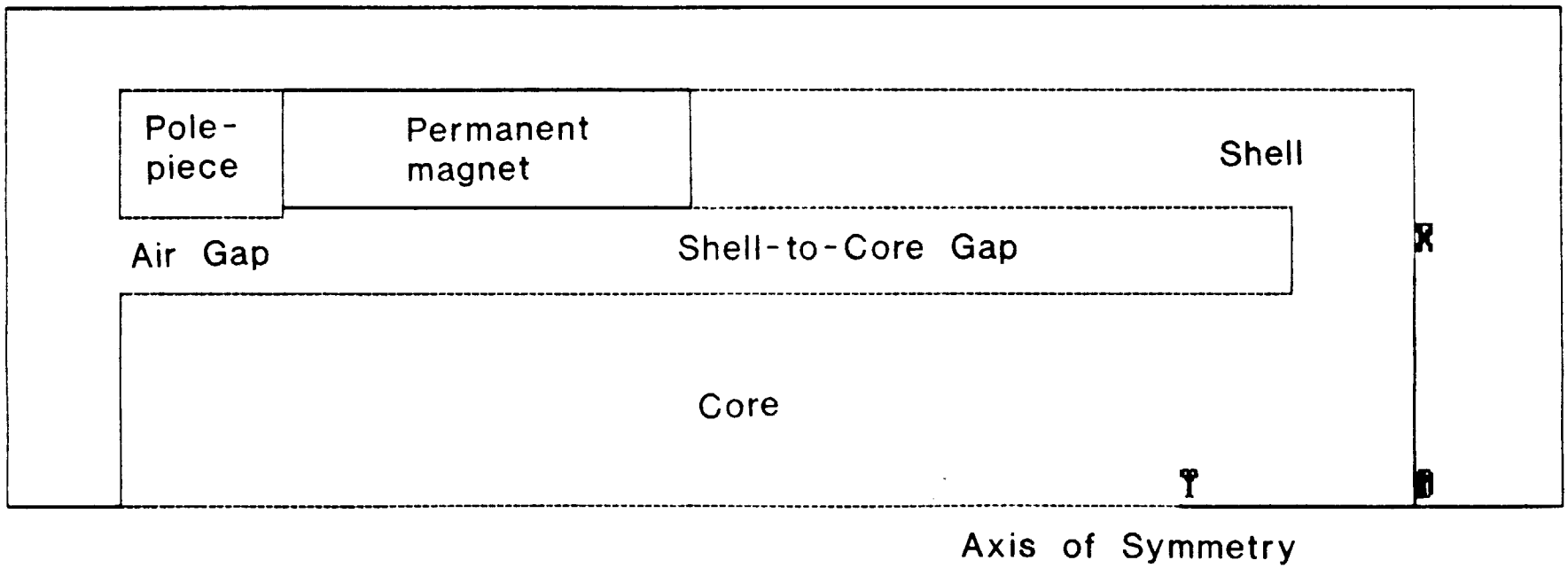

Axisymmetric Section of Lorentz Actuator

University of Virginia / NASA Lewis

LORENTZ ACTUATOR : DESIGN EQUATIONS

1. Assume permanent magnet operating point for maximum energy product : ($-H1$, $B1$).
2. Compute magnet flux, $fm = B1 * Am$.
3. Compute circuit flux, $fc = H1 * Lm / R$, where R is the circuit reluctance.
4. Compare fm and fc.
5. Adjust operating point until $fm = fc = f$, when actual operating point has been found. (In case of saturation, f = saturation flux in saturated circuit segment.)
6. Calculate air gap flux density, $Bg = f / Ag$.
7. Compute force capability, $F = i * l * Bg$, where i is the actuator current and l is the total length of coil wire in the air gap.
8. Change actuator geometry or circuit / magnet material until desired force level is achieved.

Crucible Magnetics

Crumax 355
Demagnetization Curve and Energy Product Values

COMPARISON DATA

	Br(kG)	Hc(kOe)	Hci(kOe)	BH max(mega-G-Oe)
CRUMAX 261	10.4	10.0	20	26
CRUMAX 282	10.8	10.1	17	28
CRUMAX 301	11.0	10.6	20	30
CRUMAX 315	11.5	10.9	14	31
CRUMAX 322	11.6	10.8	17	32
CRUMAX 355	12.3	11.3	14	35

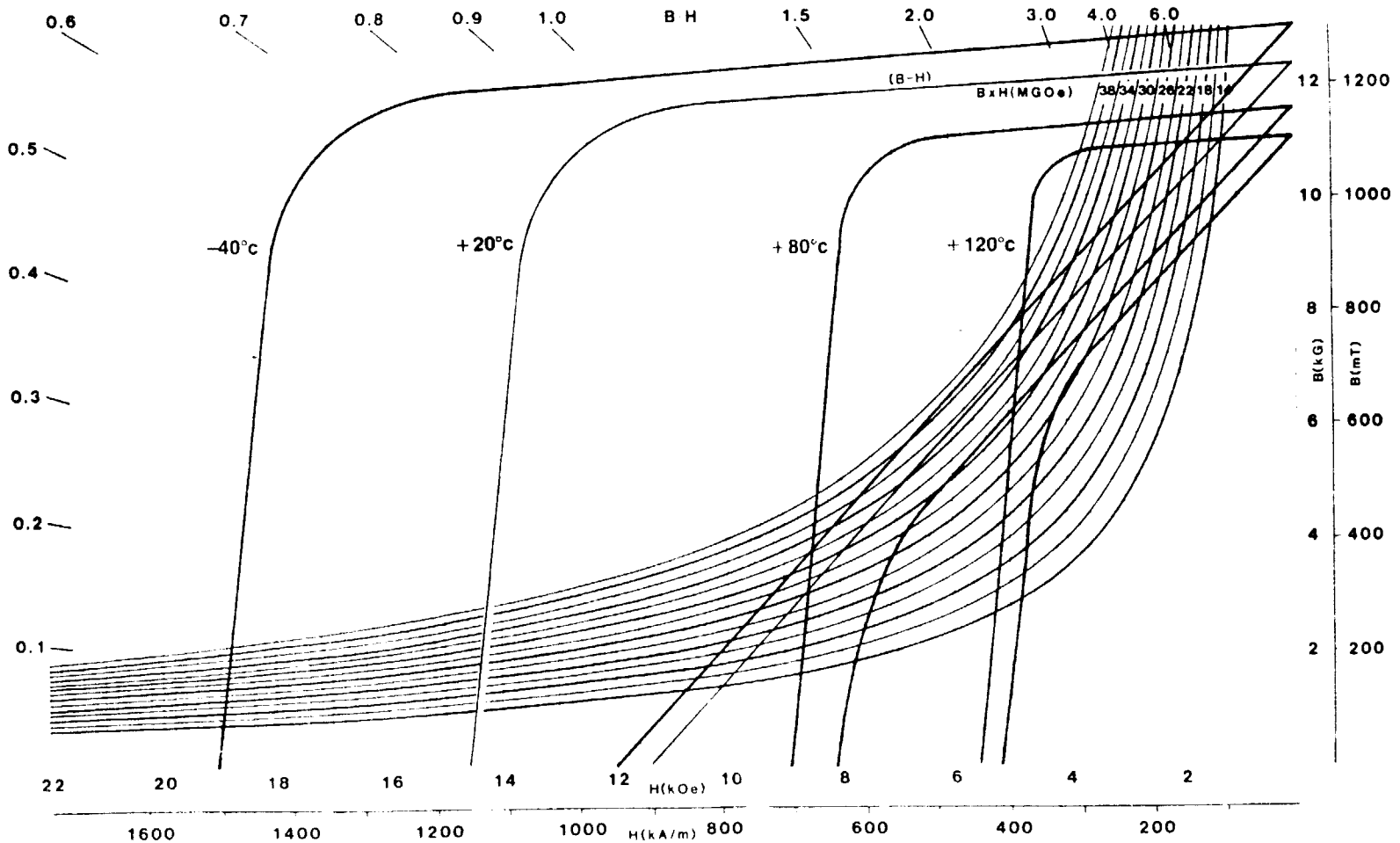

A Division of Crucible Materials Corporation
101 Magnet Drive
Elizabethtown, Kentucky 42701
502/769-1333

University of Virginia / NASA Lewis

LORENTZ ACTUATOR : INITIAL DESIGN

Total length	=	3.17 in
Magnet outer diameter	=	3.20 in
Magnet inner diameter	=	2.10 in
Magnet length	=	1.00 in
Shell outer diameter	=	2.80 in
Shell base thickness	=	0.30 in
Pole-piece thickness	=	0.40 in
Core diameter	=	1.10 in
Air gap	=	0.17 in
Shell-to-core gap	=	0.50 in
Gap ratio	=	1 : 2.94
Coil wire diameter	=	26.67 mils
Number of layers	=	4
Total number of turns	=	450
Maximum coil current	=	2.52 A
Air gap flux density	=	0.50 T
Saturation flux density	=	1.20 T
Maximum force generated	=	2.33 lbf
Actuator weight (excl. coil)	=	4.12 lbf

University of Virginia / NASA Lewis

LORENTZ ACTUATOR : COMPACT DESIGN

Total length	= 3.17 in
Magnet outer diameter	= 1.95 in
Magnet inner diameter	= 1.40 in
Magnet length	= 1.00 in
Shell outer diameter	= 1.95 in
Shell base thickness	= 0.30 in
Pole-piece thickness	= 0.40 in
Core diameter	= 1.00 in
Air gap	= 0.17 in
Shell-to-core gap	= 0.20 in
Gap ratio	= 1 : 1.18
Coil wire diameter	= 26.67 mils
Number of layers	= 4
Total number of turns	= 450
Maximum coil current	= 2.52 A
Air gap flux density	= 0.45 T
Saturation flux density	= 1.20 T
Maximum force generated	= 1.93 lbf
Actuator weight (excl. coil)	= 2.18 lbf

University of Virginia / NASA Lewis

LORENTZ ACTUATOR: FINITE ELEMENT ANALYSIS

Motivation

- Different geometric configurations
- Leakage across shell-to-core gap
- Saturation in core
- Minimum weight
- Reasonable cost
- Circuit materials with different saturation levels
- Effect of current-carrying coil on air gap flux
- Fringing

Other Considerations

- Mesh effects (coarse/fine)
- Nonlinear analysis (B-H curves)
- High gradient regions

MODEL: lrntz1 DATE: SEP-14-90

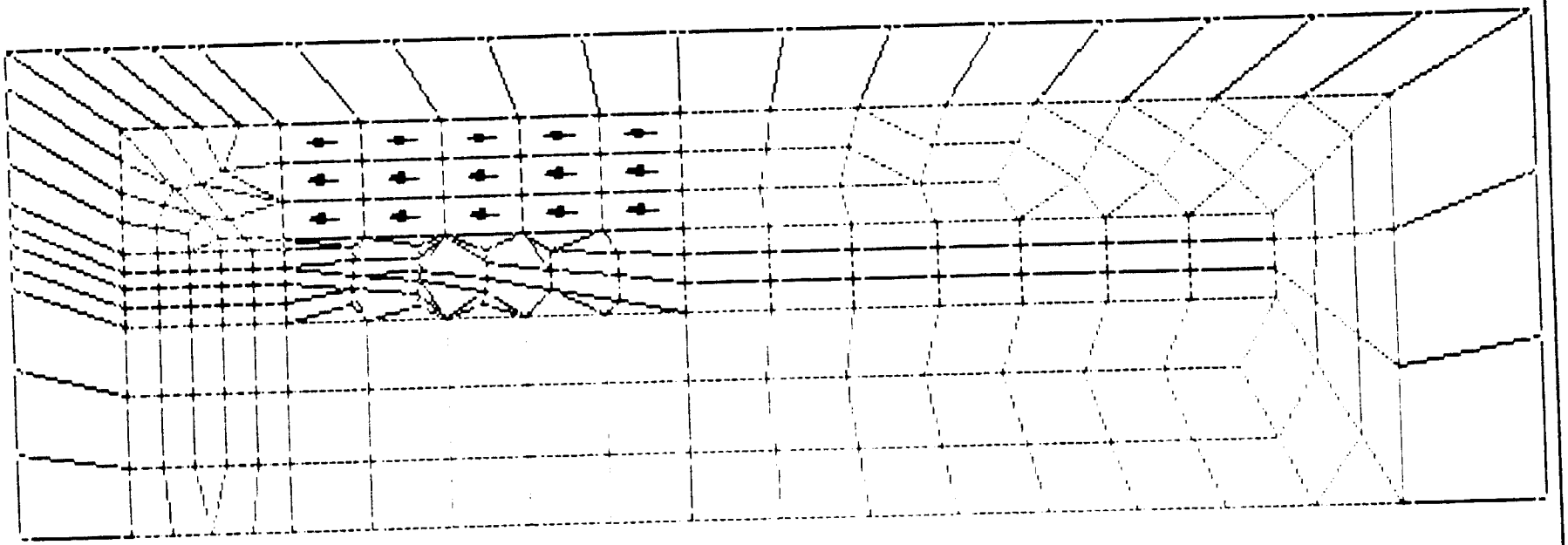

Finite Element Mesh for Lorentz Actuator

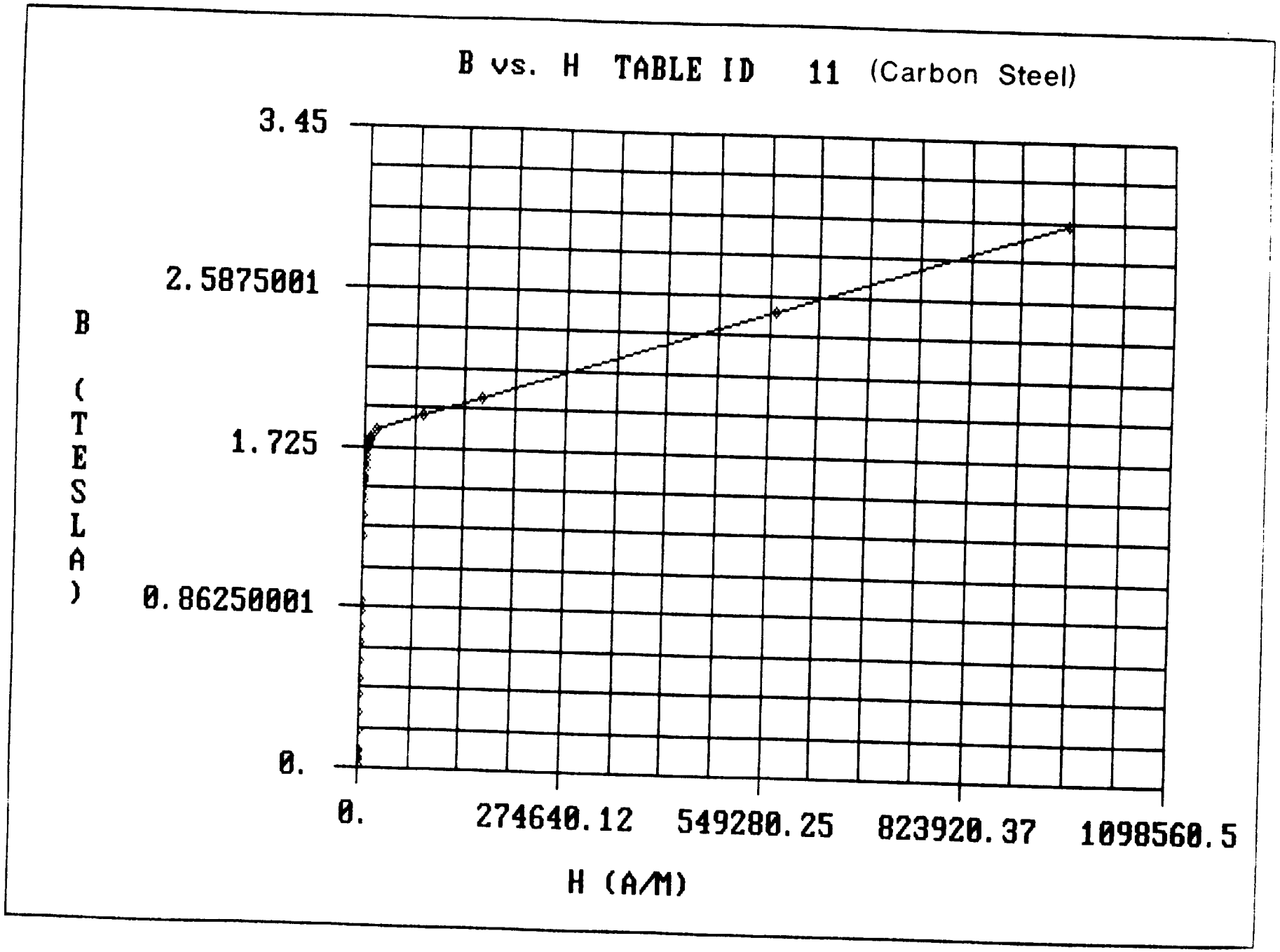
B vs. H TABLE ID 11 (Carbon Steel)
3.45
2.5875001
1.725
0.86250001
0.
B (TESLA)
0.
274640.12
549280.25
823920.37
1098560.5
H (A/M)

MODEL: lorentz

DATE: SEP-19-90

MAGNETIC FLUX DENSITY (TESLAS)

MAXIMUM = 1.456

1.456
1.214
0.9710
0.7282
0.4855
0.2427
0.0000E+00

MINIMUM = 0.0000E+00

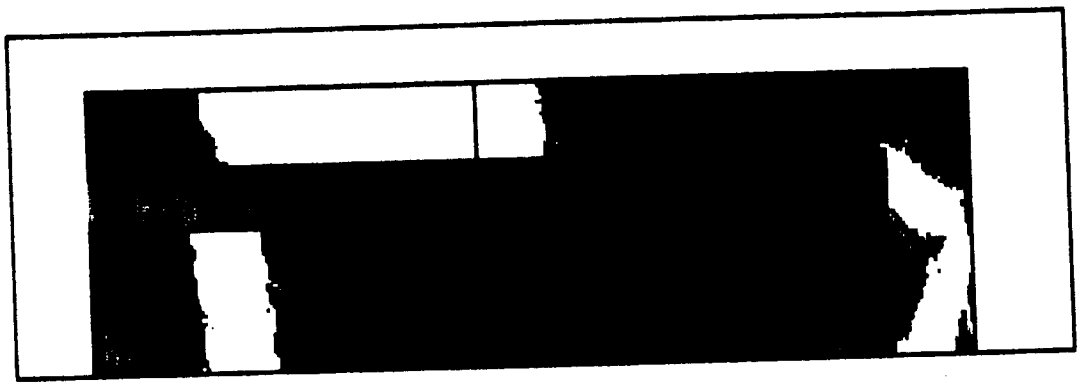

Case 1 : Circuit Material -- Carbon Steel;
No Current in Coil

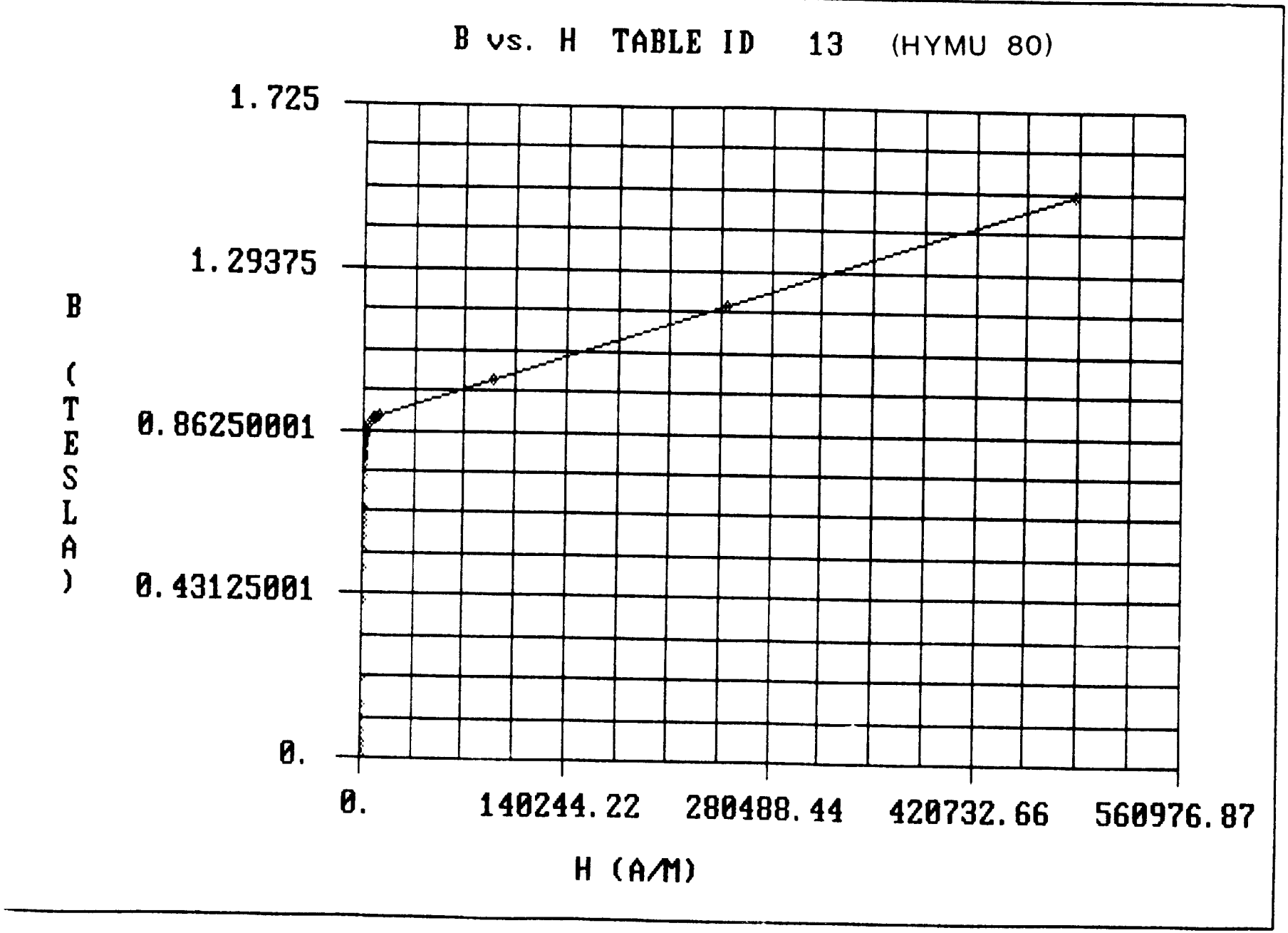
B vs. H TABLE ID 13 (HYMU 80)
1.725
1.29375
0.86250001
0.43125001
0.
B (TESLA)
0.
140244.22
280488.44
420732.66
560976.87
H (A/M)

MODEL: lrntz1 DATE: SEP-17-90

MAGNETIC FLUX DENSITY (TESLAS)

MAXIMUM = 1.050

1.050
0.8751
0.7001
0.5251
0.3500
0.1750
0.0000E+00

MINIMUM = 0.0000E+00

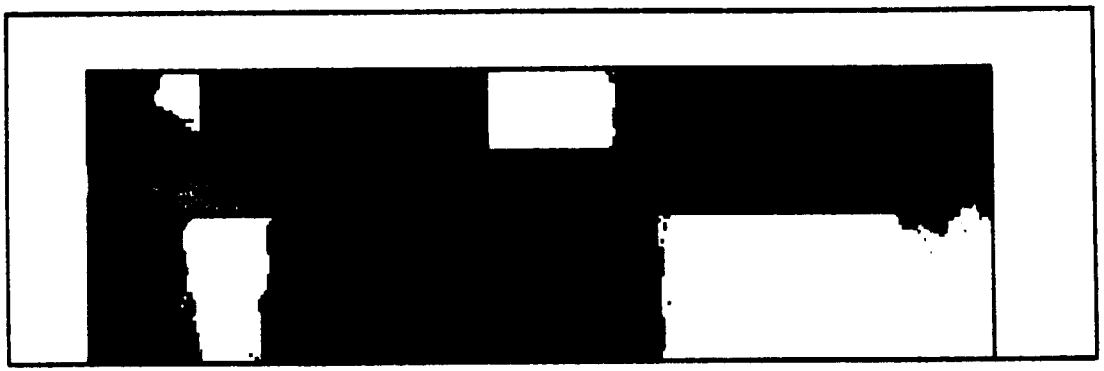

Case II : Circuit Material -- HYMU 80;
No Current in Coil

MODEL: lrntz2 DATE: SEP-17-90

MAGNETIC FLUX DENSITY (TESLAS)
MAXIMUM = 1.024

1.024
0.8529
0.6823
0.5118
0.3412
0.1706
0.0000E+00

MINIMUM = 0.0000E+00

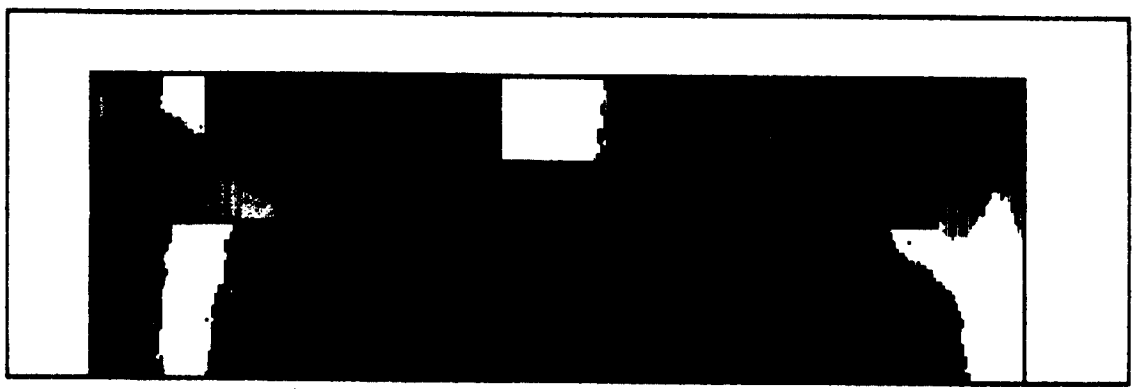

Case III : Circuit Material -- HYMU 80;
2.52 A in Coil, at 0 degree Phase

MODEL: lrntz3

DATE: SEP-19-90

MAGNETIC FLUX DENSITY (TESLAS)

MAXIMUM = 1.018

1.018

0.8485

0.6788

0.5091

0.3394

0.1697

0.0000E+00

MINIMUM = 0.0000E+00

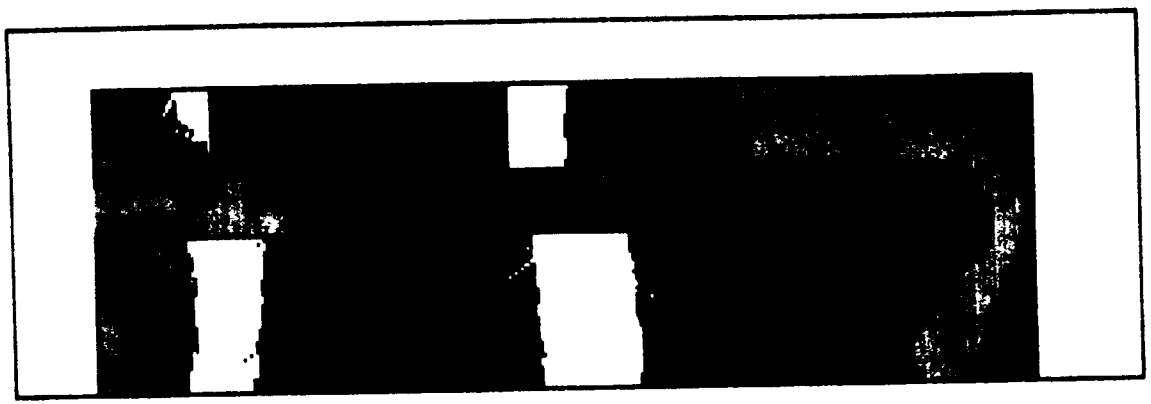

Case IV : Circuit Material -- HYMU 80;
2.52 A in Coil, at 180 degrees Phase

University of Virginia / NASA Lewis

CONCLUSIONS

- Design complete
  - Experiment
  - Lorentz Actuator

- Construction in progress
  - Concrete base in place
  - Shaker and its amplifier bought
  - Magnetic supports under construction
  - Data acquisition system being developed

- Experiment operational by late 1990
  - Background vibration measurements
  - Testing with "disturbances" generated by the shaker

DEVELOPMENT of a SUITABLE INDUCTIVE SENSOR for MAGNETIC BEARINGS

David P. Plant
FARE Incorporated
4716 Pontiac Street, Suite 304
College Park
MD 20740

Ronald B. Zmood
Royal Melbourne Institute of Technology

James A. Kirk
University of Maryland

DEVELOPMENT OF A SUITABLE INDUCTIVE DISPLACEMENT SENSOR FOR MAGNETIC BEARINGS

David P. Plant
FARE, Inc.

Dr. Ronald B. Zmood
Royal Melbourne Institute of Technology

Dr. James A. Kirk
University of Maryland

I. ABSTRACT

The work presented in this paper covers the recent developments in the area of non-contacting displacement sensors for a 500 Watt-hour magnetically suspended flywheel energy storage system. "Pancake" [permanent magnet, PM, and electromagnet, EM] magnetic bearings are utilized to suspend the flywheel. The work includes a detailed review of commercially available non-contacting displacement sensors and their suitability of operating with magnetic bearings. In addition, several non-contacting displacement sensors were designed and constructed for this magnetic bearing application. The results will show, currently available, commercial non-contacting displacement sensors will not function as desired and that an inductive sensor was developed to operate within this magnetic bearing.

II. INTRODUCTION

A prototype 500 Wh flywheel energy storage system is being built for the NASA Goddard Space Flight Center. This energy storage system is targeted for spacecraft applications, for it exhibits high specific energy densities and can be used for attitude control. A conceptual view of the 500 Wh energy storage system can be seen in Figure 1. The energy storage system incorporates three key technologies, interference assembled multi-ring composite flywheel, high efficiency brushless motor and generator, and magnetic bearings. This paper focuses on displacement transducers, which are a vital element in the suspension of flywheels, via magnetic bearings. These transducers or sensors detect the displacement of the flywheel relative to the stator portion of the magnetic bearing. This displacement is referred to as the measurand. In practice, measurement systems seldom respond directly to the measurand. More often, for ease in measuring, it is desirable to

convert from one physical quantity to another by means of a transducer. The conversion in this case is from displacement to a voltage level which is proportional to the displacement of the flywheel. Next this voltage signal is fedback through the control system, compared to a reference voltage, and a control current is applied to the electromagnetic coils, in the magnetic bearings, to center the flywheel.

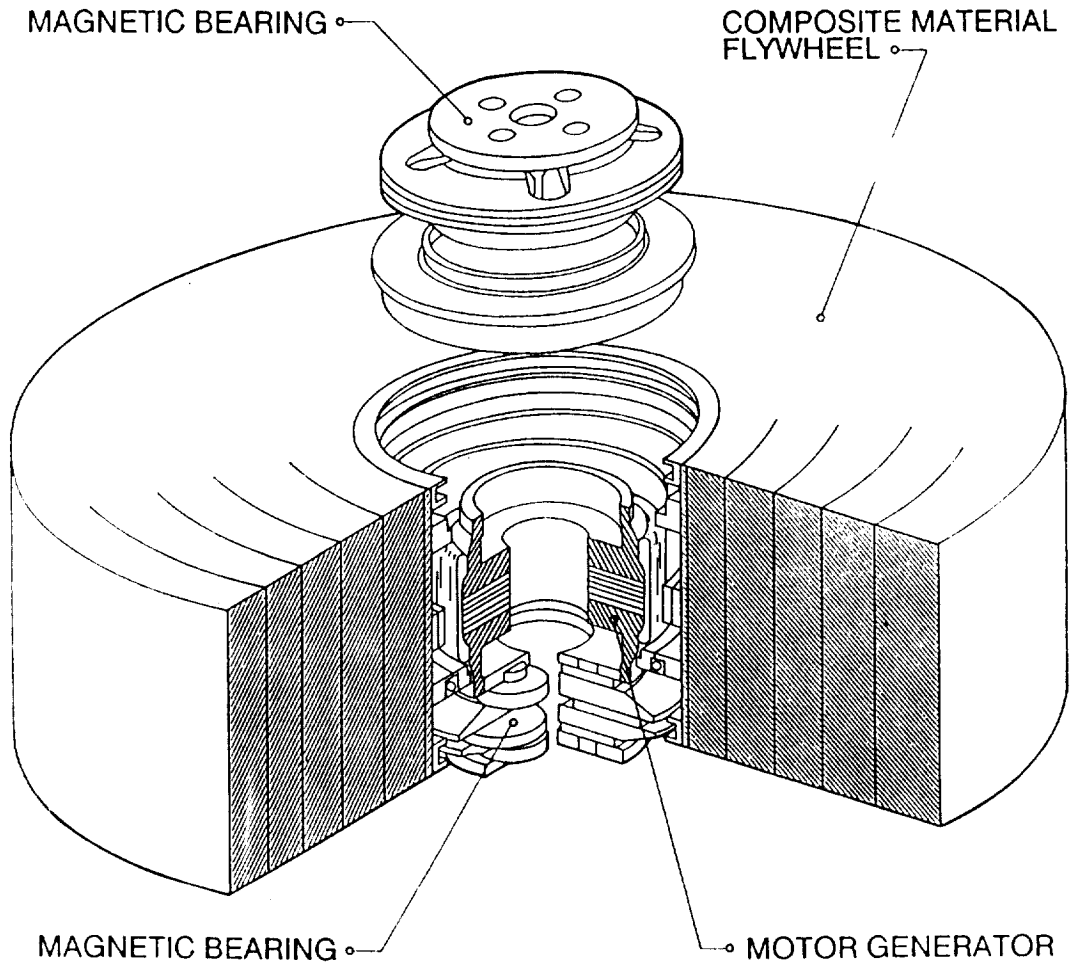

Figure 1. 500 Wh Flywheel Energy Storage System

In selecting a non-contacting displacement transducer for a magnetic bearing application, requirements for these sensors must be specified. The requirements include, the nominal linear range, the resolution, the sensitivity, the frequency response, the size of the transducer, the wire bend radius of the sensor's lead wire, and the power consumption. The main performance requirements of the displacement transducer for the 500 Wh energy storage system are listed in Table 1. For this 500 Wh energy storage system the displacement transducers were to be moved from sensing the outside periphery of the flywheel to sensing the inside surface of the flywheel. The initial location chosen for the sensor was on the inside of the magnetic bearing.

Linear Range:	20 mils
Sensitivity:	60 V/in.
Resolution:	20 μinches
Power Consumption:	less than 40 mW
Size:	Must fit on inside of a magnetic bearing 0.250" dia. 1.000" lenght
Operating Environment:	Must operate in strong magnetic fields

Table 1. Sensor Specifications for 500 Wh Energy Storage System

III. BACKGROUND ON COMMERCIALLY AVAILABLE TRANSDUCERS

Some of the types of non-contacting displacement transducers presently accessible are inductive, capacitive, and optical transducers. Although there are other types of non-contacting displacement transducers, such as radiation, ultrasonic, and air gauging, only inductive, capacitive, and optical types were investigated. The general advantages and disadvantages [for use in the 500 Wh energy storage system] of the inductive, capacitive, and optical sensors are presented next. Inductive sensor have adequate frequency response, small size, and have a relatively large linear range. The main disadvantage of the inductive sensor was uncertainty of operating in a strong magnetic field. Also the inductive sensor produced a sensing area that was the shape of a cone protruding from the sensor's probe tip. Any conducting material that would intersect this conical sensing field would affect the output of the sensor. The capacitive sensor could be custom sized to tailor fit the 500 Wh energy storage system, due to several companies that build custom designed capacitive sensors. Problems of low frequency response, very high cost, and stray capacitance fields basically prohibited the use of capacitive sensors in the 500 Wh energy system. The optical sensors were quite promising with very high frequency responses, large linear ranges, very low cost, and very small probe size with the use of fiber optics. The only disadvantage of the optical sensor was the problem of non-uniform surface reflectivity of the target surface.

A survey, of the commercial vendors, was conducted to locate a displacement sensor that could be utilized with the 500 Wh energy storage system. From the search, several potential displacement transducers were identified and several sensors were obtained for testing with the 500 Wh energy storage system.

IV TRANSDUCER TESTING

The experimental testing of each displacement transducer was separated into two parts. The first consisted of voltage output of the transducer versus target displacement testing and the second dealt with performing experimental tests using the displacement transducer in an actively controlled magnetically suspended flywheel system. This test system utilized one magnetic bearing, see Figure 2. In the following paragraphs the results of several of the sensors tested are presented.

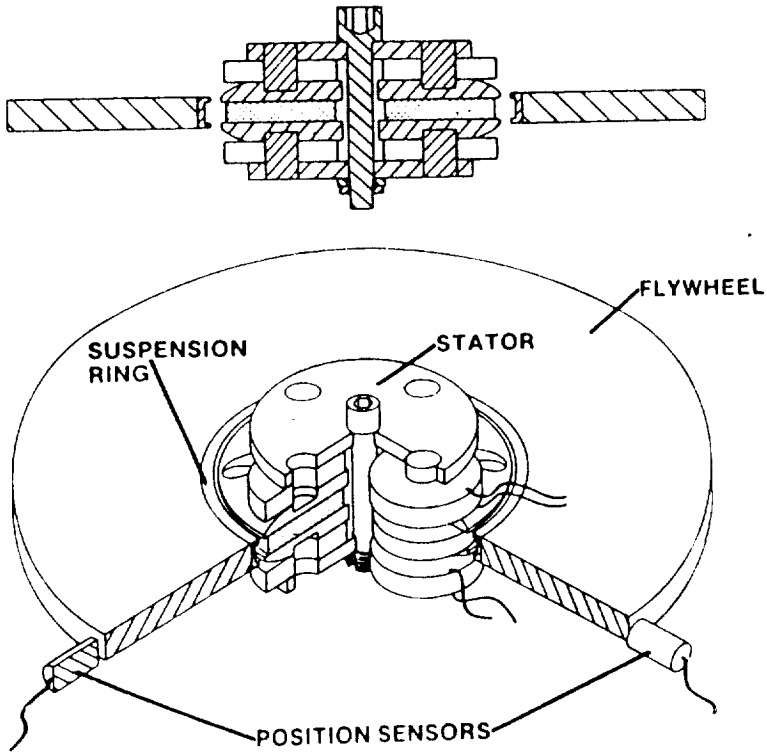

Figure 2. Actively Controlled Magnetically Suspended Flywheel System

Two different model sensors (KD-2400 and the KD-2300-1SU) were tested from Kaman Instrumentation Corporation of Colorado Springs, CO. The KD-2400 sensor was an inductive type sensor and was the sensor used in the previous magnetic bearing systems built at the University of Maryland. The voltage output curve for this sensor is shown in Figure 3. This sensor was able to meet all of the stack system's sensor requirements except for the size requirement. The sensor's probe was too large to fit on the inside of a magnetic bearing. This sensor was tested for the reason that it was readily available and worked successfully in previous magnetic bearing systems. The other Kaman sensor, KD-2300-1SU, passed all requirements for the stack system and proved to be very versatile. The voltage output versus

displacement curve is shown in Figure 4. The sensitivity was easily adjustable to 60 volts per inch. The linear range for the KD-2300-1SU was only approximately 40 mils for an aluminum target and 35 mils for a stainless steel target. An advantage of this sensor was that it did not detect ferromagnetic materials.

The last sensor tested was the SPOT optical sensor designed and built at the University of Maryland. This sensor's voltage output versus displacement curve is shown in Figure 5. Optical sensors produce voltage output versus displacement curves that have two linear portions, these portions are named the front slope and the back slope. Since this sensor was built in-house it proved to be quite flexible. The sensitivity and linear range were easily adjustable to match the required specifications of the stack system.

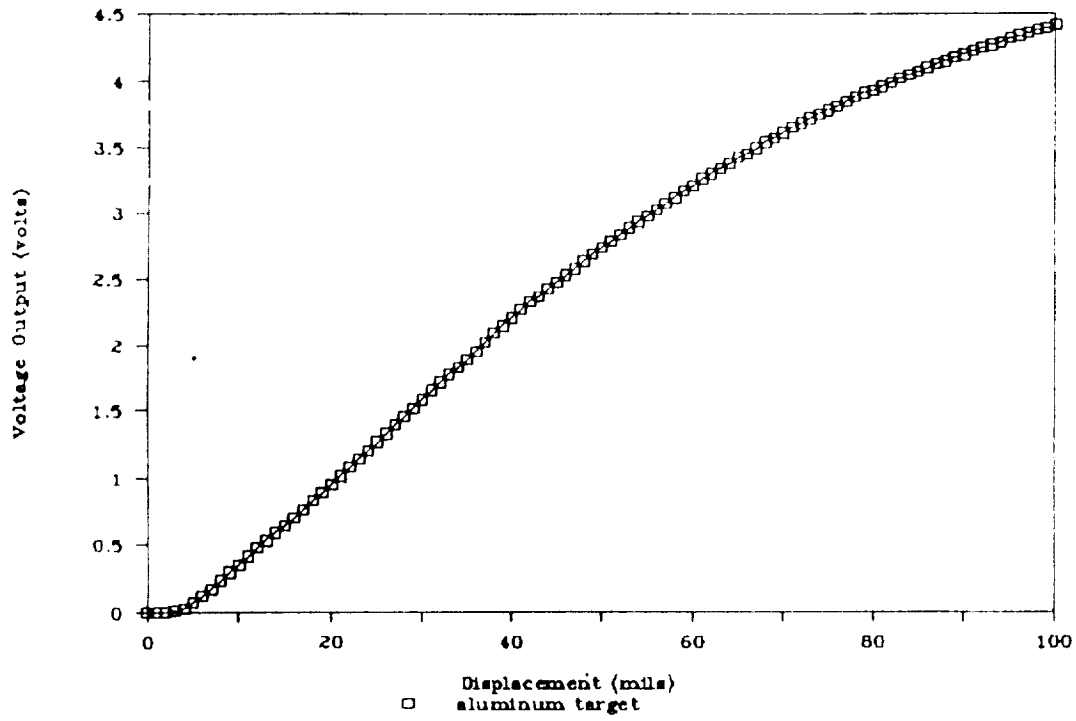

Figure 3. Voltage Versus Displacement for Kaman KD-2400 Sensor

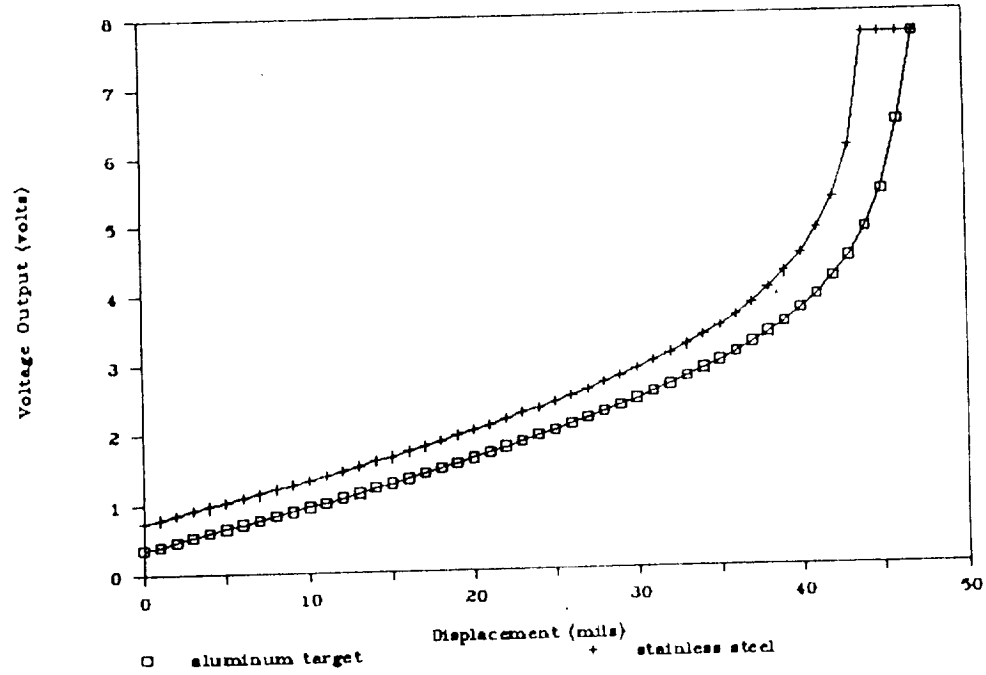

Figure 4. Voltage Versus Displacement for Kaman KD-2300-1SU Sensor

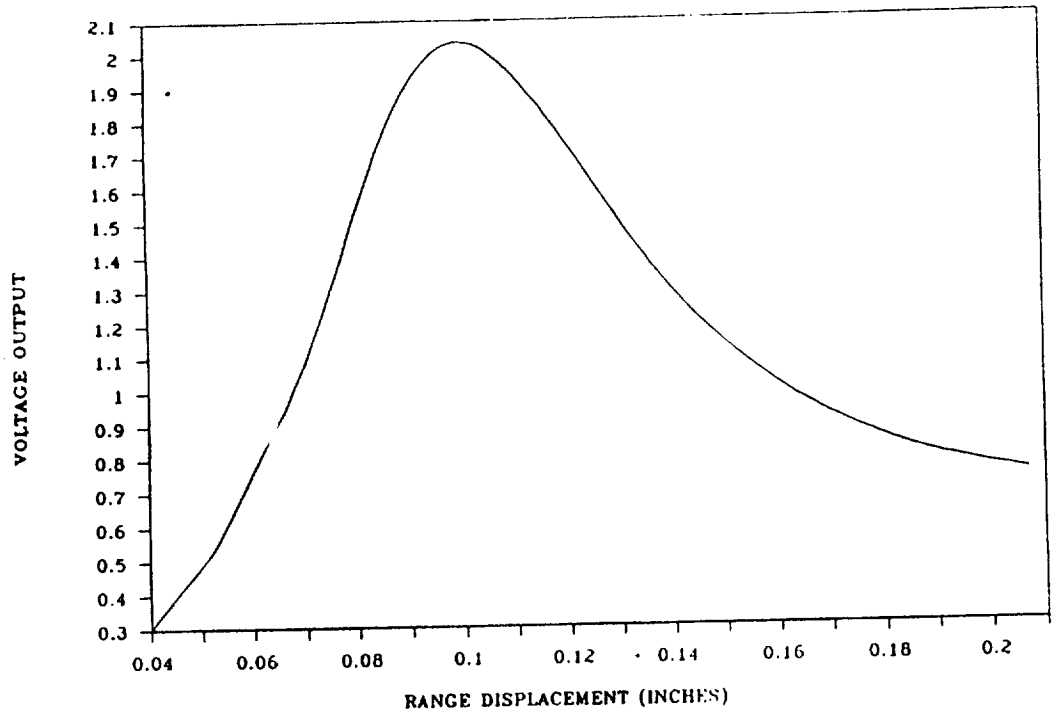

Figure 5. Voltage Versus Displacement for SPOT Sensor

Once all the displacement transducer's sensitivities were calibrated to 60 volts per inch, further experiments on the sensors were performed to reveal if these sensors could function on the inside of a magnetic bearing. The first experiment that was performed on all displacement transducers was to substitute one of the displacement transducer being tested with an existing Kaman KD-2400 inductive sensor in an existing magnetic bearing. All of the displacement transducers passed this test except for the SPOT optical transducer. The SPOT displacement transducer failed the test because of the target's non-uniform surface reflectivity. The target in this case was the outside surface of the magnetic bearing system's flywheel which is constructed of aluminum. The problem of non-uniform surface reflectivity was documented in Figure 6. This figure displays the voltage output of the SPOT and Kaman KD-2400 transducers versus time for a flywheel speed of 100 rpm. The peak to peak displacement of the Kaman KD-2400 sensor was approximately 0.05 volts, which translates at 60 volts per inch to 0.8 mils. The peak to peak displacement of the SPOT sensor was approximately 0.14 volts or 2.3 mils. In an attempt to eliminate the non-uniform surface reflectivity problem, different colored target surfaces and polished target surfaces were utilized. All these types of surfaces did not correct the problem. For this reason the SPOT sensor was dropped from further consideration.

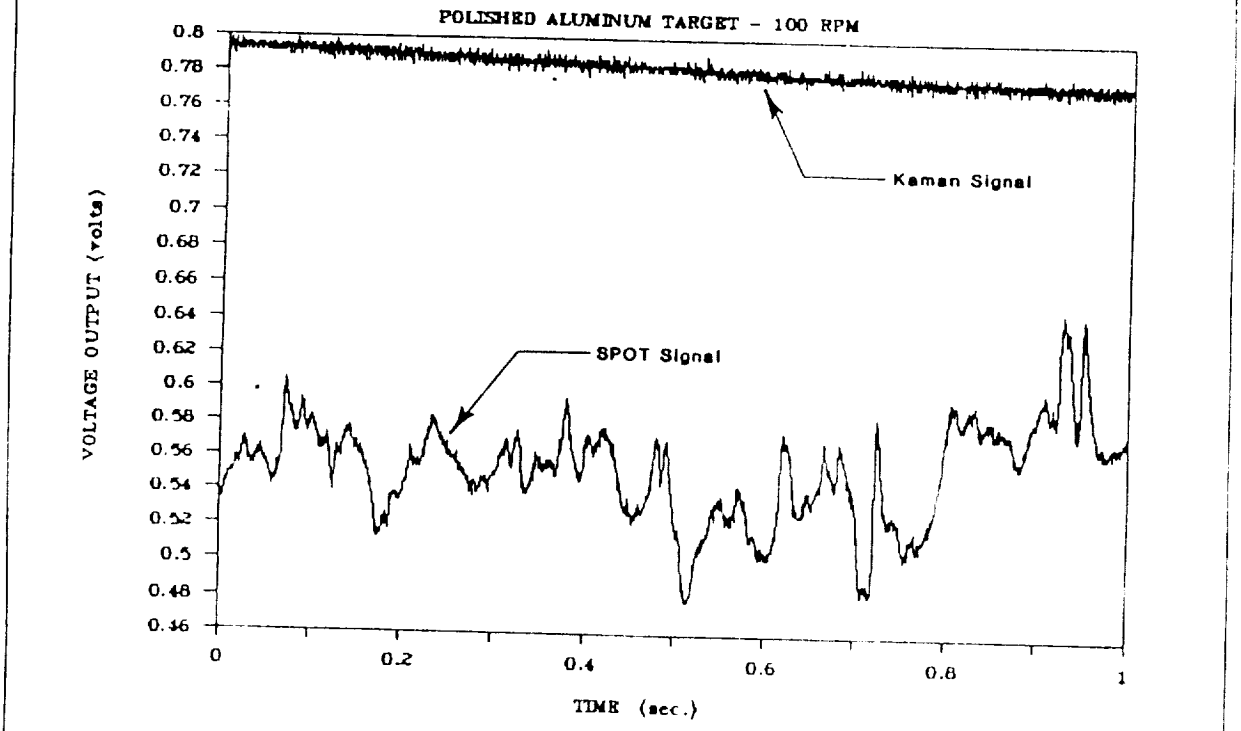

Figure 6. Reflectivity Testing of Spot Sensor

All the inductive sensors passed the suspension test. To conduct further experiments it was necessary to design and fabricate a mechanical fixture to house the displacement transducers within the magnetic bearing. Once the sensors were placed in the magnetic bearing two experiments were conducted, a voltage output versus displacement experiment and a suspension test. The voltage output versus displacement test was conducted using both the Scientific Atlanta and Kaman KD-2300-1SU sensors. For this experiment, an aluminum ring had to be placed on the inside of the return ring to provide the sensors with an aluminum target to detect. Figure 7. shows the curves created by the Scientific Atlanta sensor. There are three curves in Figure 7., one curve for no current applied to the EM coils and two curves with different currents applied to the EM coils. These three curves show that an inductive sensor can still function within a static magnetic field. For both the Kaman and

Scientific Atlanta sensors the sensitivity of the sensor decreased once inside the magnetic bearing. This change in sensitivity was due to the large magnetic fields originating from the magnetic bearing. The sensors were recalibrated to 60 volts per inch for the next test of suspension with the inside sensor. The flywheel was rotated to a low speed of a few hundred revolutions per minute and the output signals from the Scientific Atlanta and Kaman KD-2400 sensors were compared. The Scientific Atlanta sensor was tested on the inside of the magnetic bearing and the voltage output of this sensor was compared to the voltage output of one of the Kaman KD-2400 sensors, which was used to suspend the flywheel. The output signal of the Scientific Atlanta sensor did not match the signal produced by the Kaman sensor. The reason why these two graph do not correspond was because the Scientific Atlanta sensor was affected by the dynamic magnetic fields produced when the magnetic bearing was actively suspending the flywheel. To confirm this hypothesis a second experiment was run. This experiment produced a strong alternating electromagnetic field directly in front of the Scientific Atlanta sensor. The sensor was fixed relative to the target which was the iron pin at the center of the EM coil. The output of the sensor was monitored and found to vary although the sensor and target were fixed. This test concluded that inductive sensors were affected by varying magnetic fields and could not be utilized within the magnetic bearing. This test was also conducted on the Kaman and Bently Nevada sensors and similar results were obtained.

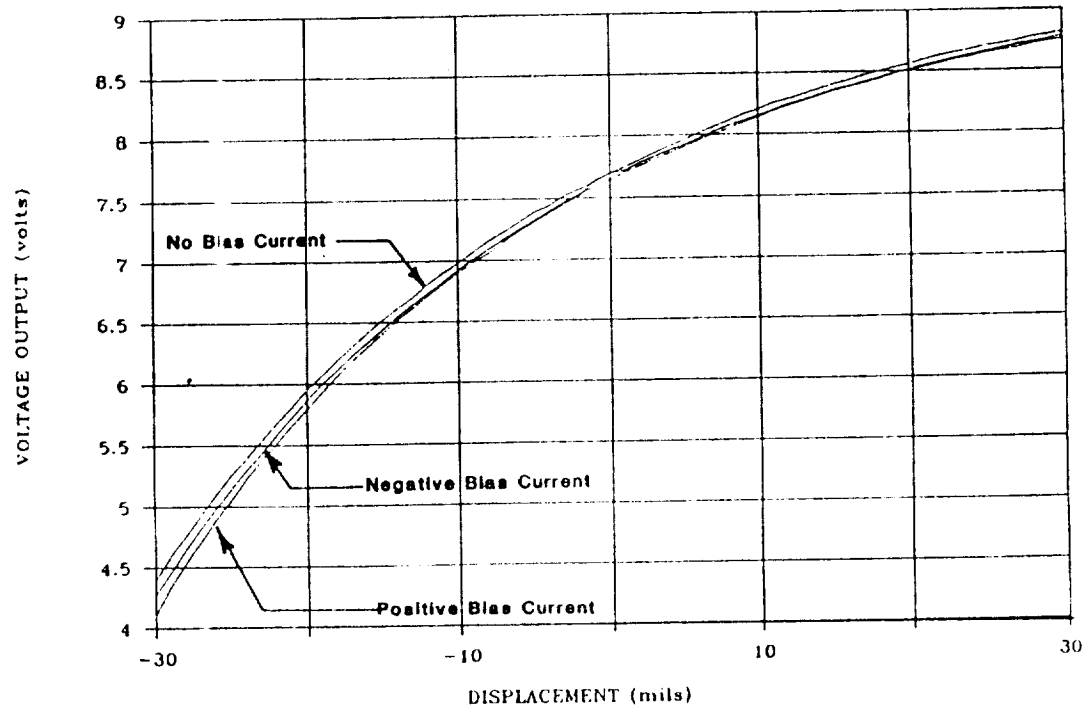

Figure 7. Testing of Sensor Within Magnetic Bearing

Since inductive transducers rely upon magnetic effects they are particularly prone to interference from external magnetic fields generated by the magnetic bearings actuators. Subsequent experimental investigation of one commercial transducer has shown the probable cause to be due to the transducer sensor casing. This casing is manufactured from a stainless steel which is mildly, but sufficiently, ferromagnetic so that the transducer calibration is affected by changes in the saturation level of the steel when it is immersed in an external magnetic field.

V. UOMD, RMIT & FARE TRANSDUCER DEVELOPMENTS

From the above experimental work, it was concluded that the displacement transducers tested could not be adapted to the inside of the magnetic bearing. Commercial inductive sensors will not work because of the alternating magnetic fields and the optical sensors have problems with non-uniform surface reflectivity. It is for this reason that effort has been devoted to developing suitable position transducers for 500 Wh flywheel energy storage system, which meet fairly stringent requirements of reliability, simplicity of concept, robustness, and ease of application. In this work attention has been largely concentrated on inductive transducers.

Both the inner and outer bores of the flywheel grow significantly as it spins from zero to a maximum speed of 80,000 rpm. In the case of the inner bore the radial growth has been estimated to be 0.43 mm [17 mils] at a speed of 80,000 rpm. On the other hand the rotor translational motion is limited by the touchdown bearings to $\pm$ 0.15 mm [6 mils] about its nominal center position, which it is observed is significantly less than the radial growth. Consequently any rotor position measuring system which senses the position, of either the flywheel outer rim or its inner bore, must be able to differentiate between displacements due to these two sources. To overcome this difficulty differential transducers need to be used. In the case of inductive elements positioned to sense on diametrically opposite sides of the flywheel inner bore. If these inductors are connected in an electrical bridge circuit the bridge balance will be unaffected by radial growth, and will only sense changes in inductance due to translational motion.

Experience has shown that sensitivities in the range 2 to 40 V/mm are achievable with acceptable out put signal-to-noise ratios, but the sensitivities are usually limited in applications to the range 2 to 4 V/mm. Commercially available inductive transducers typically operate with carrier frequencies of 1 to 2 Mhz, and sense physical displacement signals having bandwidths up to 10 khz.

Inductive transducers require a metallic target, and if they are to sense displacement on the flywheel outer rim then it must have a metallic surface attached by some means. The limited strength of metals combined with the very high surface speed of the flywheel makes this a difficult task. While the difficulty of attaching a metal surface to the outer rim may possibly be overcome, mounting the position transducers so as to sense displacement on the outer rim of the flywheel is not recommended for other reasons. Firstly, there are problems in maintaining concentricity between the flywheel outer rim and its inner bore, both during manufacture and especially when it is running at high speed. The latter situation arises due to the effects of large rotor growth with increase in rotor speed, and the in homogeneity of the composite structure causing an eccentricity to develop between the flywheel outer rim and the inner bore which changes as a function of speed. Secondly, the transducer sensors need to be rigidly and accurately fixed to the flywheel outer support structure which in turn must be accurately positioned with respect to the bearing stator; a complicated manufacturing problem. Thus for both manufacturing and operational reasons it is sensible to mount the position sensor internally so as to measure the displacement of the flywheel inner bore relative to the magnetic bearing stator.

VI. RELATIONSHIP TO MAGNETIC BEARINGS

The remainder of this discussion will center on how inductive sensors may be used in electrical bridge networks to solve the collocation problem by ensuring the effective displacement sensing planes are along the bearing actuator planes of symmetry. Four possible arrangements for the inductive sense coils of the transducers are shown in Figure 8. The most ideal arrangement is shown in Figure 8(a) where the coils are mounted between the pole faces, as this enables direct displacement measurement in the bearing planes X_AX_A' and X_BX_B'. For practical reasons this arrangement is difficult to implement and so will not be considered further.

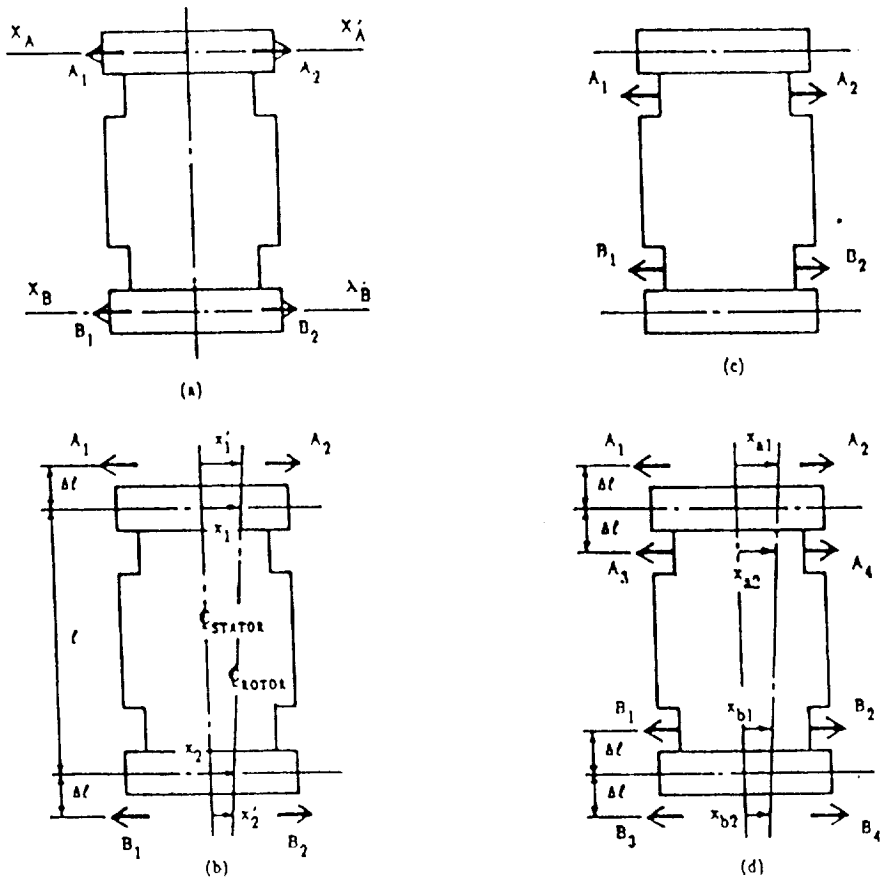

Figure 8. Alternative Location for Sensors. Sensor Positions Indicated by Arrows

The remaining possible arrangements can measure the displacements in the bearing planes of symmetry provided it is assumed that the bearing actuators and the motor/generator are rigid bodies. For example, let us consider the alternatives shown in Figures 8(b) and (c) where the inductive sense coils are shown by the arrow bars in each case. From simple geometry the displacements x_1 and x_2 can be calculated from measurements x_1' and x_2' and for the case shown in Figure 8(b) are given by

$$(1) \qquad x_1 = x_1' \left[\frac{\ell + \Delta\ell}{\ell + 2\Delta\ell}\right] + x_2' \left[\frac{\Delta\ell}{\ell + 2\Delta\ell}\right]$$

and

$$(2) \qquad x_2 = x_1' \left[\frac{\Delta\ell}{\ell + \Delta\ell}\right] + x_2' \left[\frac{\ell + \Delta\ell}{\ell + 2\Delta\ell}\right]$$

As long as $\Delta\ell/\ell$ is small the error due to uncertainties in $\Delta\ell$ can be neglected and the computed values of x_1 and x_2 can be used in place of their exact values in the respective bearing controllers.

If the motor cannot be considered to be rigid then the arrangement shown in Figure 8(d) needs to be used. Here the sense coils A_1, A_2, coils A_3, A_4, coils B_1, B_2 and coils B_3, B_4 are separately connected in a series. Since these coils are symmetrically displaced about the bearing planes of symmetry the transducer outputs will be x_1 and x_2, where

(3) $$x_1 = \frac{x_{a_1} + x_{a_2}}{2}$$

and

(4) $$x_2 = \frac{x_{b_1} + x_{b_2}}{2}$$

In Figure 9. is shown a simplified schematic of the experimental inductive bridge transducer, which can be used with any of the mechanical arrangements shown in Figure 8. The sensor inductors are connected in a Maxwell impedance bridge whose output is fed to a synchronous demodulator. The output of the demodulator passes through a low pass filter which filters the residual high frequency modulation products as well as any extraneous noise induced into the circuitry. The filter output is an analog signal whose magnitude is proportional to the displacement.

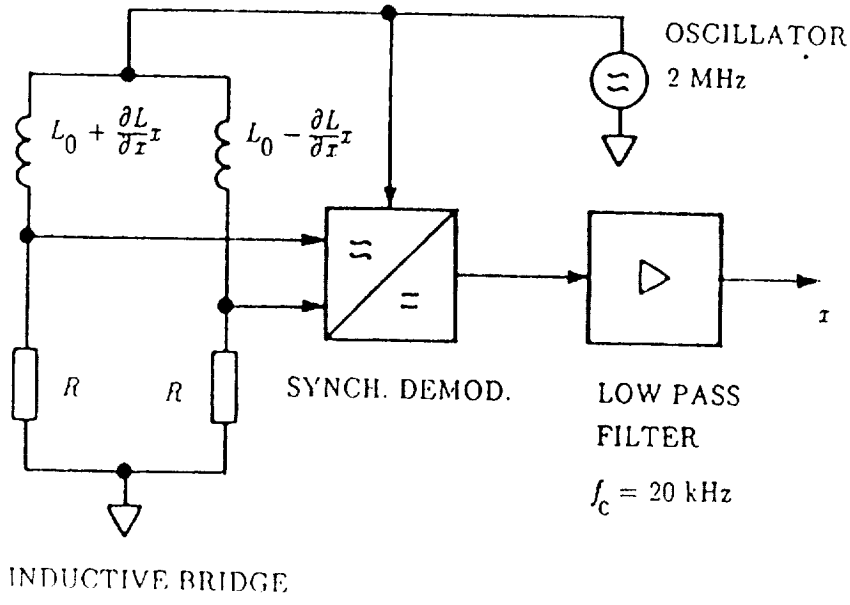

Figure 9. Schematic of Inductive Bridge Sensors

From the remarks given above concerning the use of stainless steel in commercial inductive sensors care was taken to only use non-ferrous materials, such as aluminum in the construction of the experimental sensors. Aluminum was also used for the transducer target. Experiments showed that using this construction made the transducers insensitive to changes in external magnetic fields.

The inductive sensors describe above will be utilized with the magnetic bearings in the prototype 500 Wh energy storage system. The specifications of this inductive sensor are presented in Table 2. A view of the location of these sensors within the 500 Wh energy storage system in shown in Figure 10.

Operating Principle:	Differential eddy current induction
Linear Range:	80 mils. Can be increased to 200 mils
Sensitivity:	60 V/in. Maximum exceeds 130 V/in.
Resolution:	20 μinches at 60 V/in. sensitivity
Frequency Response:	5 kHz (3dB)
Output Range:	± 10 V (offset can be adjusted to zero output)
Mounting:	Sensors remote from signal conditioning (0 - 4 ft)
Target:	Metallic - non-ferrous
Adjacent Metal:	Insensitive to external magnetic fields
Coil Inductance Range:	50 μH to 130 μH

Table 2. Inductive Sensor Specifications

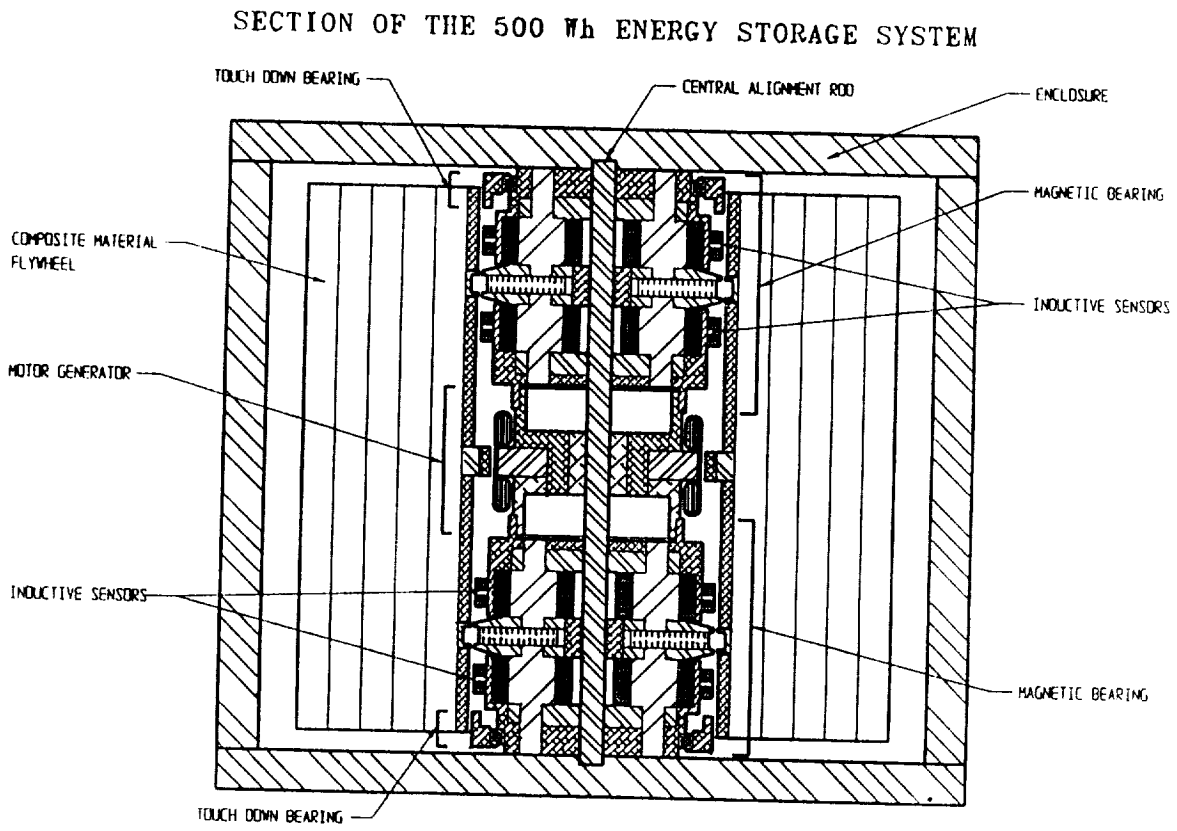

Figure 10. Location of Inductive Sensors Within 500 Wh Energy Storage System

VII. CONCLUSIONS AND RECOMMENDATIONS

The research conducted, showed that commercially available displacement sensors could not work with the 500 Wh flywheel energy storage system. Optical sensors were too sensitive to the non-uniform surface reflectivity and the inductive sensors were affected by the dynamic magnetic fields produced by the magnetic bearings. These conclusions led to the development of an inductive sensor, which was built and tested with the 500 Wh magnetic bearings. The placement of this inductive sensor within the 500 Wh energy storage system was altered and several sensors were used in a differential arrangement. The sensors will soon be incorporated with the final 500 Wh energy storage system.

VIII. REFERENCES

1. Anand, D.K., Kirk, J.A., Zmood, R.B., Studer, P.A., and Rodriguez, G.E., *"System Considerations for a Magnetically Suspended Flywheel"*, Proceedings of the 21st Intersociety Energy Conversion Engineering Conference, August 25-29, 1986, San Diego, California, pgs. 2.449-2.453

2. Kirk, J.A., Studer, P.A. and Evans, H.E., *"Mechanical Capacitor"*, NASA TND-8185, March 1976.

3. Kirk, J.A. and Huntington R.A. , *"Energy Storage - An Interference Assembled Multi-ring Super-Flywheel"*, Proceedings of the 12th Intersociety Energy Conversion Engineering Conference, Sept. 2, 1977, Washington, D.C., pgs. 517-524

4. Evans, H.E. and Kirk, J.A., *"Inertial Energy Storage Magnetically Levitated Ring-Rotor"*, Proceedings of the 20th Intersociety Energy Conversion Engineering Conference, August 18-23, 1985, Miami Beach, Florida pgs. 2.372-2.377

5. Kirk, J.A.,Anand, D.K., and Khan, A.A., *"Rotor Stresses in a Magnetically Suspended Flywheel System"*, Proceedings of the 20th Intersociety Energy Conversion Engineering Conference, August 18-23, 1985, Miami Beach, Florida, pgs. 2.454-2.462

6. Plant, D.P., Anand, D.K., Kirk, J.A., *"Prototype of a Magnetically Suspended Flywheel Energy Storage System"*, Proceedings of the 24th Intersociety Energy Conversion Engineering Conference, August 7 to August 11, 1989, Washington, D.C.

7. Jeyaseelan,M., Anand, D.K. and Kirk, J.A., *"A CAD Approach to Magnetic Bearing Design"*, Proceedings of the 23rd Intersociety Energy Conversion Engineering Conference, July 31 to August 5, 1988, Denver Co., Volume 2, pgs. 87-91.

8. Plant, D.P., Jayaraman, C.P., Frommer, D.A., Anand, D.K., Kirk, J.A., *"Prototype Testing of Magnetic Bearings"*, Proceedings of the 22nd Intersociety Energy Conversion Engineering Conference, August 10-14, 1987, Philadelphia, Pennsylvania.

9. Plant, D.P., Anand, D.K., Kirk, J.A., Calomeris, A.J., Romero, R.L., *"Improvements in Magnetic Bearings for Flywheel Energy Storage"*, Proceedings of the 23rd Intersociety Energy Conversion Engineering Conference, July 31-August 5, 1988, Denver, Colorado.

10. Plant, D.P., *"Prototype of a Flywheel Energy Storage System"*, Master of Science Thesis, University of Maryland, 1988.

11. Zmood, R.B. , Pang, D., Anand, D.K., and Kirk, J.A., *"Improved Operation of Magnetic Bearings for Flywheel Energy Storage System"*, Proceedings of the 25th Intersociety Energy Conversion Engineering Conference, August 12-17, 1990, Reno, NV.

12. Horn, D., *"Optical Fibers, Optimal Sensors"*, Mechanical Engineering, September, 1988. pp. 84-88.

13. Norton, H.N., *"Handbook of Transducers for Electronic Measuring Systems"*, Prentice-Hall, Inc., Chapters I and 3, 1969.

The NEW ELECTRO-OPTICAL DISPLACEMENT MEASURING SYSTEM for the 13 inch MSBS

Timothy D. Schott, Ping Tcheng
Mail Stop 238
NASA Langley Research Center
Hampton
VA 23665-5225

A NEW ELECTRO-OPTICAL DISPLACEMENT MEASUREMENT SYSTEM FOR THE 13 INCH MSBS

Timothy D. Schott
Engineering Technician

Ping Tcheng, Ph.D.
Senior Research Engineer

Langley Research Center, NASA
Hampton, Virginia 23665

ABSTRACT

The development of a five channel electro-optical model position measurement system is described. The system was developed for the 13 Inch Magnetic Suspension and Balance System (MSBS) located at NASA Langley Research Center. The system consists of five linear photodiode arrays which are illuminated by three low power HeNe lasers, an assembly of lenses and mirrors for shaping the beams, and signal conditioning electronics. The system is mounted to a free standing, pneumatic isolation table to eliminate vibration susceptibility. Two distinct channels are used for sensing vertical displacement and pitch, providing an angle of attack (AOA) measuring range of 40 degrees with a $\pm$.02 degree precision.

INTRODUCTION

The 13 Inch MSBS was originally constructed by Arnold Engineering and Development Center in 1965 and was relocated to NASA LaRC in 1979 [1]. Model position was sensed by a system of X-ray sources and detectors which produced an analog signal proportional to their exposure to the beams. Four beams were directed diagonally across the test section at the model to detect pitch and yaw, while a fifth vertical beam detected axial motion. A suspended model would partially block the X-ray beams, leaving a portion of the detector unexposed, or shadowed. Although the X-ray system was suited for detecting model position through the aluminum test section, the potential safety hazard prompted development of an optical system. The optical system operated on the same principle of blocking a portion of a laser beam (light sheet) with the wind tunnel model and sensing position using light sensitive detectors. A new subsonic wind tunnel with a transparent test section was designed to accommodate the optical system.

The original optical system design was dictated by existing hardware used for mounting of the X-ray system. A series of poles

surrounding the test section allowed fore and aft sliding of the detectors for different lengths of models. Many custom adapters were required to mount the optical system components to the existing structure. The optical components themselves, were limited to very short focal lengths in order to fit in confined areas.

Installation of this system was completed in 1986 and it was successfully used for several years with minimal modifications. The system did suffer some deficiencies, however. Building vibrations were parasitic because of the critical optical alignment. The position sensors were mounted to precision translators partially constructed of magnetic materials. Magnetic field intensity variations would sometimes vibrate the position sensors into a resonance. Optical realignment for various models was tedious and time consuming, often consuming an entire day. The limited AOA range of ± 8 degrees did not meet the requirements of the 13 Inch MSBS, initiating design improvements.

SYSTEM DESCRIPTION

The original system consisted of five identical channels using the same 1-inch position sensors. The new system uses longer position sensors for two of the channels to improve the AOA range, resulting in a combination of two separate subsystems. In addition, a new mounting system for the optics and sensors has been implemented. The following is a detailed description of the new system components.

Position Sensors

Linear, self-scanning photodiode arrays (PDA) were chosen to detect model position. A pair of 1-inch arrays are used for sensing position in side and yaw while a third senses axial position. Each of the 1-inch PDAs contains 1024 individual elements on 25 micron centers. Each device is mounted to a 3 inch square factory supplied circuit board. The circuit boards contain all necessary clock circuits for operation. Modifications allowed the circuits to be operated in a master-slave configuration, driving the arrays with the same 500 KHz clock.

A pair of 2.4-inch arrays are used to detect vertical and pitch position. Each of these arrays contains 4096 elements on 15 micron centers. The commercially available units are presently driven by modified factory circuit boards. A master-slave configuration with a 1.1 MHz clock is also used for these units. The 13 Inch MSBS system computer provides a 256 Hz scan initiate signal, which is synchronized with both of the PDA sampling clocks.

Light Sheet Generating Optics

Two different light sheet generating methods are used for PDA

illumination to accommodate different requirements for each subsystem. The method used to illuminate the 1-inch PDAs is less critical since these are normally operated in saturation. While the device is saturated, it is not sensitive to small intensity variations along its aperture. Minor scratches on the test section windows and dust on the optics generally do not degrade the system operation.

A 5mw HeNe laser beam is fanned by using a 4mm diameter glass rod as a high power cylindrical lens. This quickly expands the beam into a wide angle, reducing the optical path length and saving space. The sheet is then collimated by a 50mm diameter plano-convex cylindrical lens with a focal length of 150mm. Since this combination loses very little power, two PDAs can be illuminated by use of a plate beamsplitter. Figure 1 illustrates how the two side and yaw detectors are illuminated in this manner. The axial array is on its own axis and is, therefore, illuminated by its own 2mw laser and associated optics for simplicity.

The two 2.4-inch arrays used for detecting lift and pitch are not operated in saturation and are very sensitive to intensity variations along the aperture. Several different lens combinations for beam expansion, including commercially available units, were evaluated before satisfactory results were obtained. A double glass rod expander, which spreads a section of the first light sheet a second time to overcome the Gaussian profile was successful but very inefficient since the resulting light sheet is many times wider than the diameter of the collimating lens. A plano-convex cylindrical collimating lens was believed to be necessary to avoid increasing the thickness of the light sheet. A lens was custom ground to meet size and focal length requirements without realizing the effects of distortion on the system accuracy. A laboratory calibration revealed that the collimating lens caused large errors due to spherical aberration and was replaced by a spherical achromatic doublet of longer focal length. Construction of a second light sheet by inserting a plate beamsplitter caused diffraction patterns, ghost images, and added to the intensity variations.

Figure 2 illustrates the present light sheet generation for the two vertical sensors. The expanding optics are basically Keplerian design so that a spatial filter may be used. A 5mw multimode laser was found to improve the uniformity of the light sheet due to its flatter profile. A single plano-convex cylindrical lens with a 6.4 mm focal length spreads the beam while a plano-convex spherical lens with a focal length of 600mm and diameter of 95mm performs the collimation. The inherently small spherical aberration of the high f-number lens reduces system errors at the expense of a long optical path length. Errors may be further reduced with a substantial increase in component cost. Unlike a cylindrical lens, the spherical collimating lens causes the light sheet to change thickness over the path length. If the PDA is located near the focus of the lens, the resulting line will be extremely narrow, making alignment more critical. The greater the distance between

the detector and the lens focus, the thicker the light sheet. A small amount of spreading is desirable to make the system less susceptible to vibration.

Several advantages are gained by splitting the laser beam prior to expansion using a cube beamsplitter. The cube beamsplitter does not rely on uniform metallic deposition and the splitting process has no direct effect on the quality of the light sheets. Although a duplicate set of components is required, the height of the two optical channels may be independently adjusted to the required optical axis. By rotating the beamsplitter about the laser beam axis, the reflected beam angle is varied without affecting the original beam. This feature allows a much higher AOA when equal positive and negative angles are not required during the same test.

Signal Conditioning Electronics

Two signal conditioning schemes are used for each of the PDA types to accommodate two different video signal formats. The 1-inch arrays are operated in saturation and produce a serial train of pulses proportional in amplitude to the exposure of each of the 1024 photodiodes sampled during a scan. The 2.4-inch arrays produce a sample and hold analog signal. The longer array is also more likely to encounter two shadow edges, resulting in two level transitions on the video signal. Detecting two shadow edges and their location requires more sophisticated electronics. The following will describe the two signal processing schemes.

The pulse video signal is carried by coaxial cable to the signal conditioner where a voltage comparator with an adjustable threshold level shapes the signal into TTL compatible rectangular pulses. The pulses are fed to binary ripple counters which count the total number of pixels exceeding the threshold level. The total number of illuminated pixels is then retained by latches for the duration of the following scan. The actual location of the shadow edge is easily determined by the system computer since one end of the PDA must always remain illuminated.

As with the pulse video processing, a voltage comparator is used at the input of the sample and hold video signal conditioner. The comparator transforms the video signal into a clean TTL level pulse by triggering on the voltage level changes occurring at the shadow edges. The comparator's hysteresis band along with various timing delays of other components help reject the diffraction effects on the video signal level transitions. Polarity sensitive monostable multivibrators are used to detect light-dark and dark-light transitions.

The location of a shadow edge is determined by counting PDA sampling clock pulses during each scan. The count is continuously fed to two separate registers during the scan. At the occurrence of a video level change, the appropriate register is enabled, temporarily storing the data until the end of the scan. The data is then shifted to the output registers, where it remains for the

duration of the following scan. An output enable pulse from the system computer controls which tri-state register will be accessed, requiring only one set of lines for both outputs. A balanced, optically isolated, line driver/receiver system is used for signal transfer between the computer and signal conditioner. The 256 Hz scan initiate pulse from the system computer is used for various resetting and clock synchronization. Shown in Figure 3 is a block diagram for one of the two channels.

Mechanical Assembly

An aluminum framework was designed for mounting the position sensors and a portion of the optical components. The mounting system basically consists of two arches joined by two sets of poles allowing fore and aft translation of the three 1-inch PDAs. Precision linear translators allow fine lateral positioning of the 1-inch arrays. The arches were designed to fit between the test section and the electro-magnets. Optical rails mount to either side of the assembly, supporting the entire optical system for the vertical sensing channels. The 2.4-inch PDAs are mounted to custom built aluminum translators for vertical adjustment. The framework assembly is attached to a commercially available 36" X 24" optical breadboard on which the remaining optical components are mounted. The aluminum breadboard provides flexibility of optical layout as well as accepting a broad range of optical holders. Ambient building vibration and magnetic field induced vibrations are minimized by floating the entire system on a pneumatic isolation table. The table, which suppresses vibration above 2 Hz at a rate of 12 db/octave, physically isolates the position sensors from the electro-magnet structure. Figures 4 and 5 are photographs of the optical system before and after installation.

CONCLUSIONS

A new model position detection system has been installed and demonstrated at the 13-Inch MSBS. System AOA range and general reliability is superior to that of the original system while meeting cost and development time requirements. Although the system has not been calibrated in the test environment, separate laboratory calibrations of the 2.4-inch and 1-inch systems were performed [2], [3]. Overall precisions of $\pm.002$ and $\pm.0005$ were displayed in linear measurements while angular precisions of $\pm.02$ degrees and $\pm.015$ degrees were exhibited by the 2.4-inch and 1-inch systems respectively. Mechanical difficulties remain to be a primary shortcoming. The physical size of the factory circuit boards limit the vertical adjustment range of the 2.4-inch PDAs, directly affecting the AOA range. Smaller clock-generating circuit boards are currently under development to alleviate this problem.

REFERENCES

[1] Mathews, R.K.; Brown, M.D.; Langford, J.N., "Description and Initial Operation of the AEDC Magnetic Model Suspension Facility: Hypersonic Wind Tunnel (E)", AEDC-TR-70-80, May 1970.

[2] Tcheng, P. and Schott, T.D., "A Five Component Electro-Optical Positioning System", ICIASF '87 Record. International Congress on Instrumentation in Aerospace Simulation Facilities, pp. 322-337.

[3] Schott, T.D., and Tcheng, P., "A High Resolution Electro-Optical Displacement Measurement System", Proceedings of the 35th International Instrumentation Symposium, Instrument Society of America, 1989, pp. 441-454.

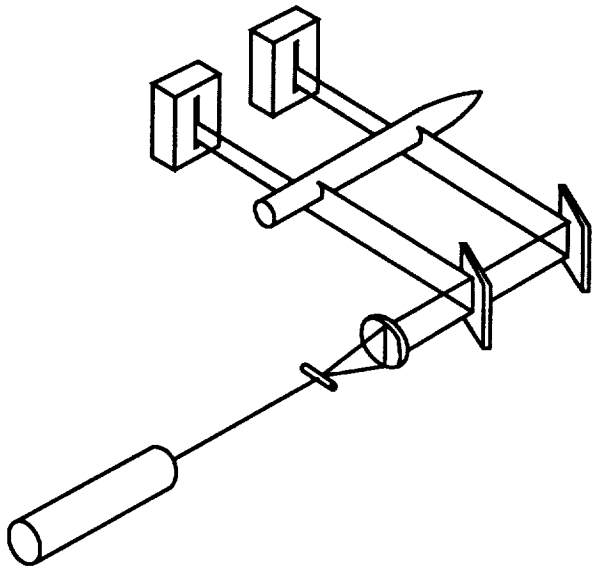

Figure 1

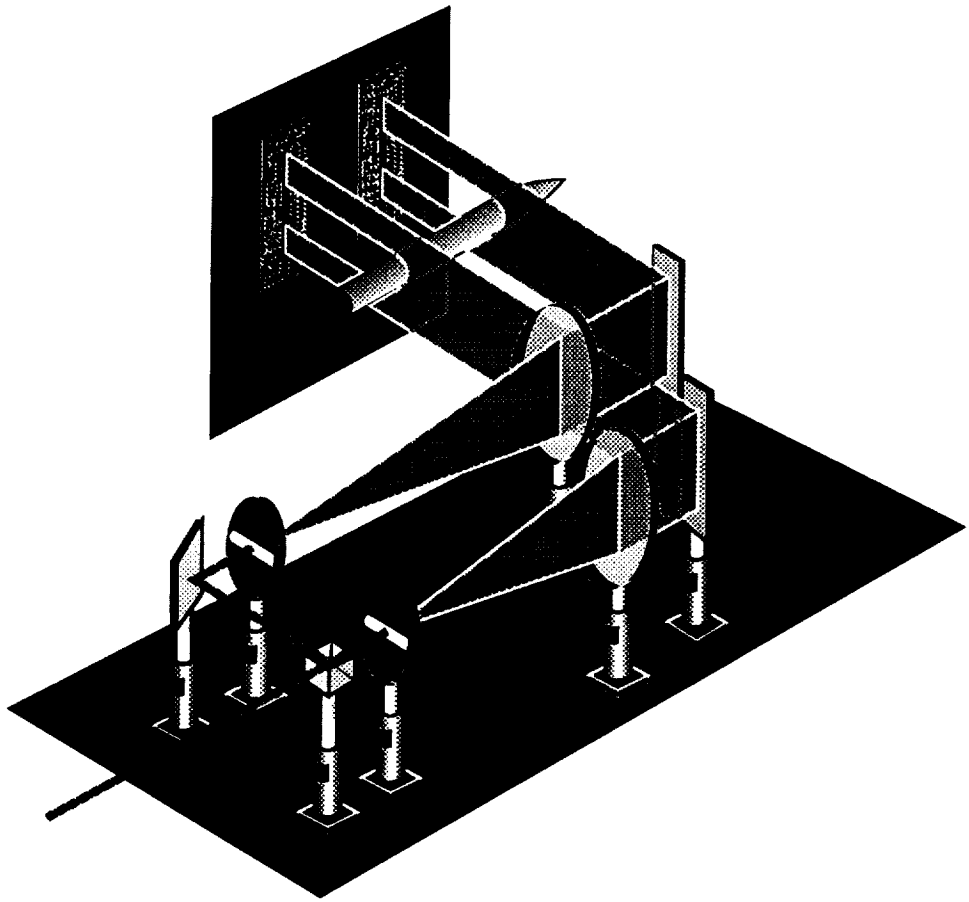

Figure 2

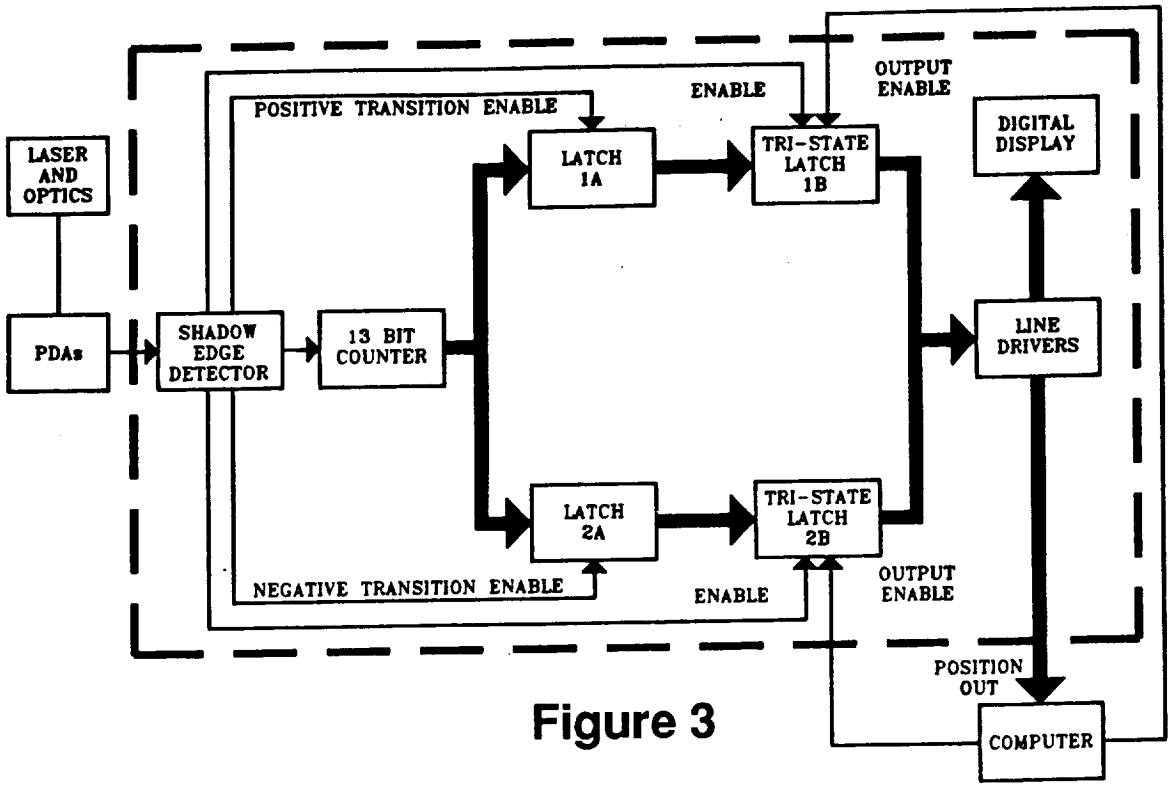

Figure 3

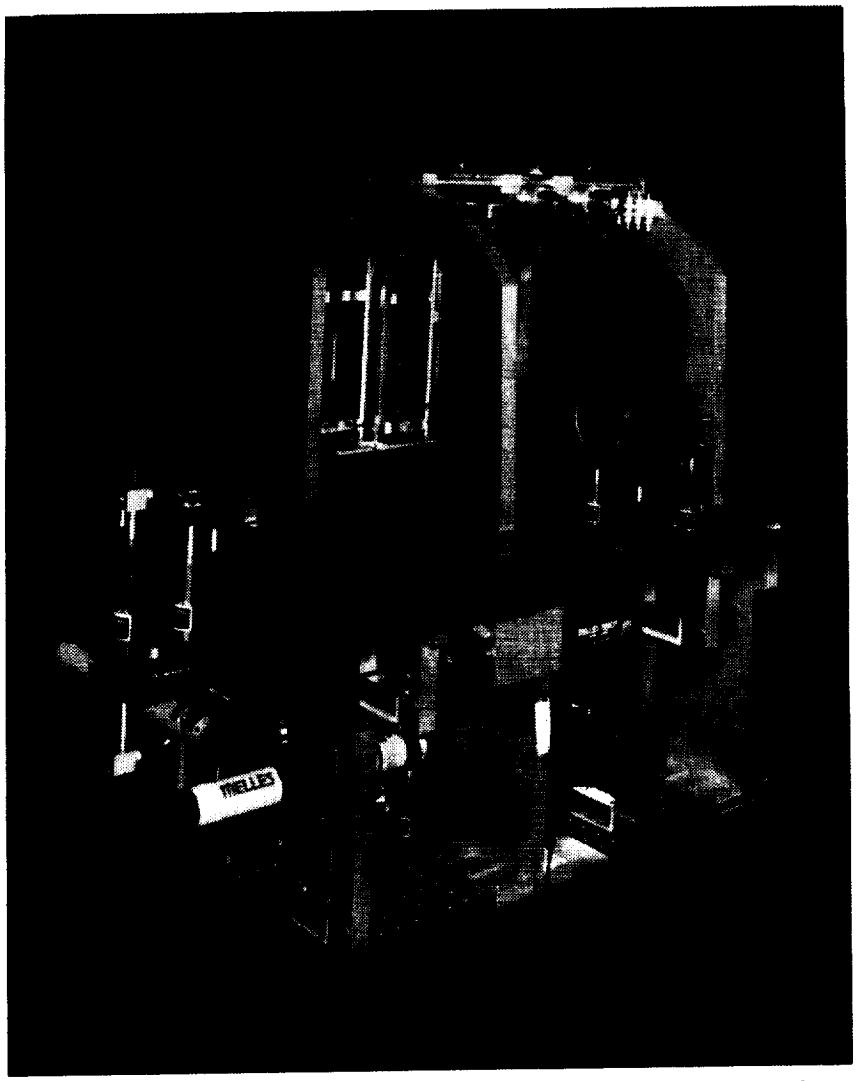

Figure 4

ORIGINAL PAGE
BLACK AND WHITE PHOTOGRAPH

ORIGINAL PAGE IS
OF POOR QUALITY

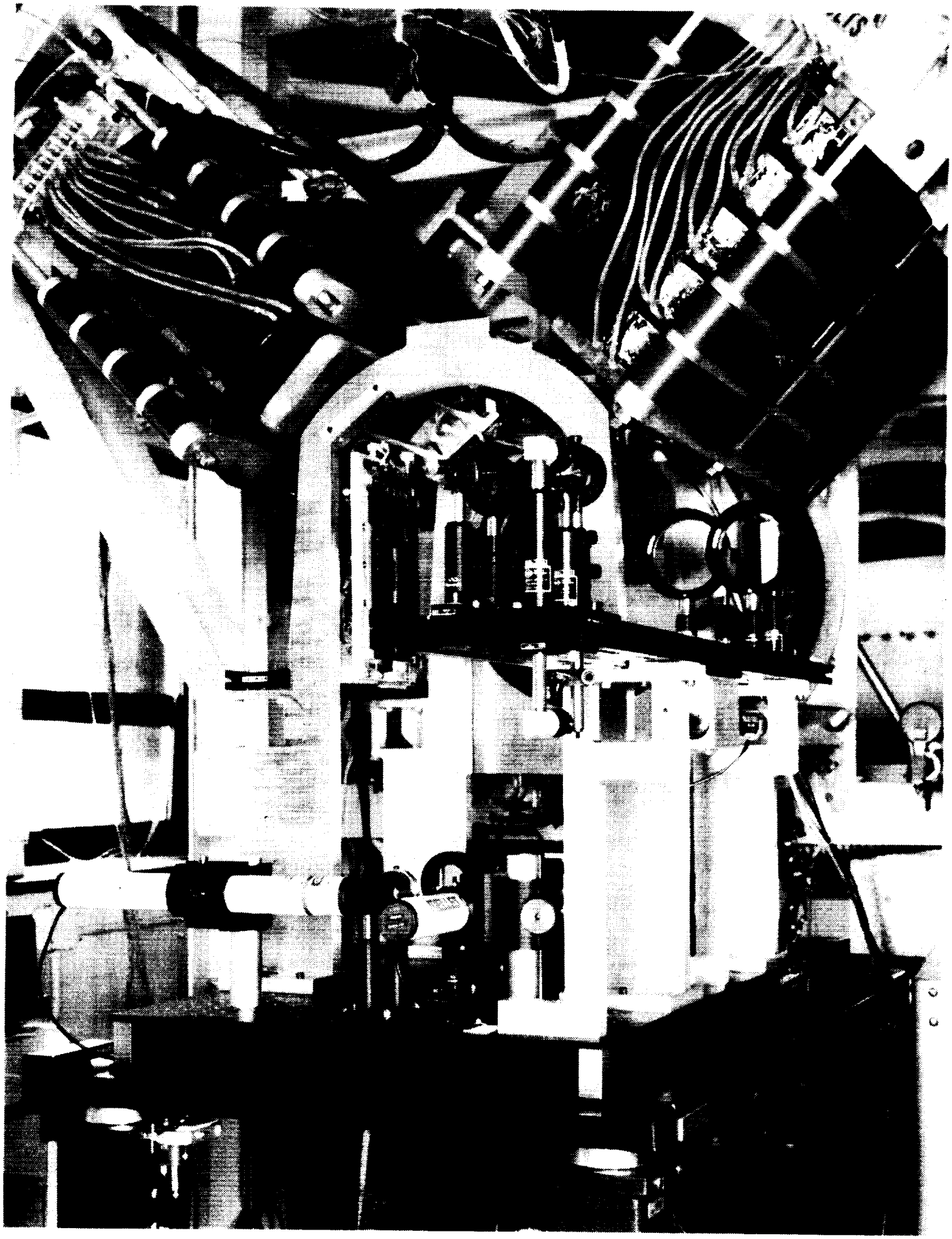

Figure 5

ORIGINAL PAGE
BLACK AND WHITE PHOTOGRAPH

The OPTICAL POSITION MEASUREMENT SYSTEM for a LARGE-GAP MAGNETIC SUSPENSION SYSTEM (LGMSS)

Sharon S. Welch
Mail Stop 161
NASA Langley Research Center
Hampton
VA 23665-5225

James I. Clemmons Jr.
Vigyan Research Associates
30 Research Drive
Hampton
VA 23665

Summary

A photogrammetric optical position measurement system is currently being built as part of the NASA Langley Research Center Large-Gap Magnetic Suspension System (LGMSS). The LGMSS is a five degree-of-freedom, large-gap magnetic suspension system to be built in the Advanced Controls Test Facility (ACTF). The LGMSS consists of a planar array of electromagnets which levitate and position a model containing a permanent magnet core. Information on model position and attitude is required to control the position of the model and stabilize levitation. The optical position measurement system determines the position and attitude of a levitated model in six degrees of freedom and provides this information to the system controller. Eight optical sensing units positioned above the levitated model detect light emitted by small infrared Light Emitting Diodes (LEDs) embedded in the surface of the model. Each LED target is imaged by a cylindrical lens on a linear Charge Coupled Device (CCD) sensor. The position and orientation of the model are determined from the positions of the projected target images. A description of the position measurment system, tracking algorithm, and calibration techniques, as well as simulation and preliminary test results of the position measurement system will be presented.

Introduction

A Large-Gap Magnetic Suspension System (LGMSS) is currently being built at NASA Langley Research Center to test control laws for magnetic levitation for vibration isolation and pointing. A photogrammetric optical position measurement system has been designed and is currently being fabricated at NASA Langley as a part of the LGMSS. The optical position measurement system will measure the position and attitude of a levitated body in six degrees of freedom and supply this information to the LGMSS control system. This paper will describe the requirements for the position measurement system, and present the design of the system as well as some preliminary test results on a prototype sensor. A high level description of the system will first be presented. This will be followed by a discussion of the tracking and calibration techniques. Lastly, details of the system design will be presented and some conclusions about the performance of the optical sensing system.

Presentation Outline

Position Measurement System Requirements

Overview of the Sensing System

Tracking and Calibration Techniques

Closeup of the Sensing System

Experimental Results

Position Sensing Requirements

The requirements for the position measurement system are derived from the requirements for the LGMSS. There are three fundamental requirements for the position measurement system. These requirements are: 1) that the sensing system be able to track the levitated body to an accuracy consistent with the accuracy requirements for the LGMSS; 2) that the position information supplied by the sensing system be supplied at a high enough rate that the LGMSS can stabilize levitation of the model; and 3) that the measurement made by the sensing system not interfere with the function of the LGMSS.

To meet the three requirements specified above, a photogrammetric optical sensing approach was selected. Small point targets embedded in the surface of the levitated body are detected by multiple cameras positioned about the model. The locations of the projected target images are determined and triangulation techniques are used to determine the position and attitude of the model from this information. The accuracy requirement for the optical sensing system is set by the accuracy requirement for the LGMSS. The LGMSS is required to position a levitated model to an accuracy of +/- 0.01 inches in x, y, and z, and +/- 0.02 degrees in yaw, pitch, and roll (defined by the Euler angles psi, theta, and phi). The optical sensing system is allowed thiry percent of the error budget and thus the required accuracy for the sensing system is +/- 0.003 inches in x, y, and z, and +/- 0.006 degrees in psi, theta, and phi. The frequency response for the optical sensing system is 20 samples/second. This is not a fast update rate, but is fast enough that the LGMSS can control the levitation of the model to the accuracy specified for the system.

Position Sensing Requirement

Position Measurement Accuracy

+/- 0.003 inches xcm, ycm, zcm
+/- 0.006 degrees in psi, theta, phi

Frequency Response

20 samples/second

Noninvasive Measurement

Overview of the Optical Sensing System

In figure 1 is a block diagram of the optical sensing sytem. Eight infrared light emitting diode (LED) targets are embedded in the surface of the levitated model. The targets are multiplexed in time for target identification. As each target is flashed on, it is detected by sixteen linear charge coupled device (CCD) array sensors. A cylindrical lens, positioned in front of the detector focuses the light emitted by a target as a line of light on the detector array. Each array has 2048 photosensitive elements. A voltage signal is output from the array which is proportional to the light falling on each element or pixel. (figure 2) The location of each target image along the CCD array is determined by calculating the location of the centroid of the light distribution falling on the detector. The analogue video signal output of each CCD sensor is digitized and stored in a random access memory (RAM) which can be accessed by a high speed digital signal processor (DSP). There are a total of sixteen analogue to digital converters (one for each sensor), and sixteen DSPs (Texas Instruments TMS320C30s). The location of the centroid of light is calculated by the DSP and stored in a central memory. The locations of the target images in the sensors are used to determine the position and attitude of the levitated model. Data flow from the DSPs to the central memory is controlled by a 68000 based microcontroller. The calculation of model position and attitude is performed in an I860 based array processor. The array processor resides on a VME bus and is controlled by a SUN computer.

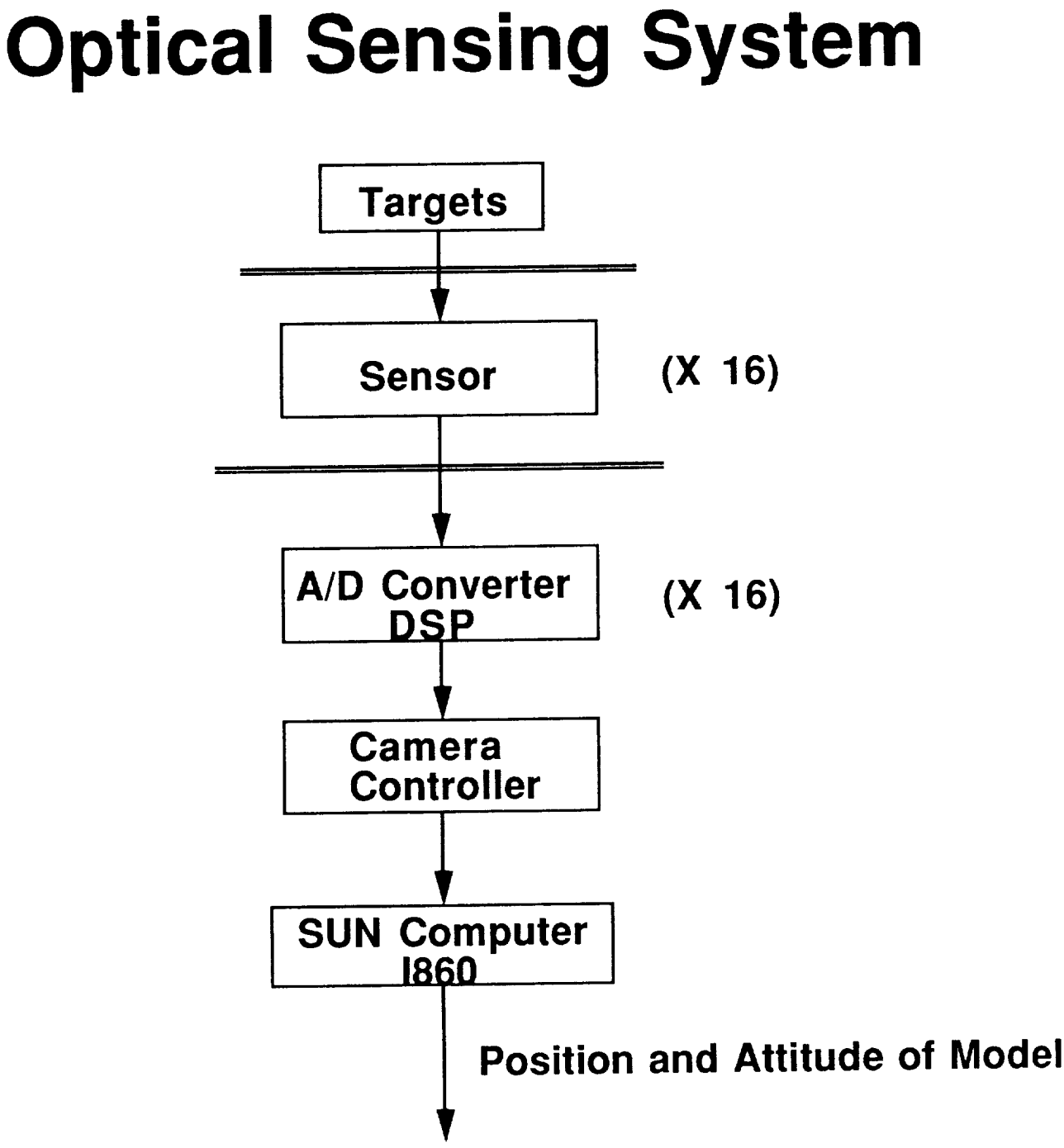

Figure 1. Block diagram of the optical sensing system showing signal flow.

LIGHT DISTRIBUTION

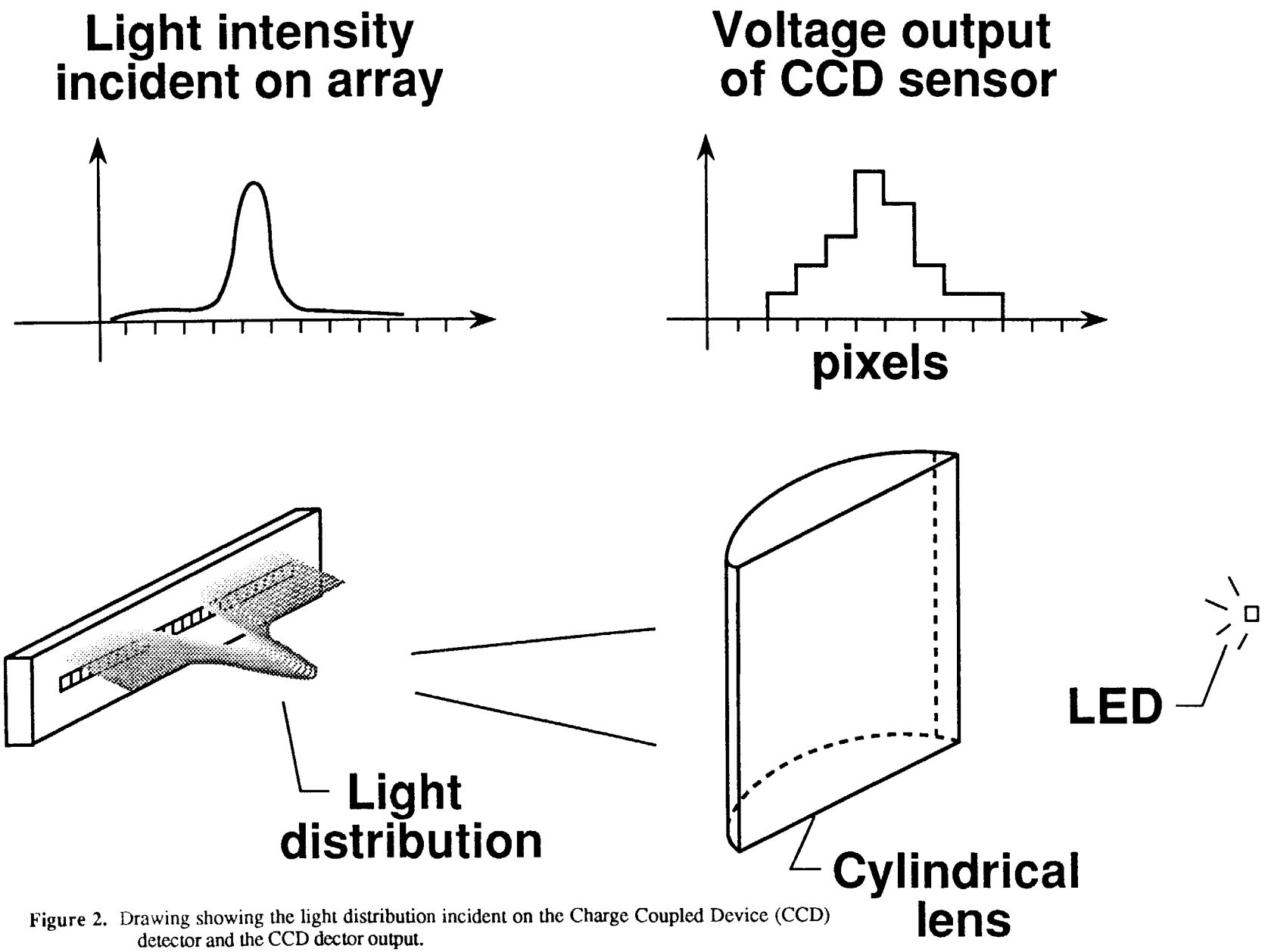

Figure 2. Drawing showing the light distribution incident on the Charge Coupled Device (CCD) detector and the CCD dector output.

Sensing Unit

Eight sensing units are located symmetrically about, and approximately five feet above the levitated model. Each sensing unit consists of two linear CCD sensors oriented orthogonally with respect to one another.(figure 3) The output of each sensing unit is thus an x and y camera location for each projected target image. Each sensing unit is mounted to the sensing system support structure. The sensing unit mount allows the orientation of the sensing unit to be adjusted in two angular directions as well as the verticle direction.(figure 4)

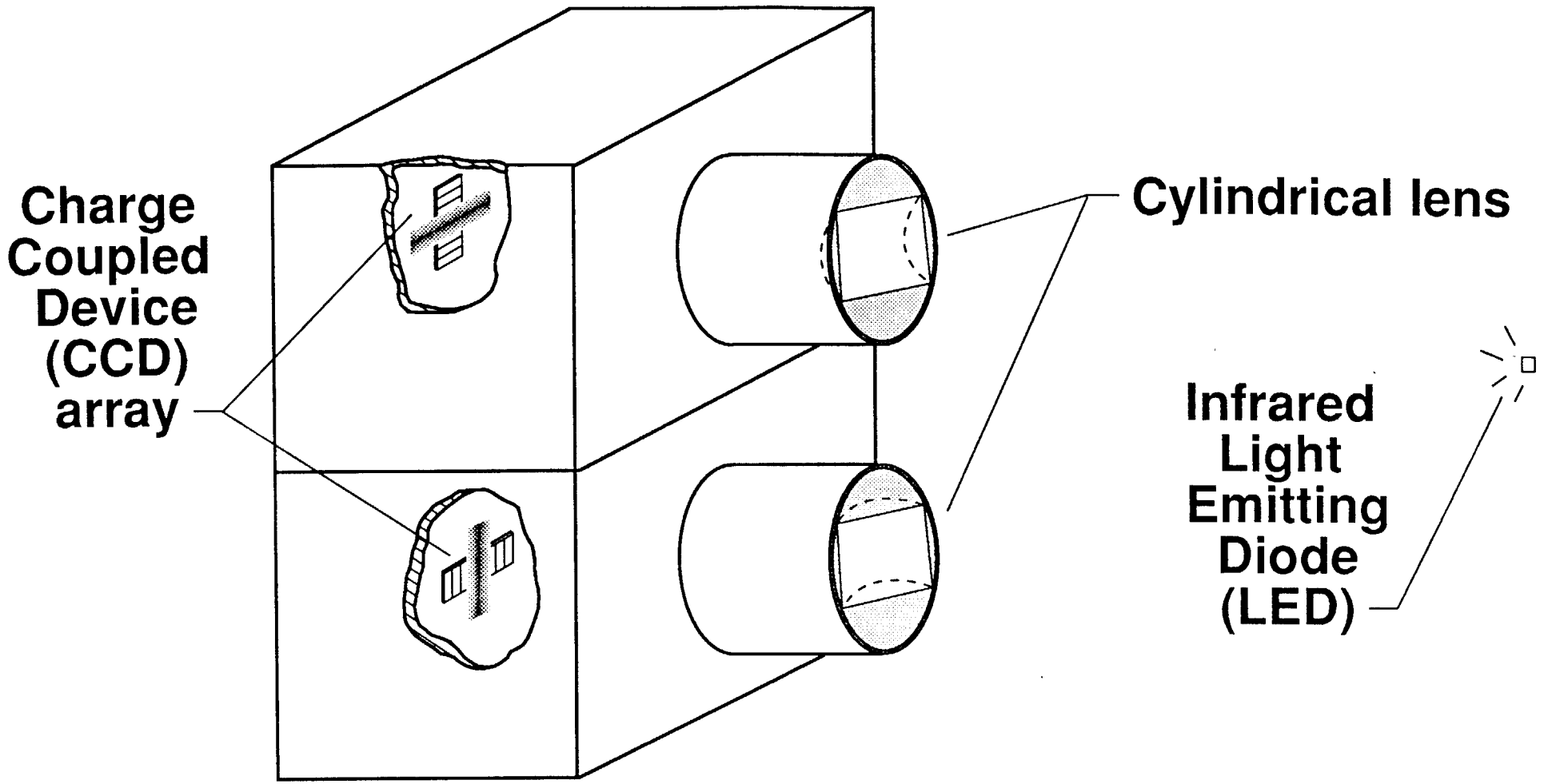

Figure 3. Drawing of a sensing unit. Each sensing unit consists of two CCD cameras oriented orthogonally.

DIAGRAM OF SENSING UNIT MOUNT

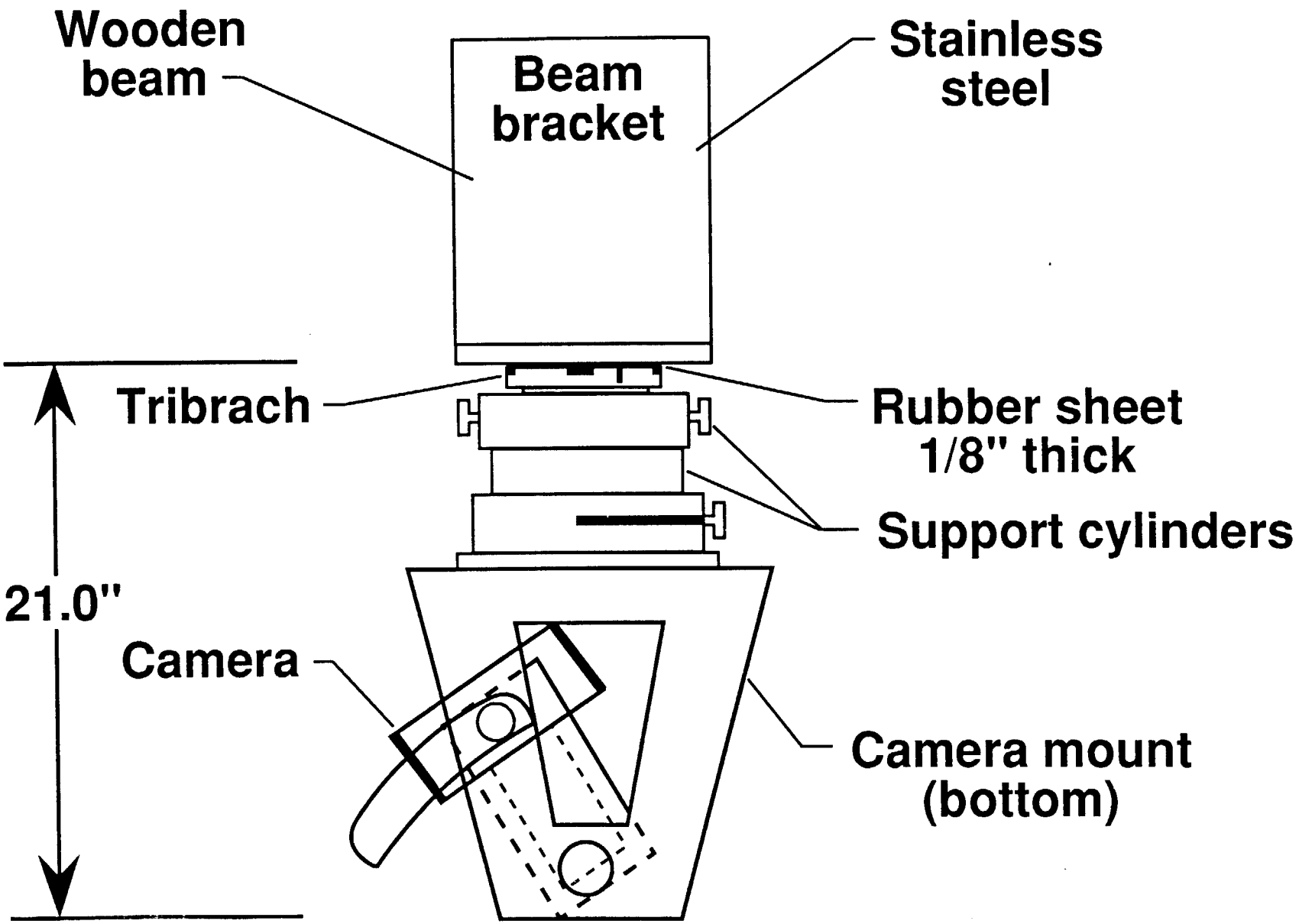

Figure 4. Drawing of sensing unit mount.

Coordinate System Definition

The coordinate system for the LGMSS and position measurement system is a right hand cartesian coordinate system.(figure 5) The z axis points up. The position of the levitated model is defined by the x, y, and z position of the origin of a body fixed reference frame in the laboratory (or fixed) reference frame. The orientation of the model is defined by the Euler angles ψ, θ, φ (yaw, pitch, roll). The rotation sequence is yaw, pitch, and roll.

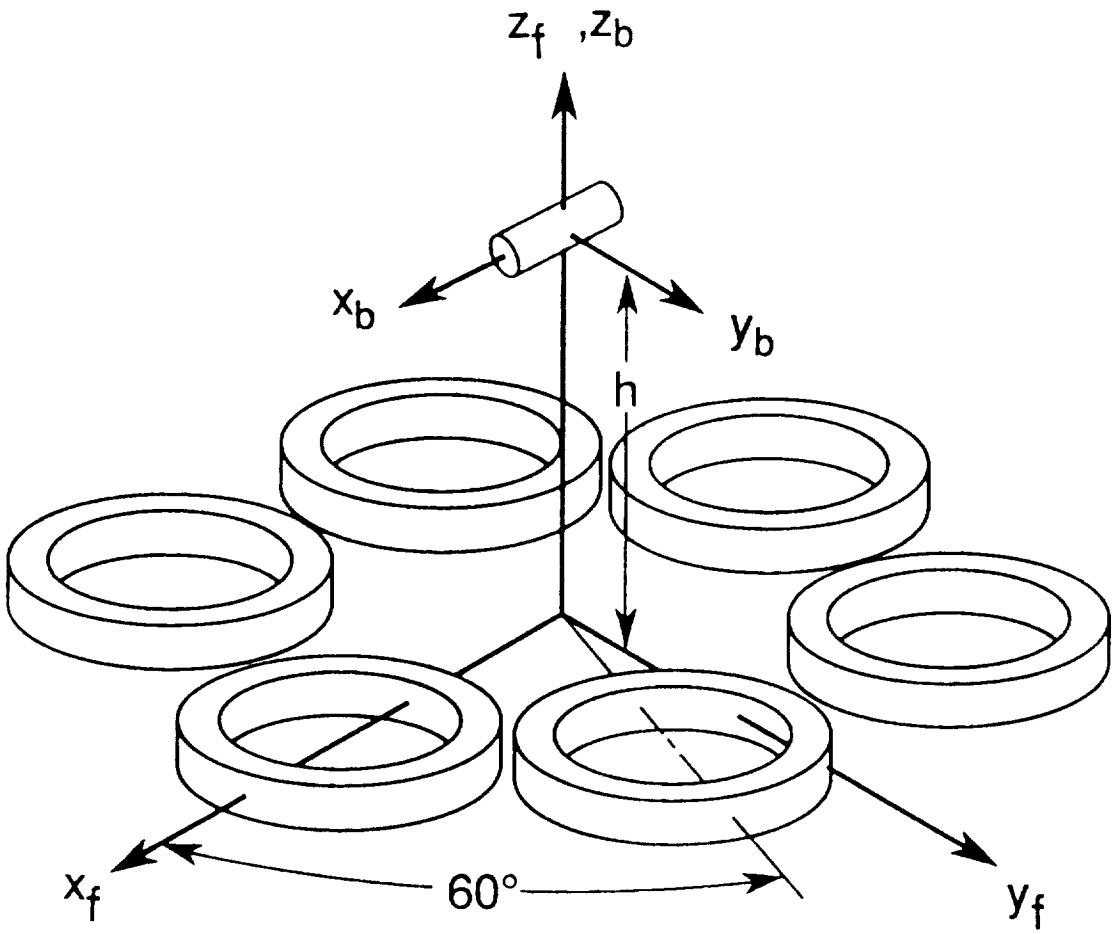

Figure 5. Diagram showing cylindrically shaped model levitated by a six coil magnetic suspension system. Coordinate systems of body and suspension system indicated by subscripts b and f, respectively.

Transformation Equations

The position and orientation of the model are determined by solving a set of nonlinear equations which relate the measured x and y camera coordinates of each target to the six parameters, x_{cm}, y_{cm}, z_{cm}, ψ, θ, and φ. Two sets of transformation equations are listed below. The first set of transformation equations describe the transformation from body fixed reference frame coordinates (x_b, y_b, z_b) to laboratory or fixed reference frame coordinates (x_f, y_f, z_f) in terms of the coordinates of the origin of the body frame in the laboratory frame (x_{cm}, y_{cm}, and z_{cm}) and the orientation of the body frame with respect to the fixed frame, given by the sines and cosines of the Euler angles psi (ψ), theta (θ), and phi (φ). The second set of transformation equations describe the transformation from laboratory reference frame coordinates for the jth target (x_{fj}, y_{fj}, z_{fj}) to the ith camera (x_{ij}, y_{ij}) in terms of the x, y, z position of the perspective center of each camera in the laboratory reference frame, denoted by X_i^c, Y_i^c, and Z_i^c, and the orientation of each camera with respect to the laboratory reference frame. In the second set of equations, the mij are elements of the rotation matrix and are functions of the camera pointing angles. The terms x_{pi} and y_{pi} are the principal points for the ith camera, and $f_{x,yi}$ is the focal length of camera i. The positions and orientations of each camera are determined by an independent survey and through calibration.

Substituting the first set of transformation equations below into the second produces a set of nonlinear equations which decribes the dependence of the xij and yij positions of the projected images of target diode j in sensing unit i in terms of the position and orientation of the model. The position and orientation of the model are given by the six parameters x_{cm}, y_{cm}, z_{cm}, ψ, θ, φ. With eight targets and eight sensing units, 128 equations are thus generated. These equations are linearized and solved using an iterative technique (Newton's Method).

$$x_{fj} = x_{cm} + x_{bj}(\cos(\theta)\cos(\Psi) + y_{bj}(-\cos(\varphi)\sin(\psi) + \sin(\varphi)\sin(\theta)\cos(\psi)) + z_{bj}(\sin(\varphi)\sin(\psi) + \cos(\varphi)\sin(\theta)\cos(\psi))$$

$$y_{fj} = y_{cm} + x_{bj}(\cos(\theta)\sin(\psi) + y_{bj}(\cos(\varphi)\cos(\psi) + \sin(\varphi)\sin(\theta)\sin(\psi) + z_{bj}(-\sin(\varphi)\cos(\psi) + \cos(\varphi)\sin(\theta)\sin(\psi))$$

$$z_{fj} = z_{cm} + x_{bj}(-\sin(\theta)) + y_{bj}(\sin(\varphi)\cos(\theta)) + z_{bj}(\cos(\varphi)\cos(\theta))$$

$$x_{ij} = x_{pi} + f_{ix}\left[\frac{m_{11}(x_{fj} - X_{xi}^c) + m_{12}(y_{fj} - Y_{xi}^c) + m_{13}(z_{fj} - Z_{xi}^c)}{m_{x31}(x_{fj} - X_{xi}^c) + m_{x32}(y_{fj} - Y_{xi}^c) + m_{x33}(z_{fj} - Z_{xi}^c)}\right]$$

$$y_{ij} = y_{pi} + f_{iy}\left[\frac{m_{21}(x_{fj} - X_{yi}^c) + m_{22}(y_{fj} - Y_{yi}^c) + m_{23}(z_{fj} - Z_{yi}^c)}{m_{y31}(x_{fj} - X_{yi}^c) + m_{y32}(y_{fj} - Y_{yi}^c) + m_{y33}(z_{fj} - Z_{yi}^c)}\right]$$

Targets

As stated previously, eight infrared light emitting diode targets are embedded in the top surface of the model. Each target consists of an LED chip soldered into a small parabolic reflector.(figure 6) The wavelength of the light is 850 nm. The diameter of the reflector is 0.047 inches. Figures 6 - 11 show a diagram of the cross section of a target, a picture of a target compared to a dime, a graph of the spatial distribution of the light output from an LED target, a picture of a cylindrical model with the targets embedded in the surface, a picture of the circuit board for the target driver electronics, and a diagram showing the timing pulses. The larger diameter shown in diagram 6 is a heat sink. Special bonding techniques had to be developed which would provide adequate heat conduction when the diodes are driven at high current levels. The materials which are used to bond the LED and leads to the reflector are noted in diagram 6.

The driver electronics and power supply for the targets are all located on the model. The size of the driver electronics package is about 1 inch in diameter and 0.25 inches in thickness. Two nickel cadmium (rechargeable) batteries are provided. The dimensions of the batteries are 1 inch in diamter and about 1 inch in length. These batteries can provide sufficient power to operate for about 2 hours.

In addition to the target diodes, two additional strobe diodes, located on the bottom surface of the model are used to time the sensor acquisition of each target and detect the flashing of the first of the eight targets (or the beginning of frame). Diagram 11 shows the timing pulses for the prototype model. The timing diodes are separated from the target diodes in wavelength. The photodetectors used to detect these diodes, which are located beneath the levitated model, are filtered..

During tracking of the model, each of the eight target diodes is turned on in sequence for a period of time which may range from approximately 1.25 ms to 3.75 ms. (The length of time is determined by resistor values which are set in driver circuitry located in the model.) During this time, the CCD sensors integrate the light falling on the array. Following integration, the signal is read out and the centroid location is determined. After all eight diodes have been illuminated they are turned off during the time the sensing system is calculating the position and attitude of the model. The length of time required to calculate the position and attitude of the model is 15 ms. Following the calculation, the computed position and attitude information is sent to the LGMSS controller and a new frame is begun.

LIGHT EMITTING DIODE TARGET

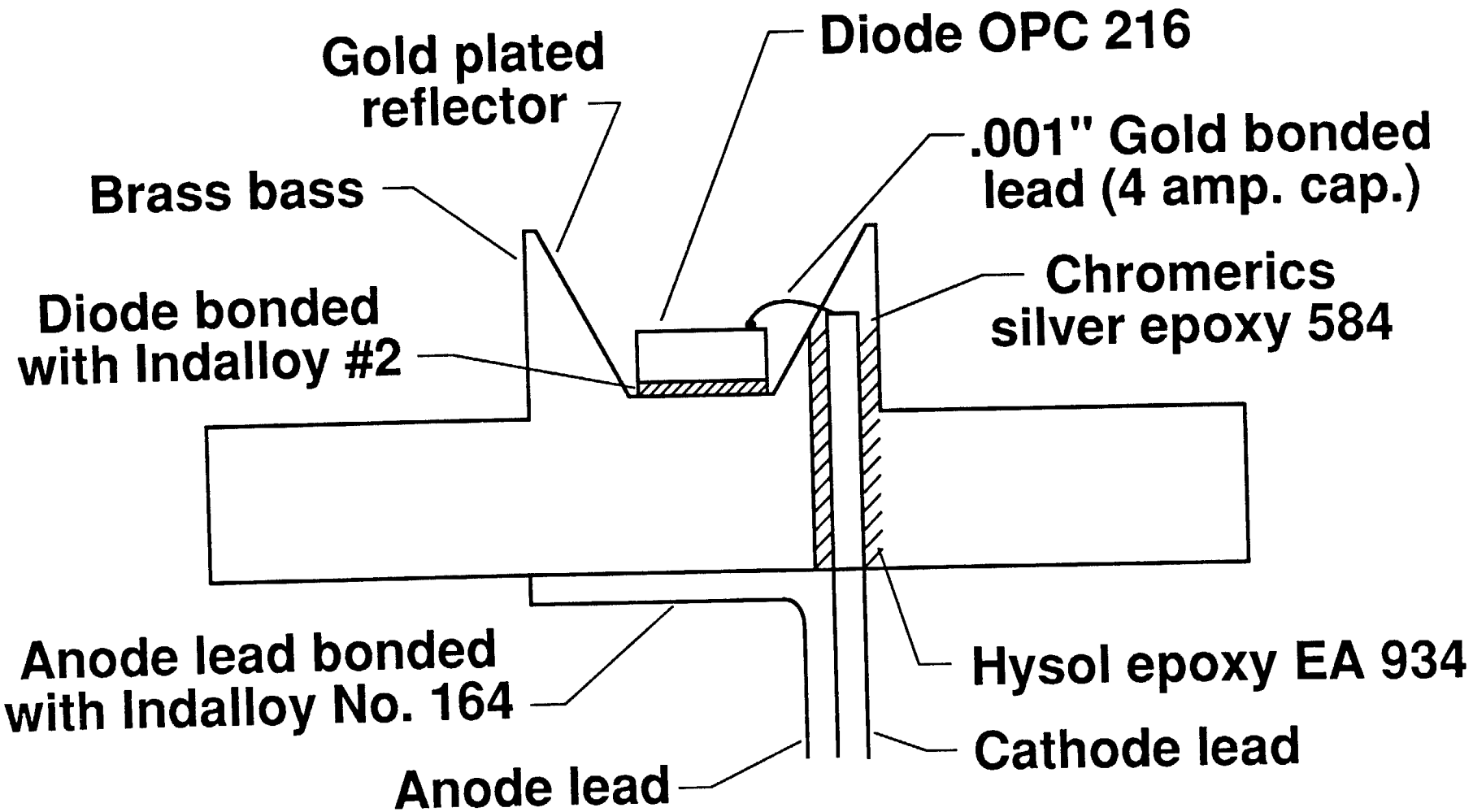

Figure 6. Drawing of a Light Emitting Diodc (LED) target cross section.

Figure 7. Picture of a target LED next to a dime.

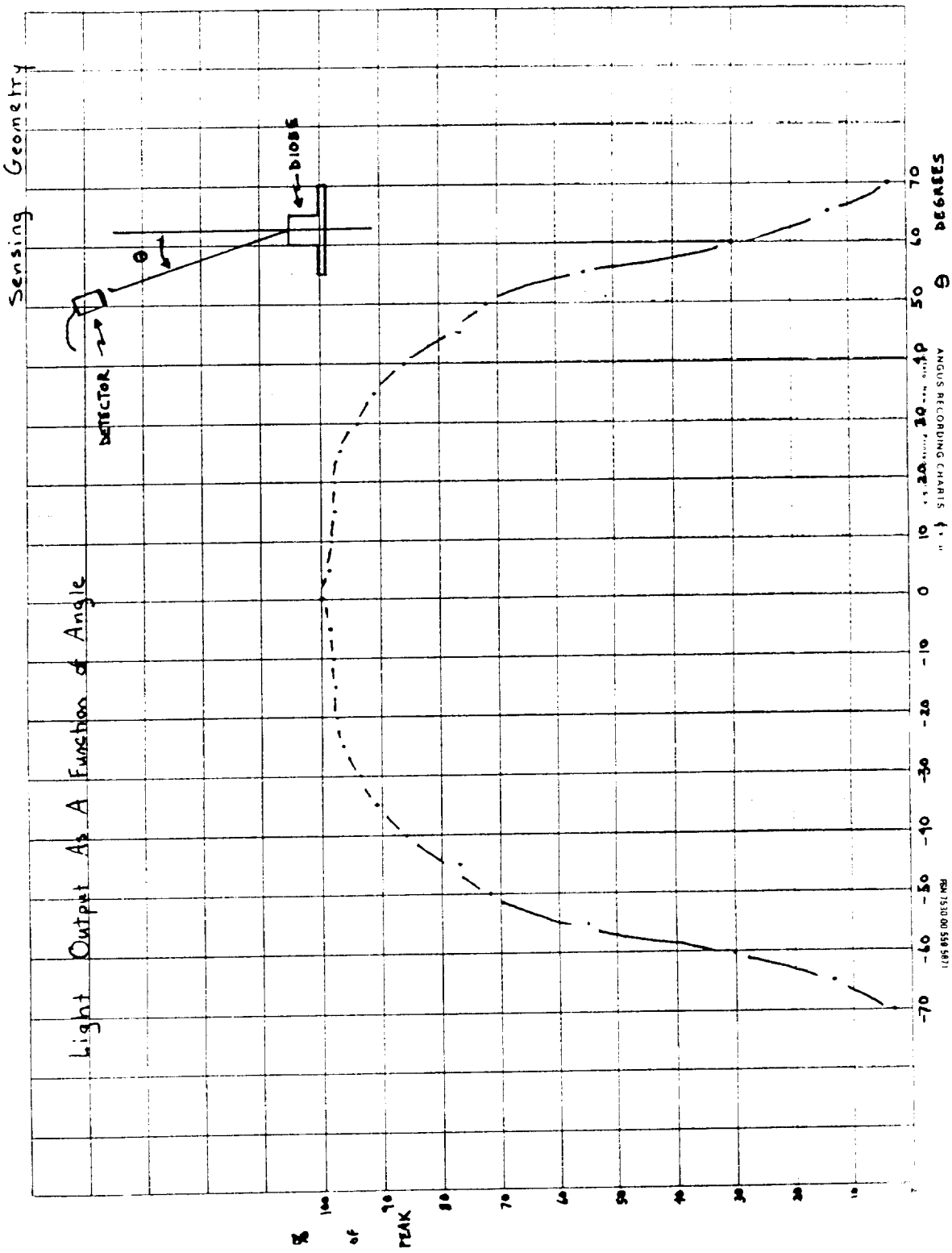

Figure 8. Graph of spatial distribution of light emitted by LED target.

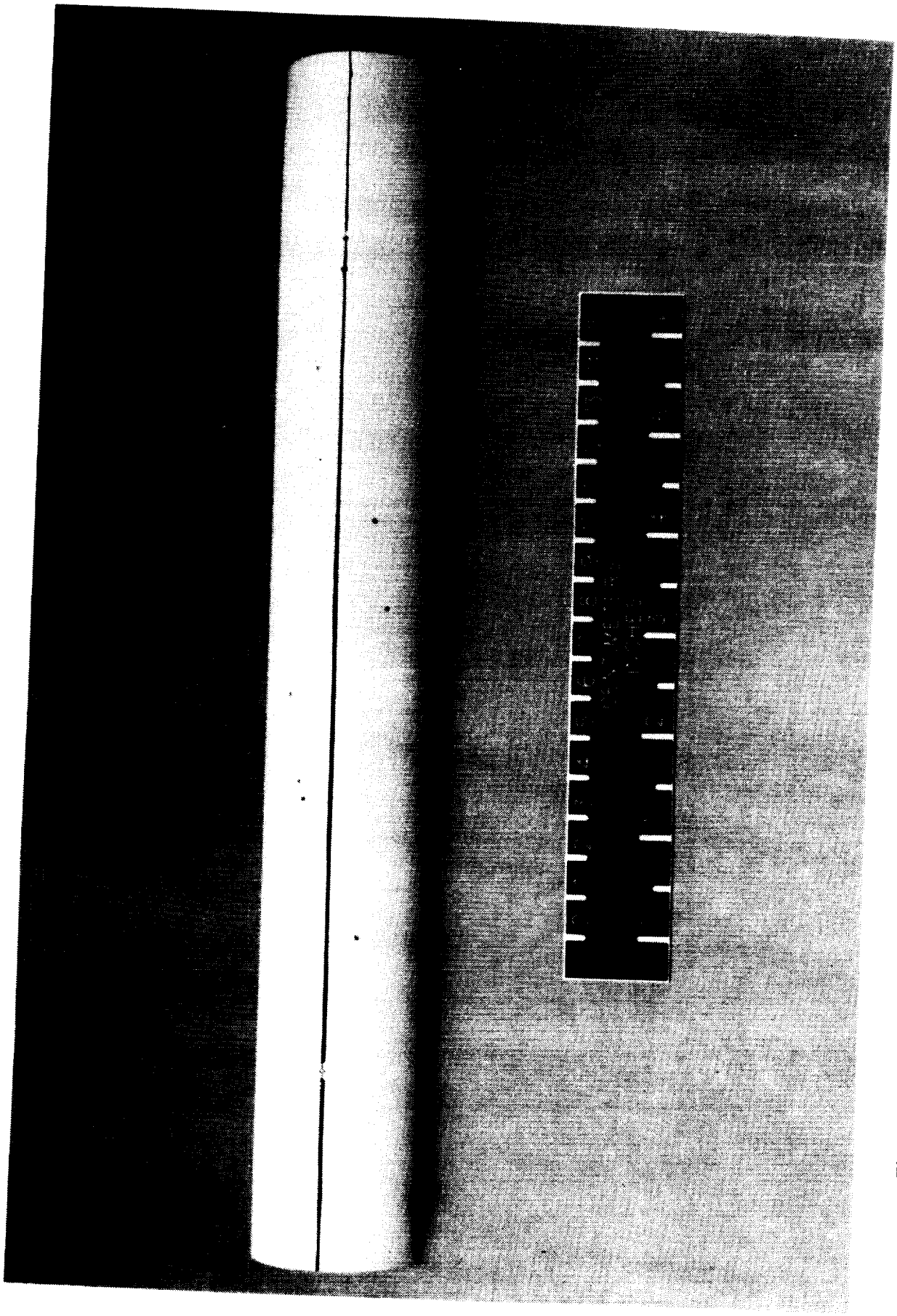

Figure 9. Picture of cylindrical model with targets embedded in the surface.

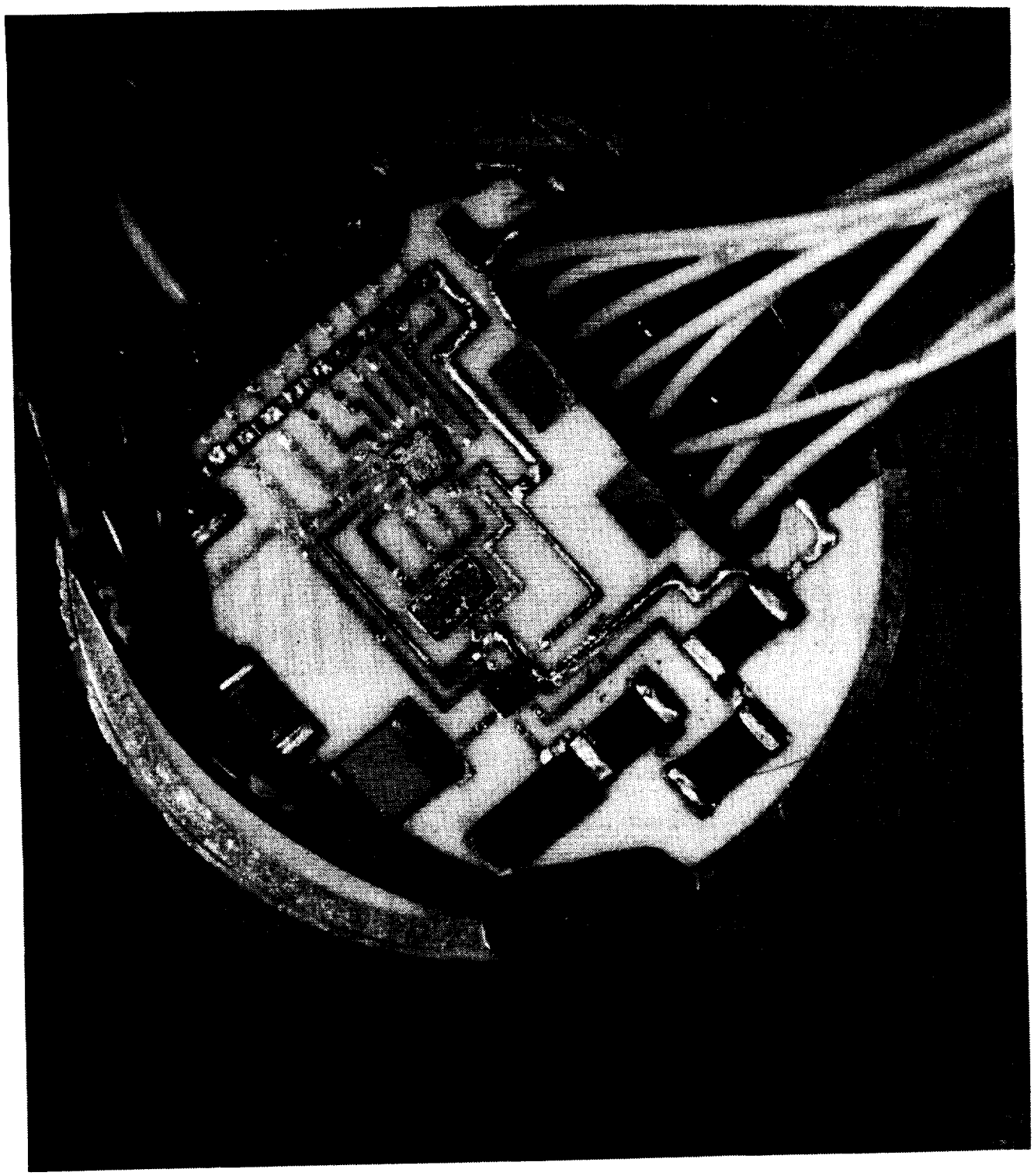

Figure 10. Picture of LED target driver electronics circuit board.

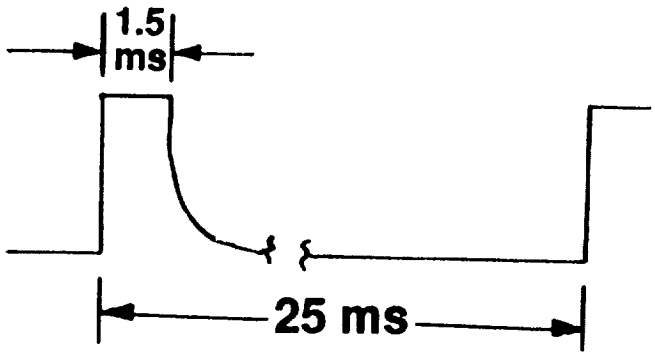

(a)

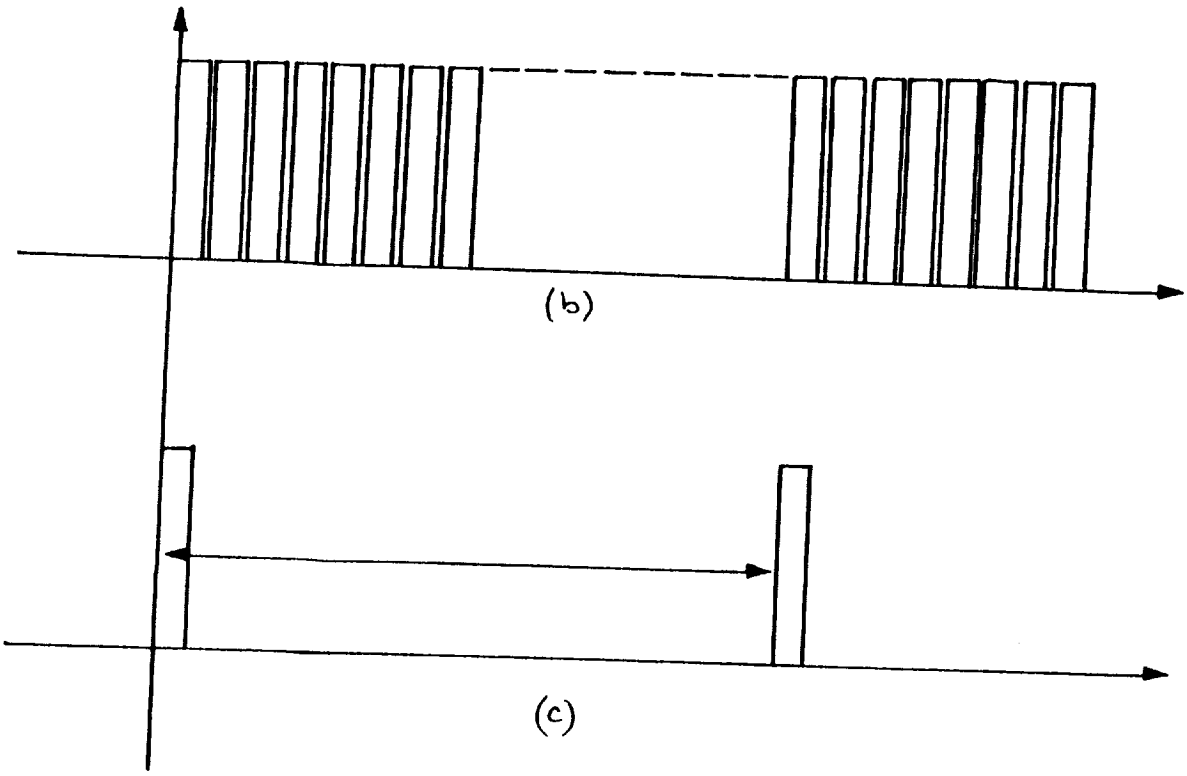

Figure 11. Diagram of the timing pulses for beginning of frame and acquisition of a single target. a) Pulse for a single diode. b) Pulses generated by strobe diode for timing. c) Pulses generated by strobe diode for timing the beginning of a set of eight diodes.

Sensor Electronics

Figures 12 - 14 show pictures of the various sensor components. Figure 12 shows the front and back view of the camera board. Also shown is the thermoelectric cooler circuitry. Some of the components on the camera board are being operated at high clock speeds. As a result, without active cooling, these parts will overheat and be destroyed. A thermoelectric cooler is provided to actively cool these parts. A thermoelectric cooler was used to avoid inducing vibrations which could disturb the optical measurement. Figures 13 and 14 show pictures of the analogue to digital converter and digital signal processor boards, respectively.

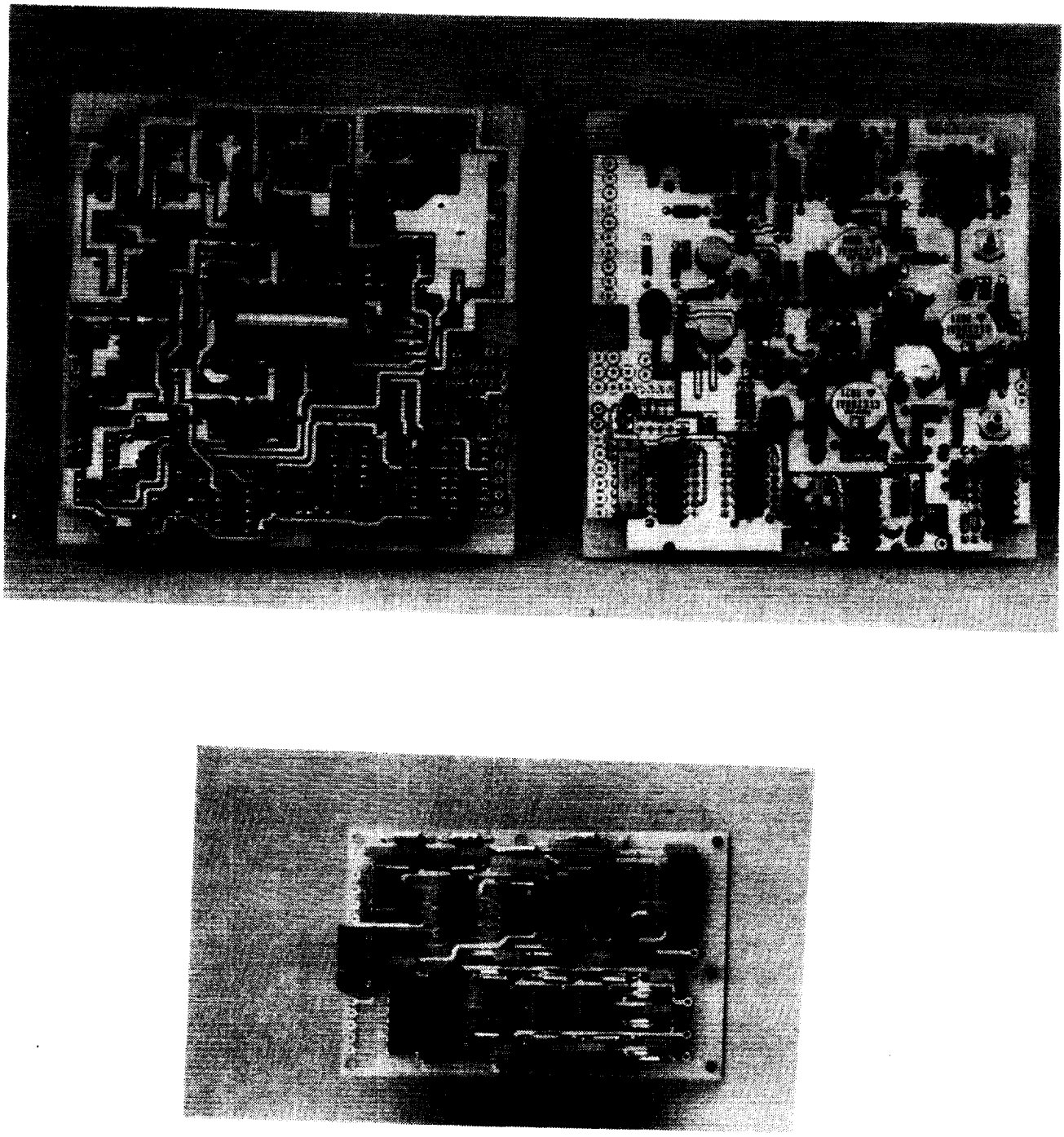

Figure 12. Pictures of camera board (front and back view) and thermoelectric cooler board.

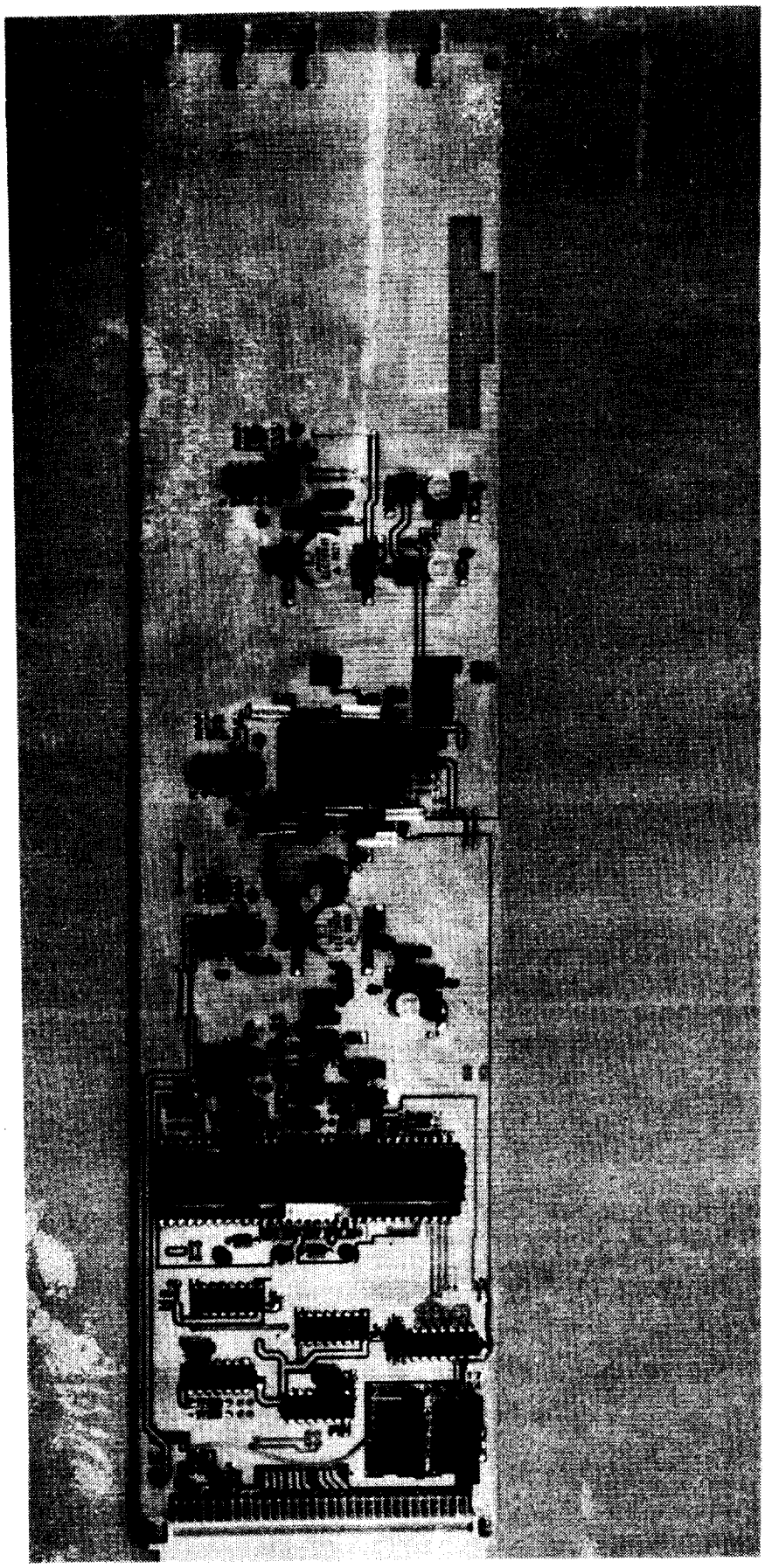

Figure 13. Shown in this picture is the analogue-to-digital (A/D) converter board. The A/D is a 10 bit flash capable of a maximum data conversion rate of 20 megasamples/second.

Figure 14. On the following page is a picture of the digital signal processor (DSP) board. The DSP is a Texas Instruments TMS320C30. The clock speed is 32 mHz which yields an instruction cycle time of approximately 60 ns. The total time to perform the calculation of the centroid, background, and signal-to-noise ratio is about 1 ms.

ORIGINAL PAGE
BLACK AND WHITE PHOTOGRAPH

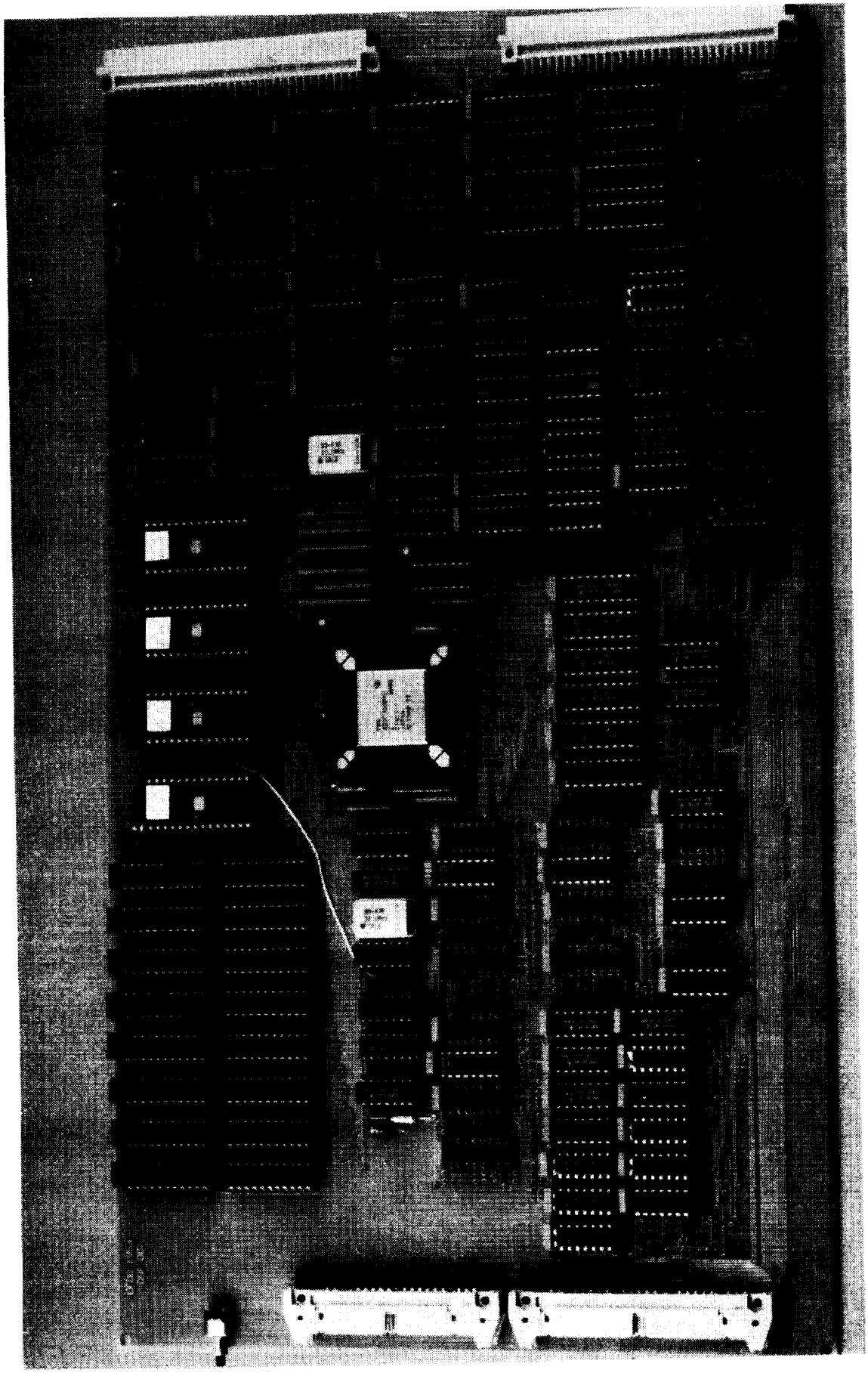

Graphs of Output of Prototype Sensor

Figure 15 is a graph showing the digital output of a prototype CCD sensor when imaging the cylindrical model of figure 9. The integration time of the camera was set to integrate over the entire frame time of all eight targets. Figure 16 is a graph of a portion of the digital output of a camera when imaging a single LED target. The light distribution spans approximately 11 pixels.

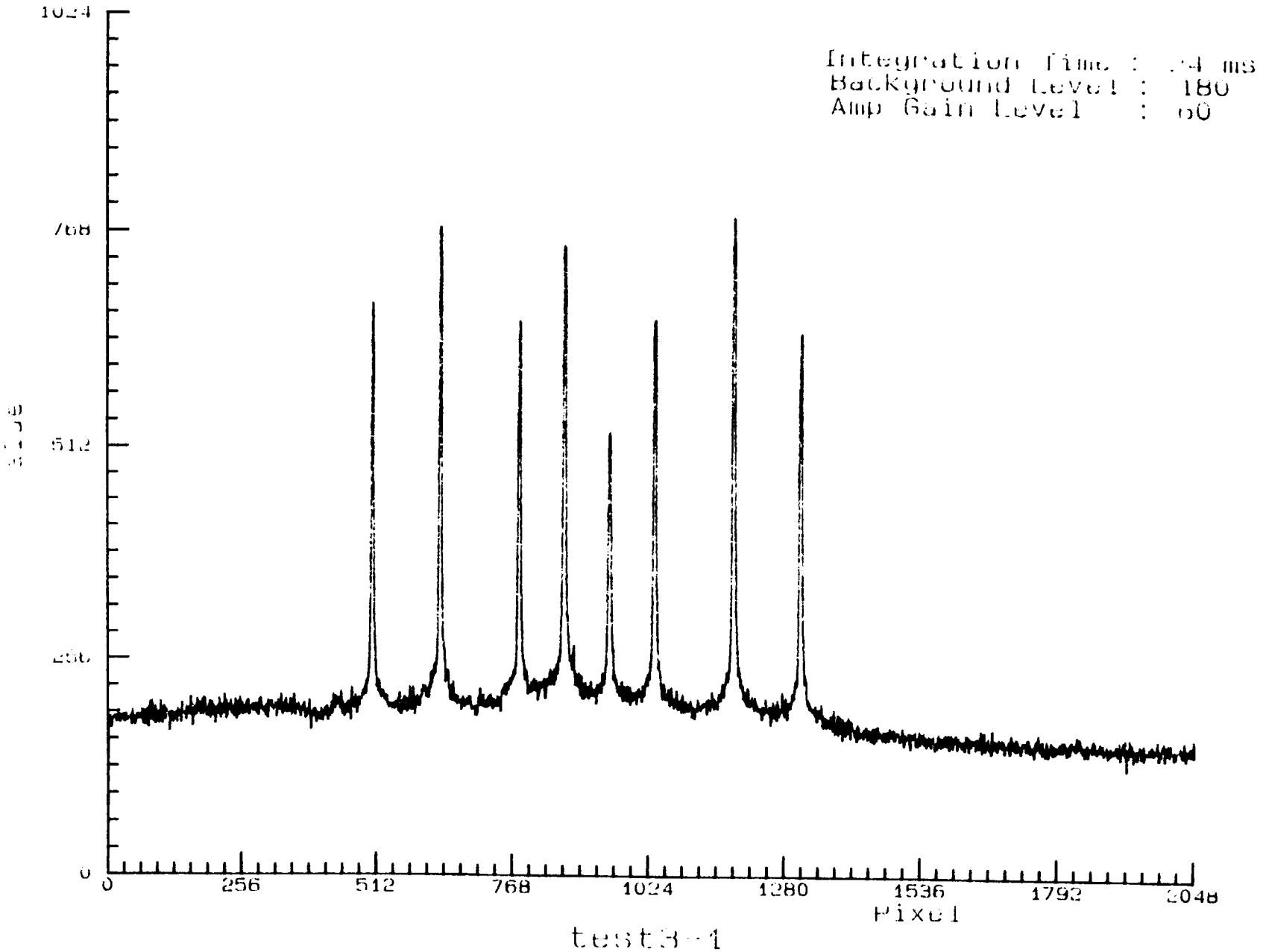

Figure 15. Graph of digital signal output of camera when imaging cylindrical model with eight targets.

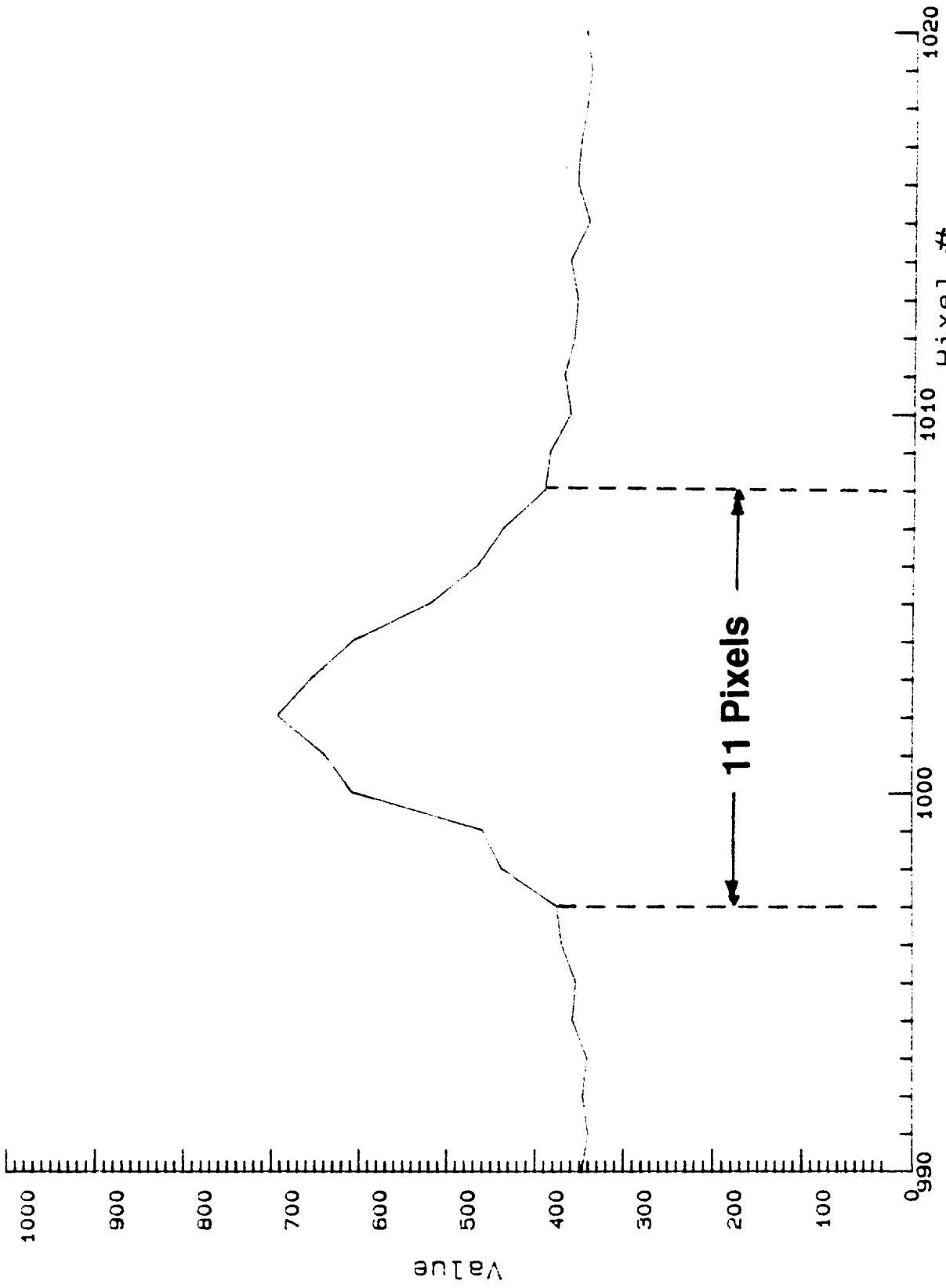

Figure 16. Graph of digital output of a camera for a single LED target.

Conclusions

Early simulation results were used to determine the level of signal-to-noise which would be needed to achieve the accuracy specified for the position measurement system. No model dynamics were taken into account in the simulation. Rather, the model was assumed to be stationary over the total 10 ms time in which the target locations were being sensed. The signal-to-noise ratio required to achieve the specified accuracy for the sensing system has been demonstrated. Also, it appears that a sample rate in excess of 20 samples/second can be achieved. However, further tests are required before it is known how much faster the system can track.

Conclusions

* Simulation and test results indicate that the accuracy requirements for the sensing system will be met

* Software is being streamlined to improve the frequency response, should be possible to sample > 20 samples/sec

APPENDIX

LIST OF ATTENDEES

Paul E. Allaire
University of Virginia
Mechanical Engineering Department
Thornton Hall
Charlottesville, VA 22901
Bus. Phone: (804) 924-3292

Dr. Willard W. Anderson
NASA Langley Research Center
Mail Stop 479
Hampton, VA 23665

Bus. Phone: (804) 864-1718

Bill G. Asbury
NASA Langley Research Center
MS 904
Hampton, VA 23665-5225

Bus. Phone: (804) 865-1018

Bibhuti Banerjee
University of Virginia
ROMAC Labs, Mech & Aero Engrg
Thornton Hall, McCormick Road
Charlottesville, VA 22901
Bus. Phone: (804) 924-3292

Mr. David A. Barnes
Honeywell, Inc.
13350 U. S. Hwy 19 North
Clearwater, FL 34624-7290

Bus. Phone: (813) 539-4030

James G. Batterson
NASA Langley Research Center
MS 161
Hampton, VA 23665-5225

Bus. Phone: (804) 864-4059

Michael C. Beale
Newport News Shipbuilding Co.
4101 Washington Avenue
E-78/B600
Newport News, VA 23607
Bus. Phone: (804) 688-9896

Fred B. Beck
NASA Langley Research Center
Mail Stop 490
Hampton, VA 23665-5225

Bus. Phone: (804) 864-1829

Vaughn D. Behun
NASA Langley Research Center
MS 904
Hampton, VA 23665-5225

Bus. Phone: (804) 865-1018

Leo Blecher
Intermagnetics General Corp.
P. O. Box 566 Charles Park
Guilderland, NY 12084

Bus. Phone: (518) 456-5456

Robert W. Bosley
Allied-Signal Aerospace Comp.
2525 West 190th Street
P. O. Box 2960
Torrance, CA 90509-2960
Bus. Phone: (213) 323-9500

Mr. Rich Boyden
NASA Langley Research Center
Mail Stop 287
Hampton, VA 23665-5225

Bus. Phone: (804) 864-5160

Colin P. Britcher
Old Dominion University
Dept. of Mechanical Engg.
Norfolk, VA 23529-0247

Bus. Phone: (804) 683-3720

Dr. Gerald V. Brown
NASA Lewis Research Center
MS 23-3
Cleveland, OH 44135

Bus. Phone: (216) 433-6047

Thomas G. Campbell
NASA Langley Research Center
Mail Stop 490
Hampton, VA 23665

Bus. Phone: (804) 864-1772

Ms. Michelle L. H. Chun
The Pentagon
Industrial Activities Office, OASD
Washington, DC 20310-0440

Bus. Phone: (703) 834-3779

James H. Connelly
Charles Stark Draper Laboratory
555 Technology Square
MS#37
Cambridge, MA 02139
Bus. Phone: (617) 258-4729

Mr. L. P. de Rochemont
Radiation Monitoring Devices, Inc.
44 Hunt Street
Watertown, MA 02172

Bus. Phone: (617) 926-1167

Thomas C. Britton
Lockheed Engg.
NASA Langley Research Center
MS 161
Hampton, VA 23665-5225
Bus. Phone: (804) 864-6619

Gary Brown
NASA/Goddard Space Flight Center
MS 716.2
Greenbelt, MD 20771

Bus. Phone: (301) 286-3964

Ingrid Carlberg
NASA Langley Research Center
MS 416A
Hampton, VA 23665-5225

Bus. Phone: (804) 864-4174

James Clemmons
Vigyan Associates
NASA Langley Research Center
MS 383
Hampton, VA 23665-5225
Bus. Phone: (804) 864-4466

Taumi S. Daniels
NASA Langley Research Center
Mail Stop 238
Hampton, VA 23665-5225

Bus. Phone: (804) 864-4659

Jorge H. Decanini
T R W
One Space Park
R9/2181
Redondo Beach, CA 90278
Bus. Phone: (213) 814-6307

Capt. Ted A. Doederlein
Astronautics Laboratory
AL/VSSS
Edwards, CA 93523-5000

Bus. Phone: (805) 275-5483

Dr. James R. Downer
SatCon Technology Corporation
12 Emily Street
Cambridge MA 02139

Bus. Phone: (617) 661-0540

David B. Eisenhaure
SatCon Technology Corporation
12 Emily Street
Cambridge, MA 02139-4507

Bus. Phone: (617) 661-0540 Ext 201

Gerald K. Foshage
Honeywell Satellites Systems Div.
Box 52199
Phoenix, AZ 85072-2199

Bus. Phone: (602) 561-3178

Carlos M. Grodsinsky
NASA Lewis Research Center
21000 Brookpark Rd., MS500-205
Cleveland, OH 44135

Bus. Phone: (216) 433-2664

Mike Hagopian
NASA/Goddard Space Flight Center
Greenbelt, MD 20771

Bus. Phone: (301) 286-7854

Mr. Richard Dorman
Mechanical Technology, Inc.
968 Albany Shaker Rd.
Latham, NY 12110

Bus. Phone: (518) 785-2224

Mr. David Dress
NASA Langley Research Center
Mail Stop 287
Hampton, VA 23665-5225

Bus. Phone: (804) 864-5126

Karl Flueckiger
Charles Stark Draper Laboratory
MS 4C
555 Technology Square
Cambridge, MA 02139
Bus. Phone: (617) 258-3850

Melvin C. Gilreath
NASA Langley Research Center
Mail Stop 490
Hampton, VA 23665-5225

Bus. Phone: (804) 864-1817

Nelson J. Groom
NASA Langley Research Center
Mail Stop 161
Hampton, VA 23665

Bus. Phone: (804) 864-6613

David Hampton
University of Virginia
ROMAC Labs, Mech & Aero Engrg
Thornton Hall, McCormick Road
Charlottesville, VA 22901
Bus. Phone: (804) 924-3767/3292

Steven D. Harrah
NASA Langley Research Center
MS 490
Hampton, VA 23665-5225

Bus. Phone: (804) 864-1805

David H. Hibner
Pratt & Whitney
400 Main Street
MS 163-09
East Hartford, CT 06108
Bus. Phone: (203) 565-2238

Neil Holmberg
NASA Langley Research Center
Mail Stop 442
Hampton, VA 23665-5225

Bus. Phone: (804) 864-6970

R. R. Humphris
University of Virginia
Dept. of Mech & Aero Engineering
Thornton Hall
Charlottesville, VA 22901
Bus. Phone: (804) 924-3292

Mr. Ken Jacobs
NASA Langley Research Center
Mail Stop 442
Hampton, VA 23665-5225

Bus. Phone: (804) 864-6967

Dr. Bruce G. Johnson
SatCon Technology Corporation
12 Emily Street
Cambridge, MA 02139

Bus. Phone: (617) 661-0540

Michael J. Hennessy
Intermagnetics General Corp.
P. O. Box 566 Charles Park
Guilderland, NY 12084

Bus. Phone: (518) 456-5456

Richard Hockney
SatCon Technology Corporation
12 Emily Street
Cambridge, MA 02142

Bus. Phone: (617) 661-0540 X206

Mr. Stuart Hsu
Honeywell, Inc.
19019 N. 59th Avenue
Glendale, AZ 85308

Bus. Phone: (602) 561-3485

James D. Hurley
Mechanical Technology Inc.
968 Albany Shaker Rd.
Latham, NY 12110

Bus. Phone: (518) 785-2177

Dexter Johnson
NASA Lewis Research Center
21000 Brookpark Rd., MS 23-3
Cleveland, OH 44135

Bus. Phone: (216) 433-6046

Mr. V. O. Jones
Newport News Shipbuilding Co.
4101 Washington Ave.
E-78/B600
Newport News, VA 23607
Bus. Phone: (804) 688-9896

Dr. Prakash B. Joshi
Physical Sciences Inc.
20 New England Business Center
Andover, MA 01810

Bus. Phone: (508) 689-0003

Dr. Suresh M. Joshi
NASA Langley Research Center
Mail Stop 230
Hampton, VA 23665

Bus. Phone: (804) 864-6608

Mr. Haig Kalfaian
Allied-Signal Aerospace Co.
Route 46
Teterboro, NJ 07608

Bus. Phone: (201) 393-3061

Claude R. Keckler
NASA Langley Research Center
Mail Stop 479
Hampton, VA 23665

Bus. Phone: (804) 864-1716

Mr. John M. Keesee
Magnetic Bearings Inc.
609 Rock Road
Radford, VA 24141

Bus. Phone: (703) 731-4983

Warren C. Kelliher
NASA Langley Research Center
Mail Stop 416A
Hampton, VA 23665-5225

Bus. Phone: (804) 864-4172

Dr. Robert A. Kilgore
NASA Langley Research Center
Mail Stop 285
Hampton, VA 23665-5225

Bus. Phone: (804) 864-5020

Ronald W. Kipp
Kingsbury, Inc.
10385 Drummond Rd.
Philadelphia, PA 19154

Bus. Phone: (215) 824-4887

Dr. R. Gordon Kirk
Virginia Polytech. & State Univ.
Dept. of Mechanical Engg.
Randolph Hall
Blacksburg, VA 24061
Bus. Phone: (703) 231-7478

Josiah D. Knight
Duke University
Dept. of Mech. Engg. and Mat. Science
Durham, NC 27706

Bus. Phone: (919) 660-5337

Carl Knospe
University of Virginia
Dept. of Mechanical & Aerosp. Engg.
Thornton Hall, McCormick Rd.
Charlottesville, VA 22901
Bus. Phone: (804) 982-2603

Peter J. LaRocca
Charles Stark Draper Laboratory
555 Technology Square
Cambridge, MA 02139

Bus. Phone: (617) 258-1555

Pierce L. Lawing
NASA Langley Research Center
Mail Stop 267
Hampton, VA 23665-5225

Bus. Phone: (804) 864-5137

Mr. Duncan C. McCallum
Charles Stark Draper Laboratory
M. S. #4C
555 Technology Square
Cambridge, MA 02139
Bus. Phone: (617) 258-2426

Mr. James M. Michael
Lockheed Engg & Sciences Co.
NASA Langley Research Center
MS 444
Hampton, VA 23665-5225
Bus. Phone: (804) 864-7062

Mark Motter
NASA Langley Research Center
MS 442
Hampton, VA 23665-5225

Bus. Phone: (804) 864-6978

Mr. Stuart J. Olstad
FluiDyne Engineering Corp.
5900 Olson Memorial Hwy.
Minneapolis, MN 55422

Bus. Phone: (612) 544-2721

David P. Plant
FARE, Inc.
4716 Pontiac Street, Suite 304
College Park, MD 20740

Bus. Phone: (301) 982-2093

Mr. Kirk A. Logsdon
NASA Lewis Research Center
21000 Brookpark Rd.
MS 500/217
Cleveland, OH 44135
Bus. Phone: (216) 933-2836

Edward B. McCaul
Duke University
Dept. of Mech. Engg. and Mat. Science
Bldg. 144-A
Durham, NC 27706
Bus. Phone: (919) 660-5311

William E. Michaud
Magnetic Bearings, Inc.
609 Poquonnock Road
Groton, CT 06340

Bus. Phone: (203) 445-4005

John V. Murphy
Rockwell International, Sp. Sys. Div.
P. O. Box 21086
Kenn edy Space Center, FL 32815

Bus. Phone:

Lloyd A. Ormon
Newport News Shipbuilding
4101 Washington Ave.
Newport News, VA 23607

Bus. Phone: (804) 380-4795

Dr. Douglas B. Price
NASA Langley Research Center
Mail Stop 161
Hampton, VA 23665-5225

Bus. Phone: (804) 864-6605

Rhonda R. Raffi
SatCon Technology Corporation
12 Emily Street
Cambridge, MA 02139

Bus. Phone: (617) 661-0540

Mr. Dharamendra N. Rawal
Virginia Polytechnic & State Univ.
Dept. of Mechanical Engg.
Blacksburg, VA 24060

Bus. Phone: (703) 361-3798

Dr. Donald Rote
Argonne National Laboratory
Bldg. 362
9700 S. Cass Ave.
Argonne, IL 60439
Bus. Phone: (708) 972-3786

Kevin Shelton
Lockheed Engg.
NASA Langley Research Center
MS 383
Hampton, VA 23665-5225
Bus. Phone: (804) 864-4470

Dr. Jag J. Singh
NASA Langley Research Center
Mail Stop 235
Hampton, VA 23665-5225

Bus. Phone: (804) 864-4760

John Stekly
Intermagnetic General Corporation
6 Eastern Road
Acton, MA 01720

Bus. Phone: (508) 264-4099

Dantam K. Rao
Mechanical Technology Inc.
968 Albany Shaker Road
Latham, NY 12110

Bus. Phone: (518) 785-2689

Lewis Rosado
DoD - Air Force
WRDC/POSL
WPAFB, OH 45433-6563

Bus. Phone: (513) 255-1286

Raouf Selim
Christopher Newport College
Physics Department
50 Shoe Lane
Newport News, VA 23601
Bus. Phone: (804) 599-7192

Dr. Thomas A. Shull
NASA Langley Research Center
Mail Stop 488
Hampton, VA 23665

Bus. Phone: (804) 864-1837

Dr. Michael R. Squillante
Radiation Monitoring Devices, Inc.
44 Hunt Street
Watertown, MA 02172

Bus. Phone: (617) 926-1167

Mr. Stuart S. Stephens
FluiDyne Engineering Corp.
5900 Olson Memorial Hwy
Minneapolis, MN 55422

Bus. Phone: (612) 544-2721

Mr. Richard A. Swendsen
TRW
One Space Park
Bldg. R9/1885
Redondo Beach, CA 90278
Bus. Phone: (213) 814-6092

Anil Trivedi
Allied-Signal Aerospace
2525 West 190th Street
P.O. Box 2960, M/S T-41; Dept. 93190

Bus. Phone: (213) 512-4231

Mr. John Ukstins
Allied Signal Corp.-Bendix Guid. Sys.
Dept. 6401 MS 2/13
Teterboro, NJ 07608

Bus. Phone: (201) 393-2567

Bertice E. Walker
Newport News Shipbuilding
4101 Washington Ave.
Newport News, VA 23607

Bus. Phone: (804) 688-2285

Robert C. Whitestone
David Taylor Research Center
Code 2712
Annapolis, MD 21402

Bus. Phone: (301) 267-3458

Patrick Wolke
Honeywell Satellite Systems Group
19019 North 59th Ave.
Glendale, AZ 85308-9650

Bus. Phone: (602) 561-3553

Robert S. Tamosaitis
Dupont
Experimental Station 304/C118
P. O. Box 80304
Wilmington, DE 19880
Bus. Phone: (302) 695-1752

David L. Trumper
Univ. of North Carolina at Charlotte
Dept. of Electrical Engineering
Charlotte, NC 28223

Bus. Phone: (704) 547-4324

Erik Vedeler
NASA Langley Res. Center
MS 490
Hampton, VA 23665-5225

Bus. Phone: (804) 864-1825

Sharon S. Welch
NASA Langley Research Center
Mail Stop 161
Hampton, VA 23665

Bus. Phone: (804) 864-6611

Stephanie Wise
NASA Langley Research Center
MS 474
Hampton, VA 23665-5225

Bus. Phone: (804) 864-

Belle L. Wood
NASA Langley Research Center
MS 444
Hampton, VA 23665-5225

Bus. Phone: (804) 864-7257

Dr. Kamal Youcef-Toumi
Massachusetts Institute of Technology
77 Massachusetts Avenue
Cambridge, MA 02139

Bus. Phone: (617) 253-2216

W. Robert Young
NASA Langley Research Center
MS 490
Hampton, VA 23665-5225

Bus. Phone: (804) 864-1824

Millard A. Zydron
Newport News Shipbuilding Co.
4101 Washington Avenue
E-52/B600
Newport News, VA 23607
Bus. Phone: (804) 688-8693